2014

Studies of integrins' lateral dynamics at a single particle level

Dipak Mainali
Iowa State University

Studies of integrins' lateral dynamics at a single particle level

by

Dipak Mainali

A dissertation submitted to the graduate faculty

in partial fulfillment of the requirements for the degree of

DOCTOR OF PHILOSOPHY

Major: Analytical Chemistry

Program of Study Committee:
Emily A. Smith, Major Professor
Ning Fang
Robert S. Houk
Edward Yu
Javier Vela

Iowa State University

Ames, Iowa

2014

To my father

(Bishnu Prasad Mainali)

TABLE OF CONTENTS

ACKNOWLEDGEMENTS

I would like to thank my advisor, Dr. Emily A. Smith, for her continuous guidance and support throughout the course of this research and graduate career. I especially thank her for letting me do the internship at Genentech during the summer of 2013. I would like to thank my committee members, Dr. Ning Fang, Dr. Robert Houk, Dr. Javier Vela, and Dr. Edward Yu for their support. I would also like to thank Dr. Jane Li for her guidance during the internship at Genentech.

In addition, I would also like to thank my friends and colleagues who have made the life experience wonderful regardless of where and what I am doing in life. Finally, thanks to my mother (Subhadra Mainali) and sisters (Rita Mainali Pandey and Manita Mainali Sitaula) for their eternal encouragement and unconditional love.

CHAPTER 1: GENERAL INTRODUCTION

Dissertation Organization

This dissertation presents the research results focused on the class of receptors termed integrins. The primary goal of the work is to understand the lateral dynamics of integrins using single particle tracking to elucidate how other cellular factors affect integrins' lateral diffusion.

The dissertation is organized in five chapters and one appendix. The first chapter provides the general introduction to set up the background on various topics that will facilitate the understanding of subsequent chapters. The chapter highlights the research motivations, and a literature review on areas such as the cell membrane, diffusion theory, integrins, and fluorescent probes used for labeling proteins. Two popular experimental methods for measuring the lateral diffusion properties of proteins in the cell membrane are single particle tracking (SPT) and fluorescence recovery after photobleaching (FRAP). Finally the various analysis methods employed for the analysis of single particle tracking data are discussed.

Extracellular ligand-receptor binding is one of the important interactions for signal transduction across the cell membrane. Chapter 2 is a published article in *European Biophysics Journal* that reports how the binding of extracellular ligand to integrins with different ligand affinities affects integrins' lateral diffusion. Similarly, the association of cytoplasmic and membrane proteins to integrins is an inevitable event in the crowded cellular environment, and these interactions are essential for integrin function. Chapter 3 and 4 discuss how selected cytoplasmic and membrane proteins influence integrins' lateral

diffusion. Chapter 3 is a published article in *Analytical Bioanalytical Chemistry* journal. Finally, Chapter 5 is a general conclusion summarizing this dissertation.

There is an appendix to this thesis. The research work related to this appendix was performed at Genentech during the summer of 2013 as a part of curriculum practical training under the supervision of Dr. Jane Li. The project involves the use of near infrared spectroscopy in tandem with chemometric analyses for the development of a comprehensive model to determine water content in pharmaceutical tablets. The work has been published in the *Journal of Biomedical and Pharmaceutical Analysis*.

Research motivations and objectives

It is well established that a cell membrane and the receptors embedded in the cell membrane serve a multitude of functions in living cells. The cell membrane acts as an effective barrier to selectively transport macromolecules in and out of the cell for effective communication and nourishment. Receptors are the proteins that relay signals in and out of the cell and are fundamental for proper cellular function. For several decades, scientists have been pursuing the investigation of cell membranes and receptors to fully understand their biological importance, molecular design and organization, and the relation with other constituents in their environment. Cell membrane and receptors are studied such extensively because nearly all diseases and the therapeutic targets to many diseases somehow involve the membrane and receptors. The aim of this research is to focus on an important class of receptors termed integrins, whose aberrant function is known to be associated with multiple diseases such as cancer metastases, angiogenesis, inflammation, fibrosis, and thrombosis [1-

4]. Integrins primary function includes cell-extracellular matrix adhesion, bi-directional signaling, cell migration, growth and survival.

A comprehensive understanding of the structure, signaling processes, and factors affecting the lateral dynamics of receptors is essential to develop new, or improve existing, therapeutic drugs. Several advanced analytical techniques such as electron microscopy, X-ray crystallography, and Nuclear Magnetic Resonance spectroscopy have successfully provided detailed information on the structure and composition of the cell membrane, many receptors and cellular components. However, the understanding of the interaction and lateral dynamics of receptors and other molecular components in the cell membrane and their organization in two or three dimensions to form fully functioning living cells is still lacking. This is because the aforementioned techniques are not suitable to perform lateral dynamics studies of receptors in the live cell membrane.

The focus of this dissertation is understanding integrins' interaction with both downstream and upstream effectors, such as extracellular ligand, selected cytoplasmic and membrane proteins in the cell membrane by probing the lateral dynamics of integrins. The lateral mobility is essential for integrins' function. Lateral movement allows integrins to associate with extracellular ligand, and other membrane and cytoplasmic proteins to incite biological activity such as signaling and downstream effects.

Non-invasive fluorescence-based single particle tracking (SPT), fluorescence recovery after photobleaching (FRAP), and the molecular biology technique called RNA interference are the main tools utilized in this work to address the interaction of integrins with other important cellular components. SPT and FRAP provide information on the lateral

mobility of integrins in the cell membrane and RNA interference selectively reduces the expression of a protein of interest in the cell.

Literature Review

Cell membrane

In 1972, Singer and Nicholson proposed a fluid mosaic model for the cell membrane that described the structure and functions of the membrane. According to the fluid mosaic model, the membrane is made up of a two dimensional lipid bilayer where components such as proteins, carbohydrates, and cholesterol are able to change their position without altering the membrane integrity [5,6]. Proteins are either fully integrated or peripherally attached as shown in Figure 1. Proteins play an important role in carrying out various cellular functions such as signaling, transporting ions and nutrients, and providing anchorage to the cytoskeleton.

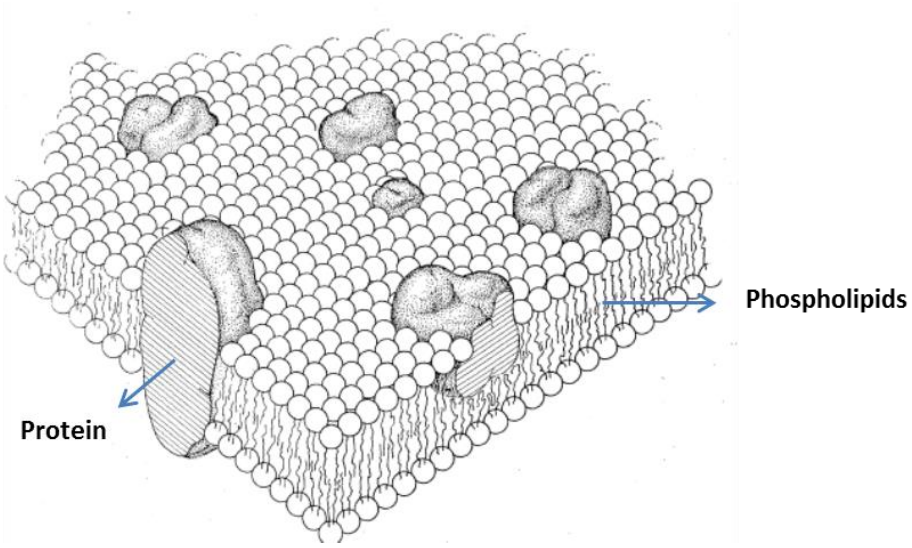

Figure 1: A structure of the cell membrane as described by the fluid mosaic model: a fluid combination of phospholipids and proteins. (Figure obtained and modified from reference [6])

Diffusion theory

One of the important factors in controlling the dynamics, structure, and functioning of the cell membrane is the lateral diffusion of membrane proteins and lipids [7-9]. Therefore, utilizing the general structural framework of fluid mosaic model, the theoretical description for the lateral Brownian diffusion of proteins and lipid molecules in a biological membrane was developed by Saffman and Delbruck in 1975 using a continuum hydrodynamic model (Equation 1) [10].

$$D = \frac{kT}{4\pi\eta_m h} \cdot \left(\ln \frac{\eta_m h}{\eta_w a} - 0.5772 \right), \qquad (1)$$

Where D is the diffusion coefficient, *k* is Boltzmann constant, T is absolute temperature, η_m is membrane viscosity, η_w is viscosity of surrounding medium, h is thickness of the membrane and 'a' is the radius of membrane component. Calculated values are on the order of 10^{-8} cm^2/s for a typical membrane protein. However, the lateral diffusion of proteins in the cell membrane is often slower than predicted by the Saffman and Delbruck equation and the experimentally measured value in model solid-supported lipid bilayers [11]. This could be due to many factors such as membrane proteins interaction with extracellular and cytoskeleton/cytoplasmic proteins, molecular crowding, or membrane confinement to domains of varying size, all of which limit lateral diffusion.

The developments in optical microscopy, labeling probes, sensitive detectors, automated image analysis, and particle tracking software have made it possible to observe the movements of a single biomolecule in the live cell membrane with nanometer level accuracy [12]. Therefore, over time the simple picture of the fluid mosaic model has evolved with

increasing information obtained from the nano-scale dynamics of proteins and lipids in a heterogeneous membrane. The concepts of lipid rafts, nanodomains, confinement zone, caveolae, and pits have appeared in the membrane picture resulting in models of non-random molecular distribution (Figure 2) [13]. With the help of optical microscopy techniques such as SPT, FRAP, and fluorescence correlation spectroscopy (FCS), it has been understood that not all membrane proteins diffuse freely as the results of anchorage to the cytoskeleton or incorporation into large oligomeric or supramolecular complexes [14,12].

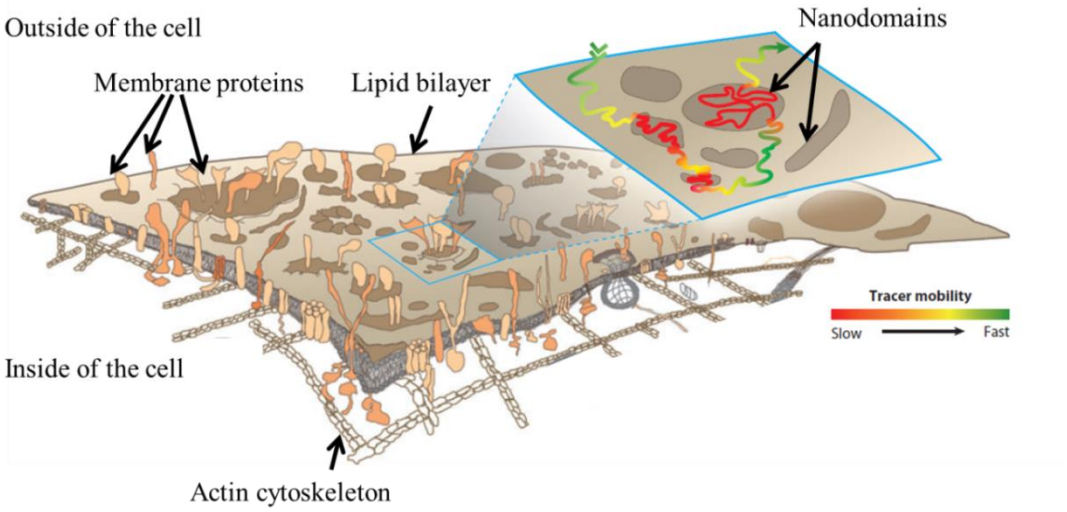

Figure 2: Cell membrane structure with protein and nanodomain organization. (Figure adapted and modified from reference [13])

Integrins

Integrins' lateral mobility and rearrangement is essential for its primary function of cell-extracellular matrix adhesion, cell-cell adhesion, and signaling [15-20]. Integrins are type 1 transmembrane heterodimeric proteins that consists of non-covalently associated α and β subunits (Figure 3).To date, there are 24 human and 5 Drosophila integrins identified [2]. Integrins are highly conserved from invertebrates to vertebrates and are structurally,

immunochemically, and functionally related to each other [21]. Integrins' ectodomain participates in extracellular matrix protein or ligand recognition, whereas the cytoplasmic tails interact directly or indirectly with the cytoskeleton signaling network [22]. Integrins' adhesiveness is dynamically regulated through inside-out signaling primed by intracellular components.

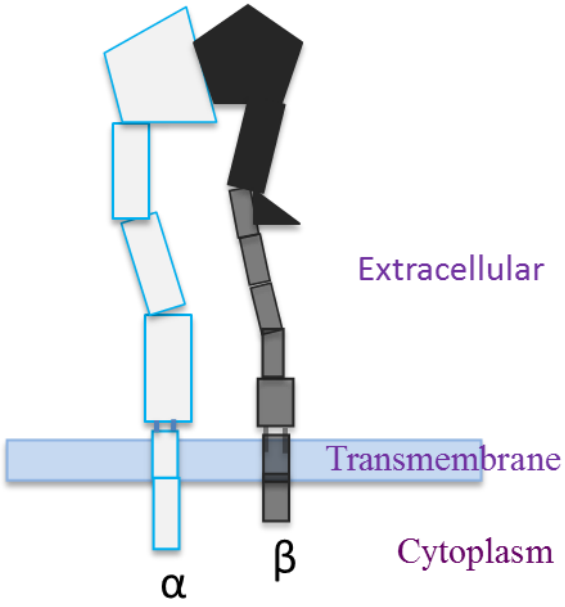

Figure 3: Integrin structure showing two subunits that consists of large extracellular domain, short transmembrane domain, and short cytoplasmic domain.

Fluorescence techniques to measure lateral diffusion of membrane receptors

One of the most widely used spectroscopic contrast mechanism at the single molecule level is fluorescence because of relatively high quantum efficiency and sensitivity of the process compared to other possible contrast mechanisms [23]. Fluorescence microscopy has become the method of choice for many experiments in biology, chemistry, and physics due to its commercial availability, non-invasiveness, and biocompatibility. Similarly, the

availability of new detectors, light source, fluorescent dyes and labeling chemistries has made fluorescence microscopy techniques increasingly popular. Particularly in cellular/molecular biology, single particle tracking (SPT), fluorescence recovery after photobleaching (FRAP), fluorescence resonance energy transfer (FRET), and fluorescence correlation spectroscopy (FCS) techniques that utilize the fluorescence principle, have revealed new and interesting dynamic and structural information of receptors.

Fluorescence principle

Fluorescence is the emission of light at the higher wavelength region compared to the excited wavelength region of light when a molecule is excited to the higher energy state. Because of the difference between emission and excitation wavelength, known as a Stokes shift, emitted light from the objects of interest can be filtered out using appropriate optics. Alexander Jablonski in the 1930s explained the fluorescence phenomenon in the form of diagram showing the details of the excitation and emission process as shown in figure 4.

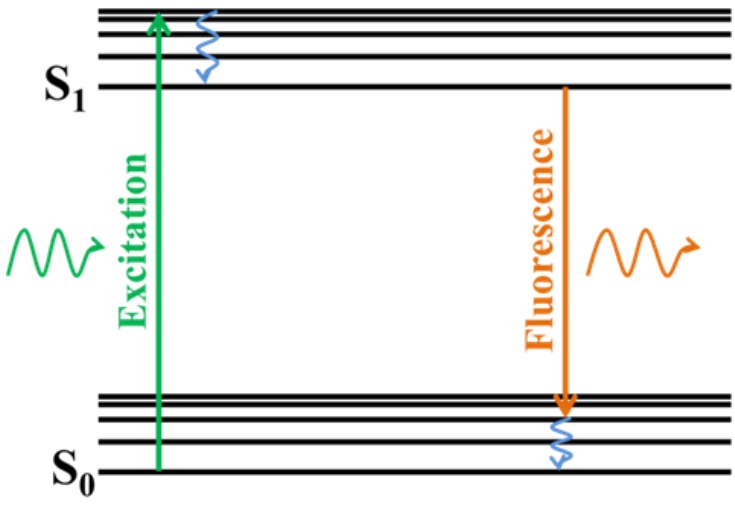

Figure 4: Jablonski diagram showing fluorescence mechanism.

Fluorescence Recovery after Photobleaching (FRAP)

FRAP and SPT are the two techniques that have been extensively used to measure the lateral diffusion of proteins in the cell membrane. FRAP measures the ensemble diffusion of fluorescently-tagged receptors. In a FRAP experiment, an intense laser pulse is used to irreversibly photobleach the fluorescently-tagged receptors in a micrometer-size area of the membrane and subsequent recovery of the fluorescence signal due to diffusion from the surrounding unbleached regions to the bleached region is monitored [24]. The data are generally analyzed by fitting the recovery curve to the equation derived for different modes of motion yielding diffusion parameters such as mobile fraction and diffusion coefficient. Since FRAP provides a snapshot of an ensemble of receptors to calculate lateral mobility, it might be insensitive to important subpopulations of receptors that exhibit different modes of motion.

Single Particle Tracking (SPT)

SPT has become a method of choice for many scientists for probing the organization and dynamics of receptors in the cell membrane. SPT has approximately two orders of magnitude higher spatial resolution compared to FRAP, which would enable observation of molecular motion in domains smaller than the diffraction limit of light [25]. The biggest advantage of SPT is that it provides information of heterogeneity in the physical, chemical, or biological properties of a single receptor that is otherwise lost in ensemble measurements such as FRAP. SPT helps to resolve the modes of motion of individual receptor such as Brownian, directed, anomalous, or immobile. In SPT, a fluorescent probe or colloidal

gold/beads is attached to the molecule of interest and the labeled molecule's movement is tracked using video microscopy.

One of the important requirements for single particle tracking is to have a high signal-to-noise ratio, which is generally achieved by the use of high efficiency optics, bright fluorescent tags, and sensitive detectors such as charged coupled devices. Moreover, SPT is achieved by using a low concentration of labeling probe so that the detection and tracking of two molecules is not convoluted in a single diffraction-limited spot. Once the movement is recorded, careful analysis of the trajectories is essential to extract diffusion parameters and modes of motion. The data analysis of SPT is discussed in a later section.

Fluorescent probes for SPT

Nanoparticles, colloidal gold, latex beads, and fluorescent tags have been used to label receptors for SPT experiments. Fluorescent tags consist of organic dye molecules, fluorescent proteins such as green fluorescent protein (GFP) or yellow fluorescent protein (YFP), and quantum dots. Before considering single receptor tracking using fluorescence microscopy, it is necessary to consider the size, photophysical properties such as quantum yield, photobleaching, blinking, and brightness of the fluorescent tag. Ideal fluorescent probes should have high extinction coefficients at the wavelength used for excitation, a high fluorescence quantum yield and have emission that is spectrally distinct from the excitation wavelength, resistance to photobleaching, and a smaller size so it has minimal effects on the diffusion properties of the species of interest [23].

One of the fluorescent probes that offer unique photophysical properties that partially compensates for the weakness of dyes and fluorescent proteins is semiconductor quantum

dots (QDs). QDs have moderate size (15-20 nm including coating), resistance to photobleaching, bright fluorescence, and high signal-to-noise ratio that would increase spatial resolution and also can be tracked over long period of time [26,27]. QDs typically consist of a core and shell that are made up of semiconductor inorganic materials such as cadmium selenide, cadmium sulfide, or zinc selenide [28,27]. For biological applications QDs are coated with biocompatible surface coatings to increase water solubility and also to provide a linker to attach with biomolecules. One of the disadvantages of QDs is blinking, which hinders the process of forming the trajectories that are used to extract diffusion properties. Sophisticated tracking algorithms exist where QD blinking is not a significant problem, and can be used to identify and confirm a single particle observation.

SPT data analysis

Meaningful information from SPT data depends on the analysis method employed. Due to the lack of universal method for SPT data analysis, different labs have developed and employed different analysis method to extract information from the trajectories of a single particle [12]. Most SPT data has been computed in terms of mean square displacement (MSD) versus time and by analyzing the probability distribution of individual displacements [29-31].

Generally SPT data analysis involves localization/detection, linking/tracking, and analysis as shown in figure 5. There are various strategies that have been reported in the literature for localizing and tracking single particles [32-34]. In localization, the x and y coordinates of the center of particle attached to a molecule that moves in the two-dimensional membrane are extracted. Various methods such as cross-correlation, centroid identification, a

Gaussian fit, or a pattern recognition method have been reported in order to find the coordinates of the particles [35]. The accuracy of position determination by each method is influenced by the number of detected photons, background noise by autofluorescence, pixelation, and dark current. Each method is suitable based on the experimental system. A two-dimensional Gaussian fit provides the best results in terms of localization when considering a single molecule labelled with fluorescent probes that are smaller than microscopic resolution at relatively low signal to noise ratio (<4) [36]. However, 2D Gaussian fit relies on a particular shape and intensity distribution of the particles. In trajectory linking, the coordinates are linked using different automated algorithms such as nearest-neighbor-algorithm, feature point tracking, or multiple-hypothesis tracking [37,38,36]. A good algorithm to calculate trajectories should take into account the issues such as particle crossover, merge, split, interact, or blink. A multiple-hypothesis algorithm takes into account the most of the aforementioned issues in trajectory reconstruction [38]. A given algorithm has its advantage or disadvantage depending on the quantity of surface density of tracking molecules it can consider for linking without being computationally intense and time consuming. Finally in analysis, the mean square displacement is computed for each trajectory from the formula (equation 2) to analyze physical parameters such as diffusion coefficient and mode of diffusion.

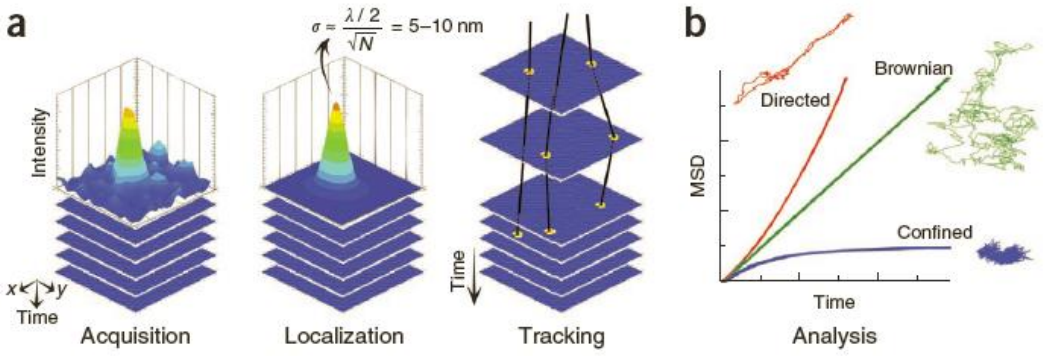

Figure 5: Processing and analysis of SPT data (a) building trajectories, (b) classification of SPT trajectories (Figure obtained from reference [26])

$$\mathrm{MSD}(n\tau) = \frac{1}{N-n}\sum_{i=1}^{N-n}[(x((i+n)\tau) - x(i\tau))^2 + (y((i+n)\tau) - y(i\tau))^2] \quad , (2)$$

where τ is the acquisition time between two successive frames, N is the total number of frames in the sequence, x and y are coordinates of the particle at a specific time lag, $0 < n < N/4$ and $1 < i < (N-n)$.

In SPT analysis, different groups differ in the way of classifying the trajectories and obtaining diffusion coefficient from calculated mean square displacement [12]. For example, Anderson et al. classified the experimental trajectory according to the model that best fit the shape of MSD vs time curve [39]. Kusumi and colleagues used the shape of the MSD curve in terms of the relative deviations by comparing the MSD behavior at short and long time lags [40]. A measure for the deviation of trajectory from free diffusion was determined by extrapolating a linear fit to the MSD at short time lags to longer time lags. Webb and collaborators used the anomalous diffusion exponent α obtained by fitting the log MSD vs log time curve to classify trajectories into different motion [41,42]. Simson et al. used the

analysis method where they classified trajectories as either confined or non-confined [43]. Trajectories were classified as non-confined if the particle remains in a region for duration of time that is considerably longer than a Brownian diffusing particle would stay. In all aforementioned analysis method, the more reliable classification can be obtained for the long trajectories if the particle didn't change the mode of motion. However, most analysis methods lack the ability to detect transitions between modes of motion such as from Brownian to confined, local stops, acceleration and deceleration of particles in a single trajectory. Many aspects of data analysis have not become standard in the scientific community yet. So it is hard to argue which one is the robust method for SPT data analysis.

References:

1. van der Flier A, Sonnenberg A (2001) Function and interactions of integrins. Cell Tissue Res 305 (3):285-298

2. Takada Y, Ye X, Simon S (2007) The integrins. Genome Biol 8 (5):215

3. Millard M, Odde S, Neamati N (2011) Integrin targeted therapeutics. Theranostics 1:154-188

4. Goodman SL, Picard M (2012) Integrins as therapeutic targets. Trends in pharmacological sciences 33 (7):405-412

5. Singer SJ (1972) A fluid lipid-globular protein mosaic model of membrane structure. Ann N Y Acad Sci 195:16-23

6. Singer SJ, Nicolson GL (1972) The fluid mosaic model of the structure of cell membranes. Science 175 (4023):720-731

7. Axelrod D (1983) Lateral motion of membrane proteins and biological function. J Membr Biol 75 (1):1-10

8. Ronchi P, Colombo S, Francolini M, Borgese N (2008) Transmembrane domain-dependent partitioning of membrane proteins within the endoplasmic reticulum. J Cell Biol 181 (1):105-118

9. Zhang F, Lee GM, Jacobson K (1993) Protein lateral mobility as a reflection of membrane microstructure. BioEssays 15 (9):579-588

10. Saffman PG, Delbruck M (1975) Brownian motion in biological membranes. Proc Natl Acad Sci U S A 72 (8):3111-3113

11. Jacobson K, Ishihara A, Inman R (1987) Lateral diffusion of proteins in membranes. Annu Rev Physiol 49:163-175

12. Saxton MJ, Jacobson K (1997) Single-particle tracking: applications to membrane dynamics. Annu Rev Biophys Biomol Struct 26:373-399

13. He HT, Marguet D (2011) Detecting nanodomains in living cell membrane by fluorescence correlation spectroscopy. Annu Rev Phys Chem 62:417-436

14. Kahya N, Schwille, P. (2005) Fluorescence correlation studies of lipid domains in model membranes. Molecular Membrane Biology 23 (1):29

15. Hynes RO (2002) Integrins: bidirectional, allosteric signaling machines. Cell 110 (6):673-687

16. Kucik DF, Dustin ML, Miller JM, Brown EJ (1996) Adhesion-activating phorbol ester increases the mobility of leukocyte integrin LFA-1 in cultured lymphocytes. J Clin Invest 97 (9):2139-2144

17. Yu T, Wu X, Gupta KB, Kucik DF (2010) Affinity, lateral mobility, and clustering contribute independently to beta 2-integrin-mediated adhesion. Am J Physiol Cell Physiol 299 (2):C399-410

18. Hynes RO (1987) Integrins: a family of cell surface receptors. Cell 48 (4):549-554

19. Giancotti FG, Ruoslahti E (1999) Integrin signaling. Science 285 (5430):1028-1032

20. Kucik DF (2002) Rearrangement of integrins in avidity regulation by leukocytes. Immunol Res 26 (1-3):199-206

21. Plow EF, Haas TA, Zhang L, Loftus J, Smith JW (2000) Ligand binding to integrins. J Biol Chem 275 (29):21785-21788

22. Petit V, Thiery JP (2000) Focal adhesions: structure and dynamics. Biol Cell 92 (7):477-494

23. Gell C, Brockwell, D., Smith, A. (2006) Handbook of Single Molecule Fluorescence Spectroscopy. Oxford,

24. Axelrod D, Koppel DE, Schlessinger J, Elson E, Webb WW (1976) Mobility measurement by analysis of fluorescence photobleaching recovery kinetics. Biophys J 16 (9):1055-1069

25. Mirchev R, Golan DE (2001) Single-particle tracking and laser optical tweezers studies of the dynamics of individual protein molecules in membranes of intact human and mouse red cells. Blood Cells Mol Dis 27 (1):143-147

26. Pinaud F, Clarke S, Sittner A, Dahan M (2010) Probing cellular events, one quantum dot at a time. Nat Methods 7 (4):275-285.

27. Bannai H, Levi S, Schweizer C, Dahan M, Triller A (2006) Imaging the lateral diffusion of membrane molecules with quantum dots. Nat Protoc 1 (6):2628-2634

28. Pinaud F, Michalet X, Bentolila LA, Tsay JM, Doose S, Li JJ, Iyer G, Weiss S (2006) Advances in fluorescence imaging with quantum dot bio-probes. Biomaterials 27 (9):1679-1687

29. Schutz GJ, Schindler H, Schmidt T (1997) Single-molecule microscopy on model membranes reveals anomalous diffusion. Biophys J 73 (2):1073-1080

30. Michalet X (2010) Mean square displacement analysis of single-particle trajectories with localization error: Brownian motion in an isotropic medium. Phys Rev E Stat Nonlin Soft Matter Phys 82 (4 Pt 1):041914

31. Iyer G, Michalet X, Chang YP, Weiss S (2010) Tracking single proteins in live cells using single-chain antibody fragment-fluorescent quantum dot affinity pair. Methods Enzymol 475:61-79

32. Schmidt T, Schutz GJ, Baumgartner W, Gruber HJ, Schindler H (1996) Imaging of single molecule diffusion. Proc Natl Acad Sci U S A 93 (7):2926-2929

33. Thompson RE, Larson DR, Webb WW (2002) Precise nanometer localization analysis for individual fluorescent probes. Biophys J 82 (5):2775-2783

34. Wieser S, Schutz GJ (2008) Tracking single molecules in the live cell plasma membrane-Do's and Don't's. Methods 46 (2):131-140

35. Cheezum MK, Walker WF, Guilford WH (2001) Quantitative comparison of algorithms for tracking single fluorescent particles. Biophys J 81 (4):2378-2388

36. Alcor D, Gouzer G, Triller A (2009) Single-particle tracking methods for the study of membrane receptors dynamics. Eur J Neurosci 30 (6):987-997

37. Sbalzarini IF, Koumoutsakos P (2005) Feature point tracking and trajectory analysis for video imaging in cell biology. J Struct Biol 151 (2):182-195

38. Jaqaman K, Loerke D, Mettlen M, Kuwata H, Grinstein S, Schmid SL, Danuser G (2008) Robust single-particle tracking in live-cell time-lapse sequences. Nat Methods 5 (8):695-702.

39. Anderson CM, Georgiou GN, Morrison IE, Stevenson GV, Cherry RJ (1992) Tracking of cell surface receptors by fluorescence digital imaging microscopy using a charge-coupled device camera. Low-density lipoprotein and influenza virus receptor mobility at 4 degrees C. J Cell Sci 101 (Pt 2):415-425

40. Kusumi A, Sako Y, Yamamoto M (1993) Confined lateral diffusion of membrane receptors as studied by single particle tracking (nanovid microscopy). Effects of calcium-induced differentiation in cultured epithelial cells. Biophys J 65 (5):2021-2040

41. Feder TJ, Brust-Mascher I, Slattery JP, Baird B, Webb WW (1996) Constrained diffusion or immobile fraction on cell surfaces: a new interpretation. Biophys J 70 (6):2767-2773

42. Slattery JP (1995) Lateral Mobility of Fc[epsilon]RI on Rat Basophilic Leukemia Cells as Measured by Single Particle Tracking Using a Novel Bright Fluorescent Probe. Cornell University, May

43. Simson R, Sheets ED, Jacobson K (1995) Detection of temporary lateral confinement of membrane proteins using single-particle tracking analysis. Biophys J 69 (3):989-993

CHAPTER 2: THE EFFECT OF LIGAND AFFINITY ON INTEGRINS' LATERAL DIFFUSION IN CULTURED CELLS

A paper published in *European Biophysics Journal*, 2013, 42, (4), 281-290

Dipak Mainali and Emily A. Smith

Department of Chemistry, Iowa State University, 1605 Gilman Hall, Ames, Iowa 50011

Abstract

The role of ligand affinity in altering αPS2CβPS integrins' lateral mobility was studied using single particle tracking (SPT) with ligand-functionalized quantum dots (QDs) and fluorescence recovery after photobleaching (FRAP) with fluorescent protein tagged integrins. Integrins are ubiquitous transmembrane proteins that are vital for numerous cellular functions, including bidirectional signaling and cell anchorage. Wild-type and high ligand affinity mutant (αPS2CβPS-V409D) integrins were studied in S2 cells. As measured by SPT, the integrin mobile fraction decreased by 22% and had a 4× slower diffusion coefficient for αPS2CβPS-V409D compared to wild-type integrins. These differences are partially the result of αPS2CβPS-V409D integrins' increased clustering. For the wild-type integrins, the average of all diffusion coefficients measured by SPT was statistically similar to the ensemble FRAP results. A 75% slower average diffusion coefficient was measured by SPT compared to FRAP for αPS2CβPS-V409D integrins, and this may be the result of SPT measuring only ligand-bound integrins, while all ligand-bound and ligand-unbound integrins are averaged in FRAP measurements. Specific binding of the ligand-functionalized QDs was

99% for integrin expressing cells. The results prove that the ligand binding affinity affects the lateral dynamics of a subset of integrins based on the complementary SPT and FRAP data.

Keywords Single particle tracking, fluorescence recovery after photobleaching, Tiggrin-functionalized quantum dot, αPS2CβPS integrins, S2 cells

Abbreviations

SPT Single Particle Tracking

QDs Quantum Dots

FRAP Fluorescence Recovery After Photobleaching

MSD Mean Square Displacement

LFA-1 Lymphocyte Function-associated Antigen 1

Introduction

Integrins are an important family of cell surface receptors that maintain a dynamic flow of information between the external and internal environments for the survival, growth, proliferation, differentiation, and proper functioning of cells (Giancotti and Ruoslahti 1999; Hynes 2002). This signal transduction occurs by ligand binding to the integrins' extracellular domain or through the stimuli received from chemokines, cytokines, and other intracellular proteins binding to integrins' cytoplasmic domain (Hynes 2002). Integrins are composed of non-covalently associated α and β subunits. Each subunit is non-homologous to one another, but overall heterodimer structure is well-conserved throughout the animal kingdom (Takada

et al. 2007). An increasing number of results from X-ray crystallography, conformational specific antibodies, and mutation studies confirm that integrins undergo significant structural changes in response to ligand binding or intracellular signals (Luo et al. 2007; Jannuzi et al. 2004). Similarly, several mutation studies have identified the important amino acids for dimer formation, association with intracellular proteins, ligand binding and regulation of ligand affinity (Luo et al. 2007; Bunch et al. 2006; Jannuzi et al. 2004). Integrins' conformational changes can lead to higher ligand affinities, whereas lateral association into clusters can increase ligand binding avidity by providing multiple contact sites (Stewart and Hogg 1996; van Kooyk and Figdor 2000). Details of integrins' lateral dynamics at the single receptor level are sparse. Many drugs target membrane proteins because of their accessibility from the exterior of cells, and aberrant integrin function is associated with numerous pathological conditions (Takada et al. 2007; Hillis and MacLeod 1996; Reddy and Mangale 2003; Huveneers et al. 2007). Therefore, it is important to study factors that affect integrins' lateral dynamics in the cell membrane.

To date, several analytical techniques have been employed to unravel the details of the lateral organization and dynamics of membrane proteins. The lateral mobility of receptors and lipids has been studied using fluorescence techniques such as fluorescence recovery after photobleaching (FRAP), fluorescence correlation spectroscopy, and single particle tracking (SPT) (Saxton and Jacobson 1997; Georgiou et al. 2002; Chen et al. 2006; Kovaleski and Wirth 1997). FRAP and fluorescence correlation spectroscopy provide an average response from many receptors, whereas SPT resolves the mode of motion for an individual receptor. In addition, the spatial resolution of SPT is approximately two orders of magnitude better than that of FRAP (Mirchev and Golan 2001). Diffusion coefficients for proteins in a cell

membrane are 5-100 times slower than the values for proteins in an artificial bilayer as measured by FRAP (Saxton and Jacobson 1997). Similarly, Jacobson et al. reports diffusion coefficients vary around two-fold at different locations on a single cell, and ten-fold from one cell to the next (1984). Sources of diffusion heterogeneity may be obstruction by other proteins, intracellular components or the extracellular matrix or confinement in domains with different compositions than the bulk membrane (Saxton and Jacobson 1997). Feder et al. analyzed FRAP data using two models: Brownian diffusion with an immobile fraction and anomalous diffusion with only mobile receptors, and found that these different modes of motion could not be distinguished by FRAP (1996). SPT provides information on sub-populations of receptors that would otherwise be indistinguishable by ensemble measurements. SPT shows heterogeneity exists in the dynamics of membrane receptors and the same proteins can exhibit both Brownian and anomalous motion (Anderson et al. 1992; Feder et al. 1996; Kusumi et al. 1993; Saxton and Jacobson 1997). Different optical techniques often use different probes to measure the lateral mobility of receptors due to their technical requirements. These probes may alter the property under study. Therefore, it is imperative to compare the results obtained from different techniques.

The effects of conformational state, clustering, cytoskeleton interactions, and cell differentiation on integrin diffusion have been studied (Bakker et al. 2012; Kucik et al. 2001; Chen et al. 2007). Bakker et al. used single dye tracking to demonstrate an intricate coupling between conformation and lateral diffusion of lymphocyte function-associated antigen 1 (LFA-1, an integrin) (2012). After the reduction of extracellular Ca^{2+} to promote high-affinity LFA-1, they observed an eight-fold increase in the percentage of immobile nanoclusters. Single particle tracking with 500-nm latex beads coated with an antibody,

which is not a ligand substitute, has been used to measure the diffusion of αIIbβ3 integrins (Kucik et al. 2001). An α cytoplasmic domain mutation that increased the ligand binding affinity decreased the average diffusion coefficient and integrin mobile fraction. The large size of the probe relative to the integrin may have affected the lateral diffusion measurements through added mass or receptor cross-linking. Recently, bioconjugated QDs have been used to image the lateral diffusion of integrins at the single particle level (Chen et al. 2007). Using QDs conjugated with integrin antibodies, slow lateral diffusion (~10^{-11} cm^2/s) of $\alpha_4\beta_1$ integrins on the surface of undifferentiated bone marrow derived progenitor cells (BMPCs) was measured. The diffusion coefficient increased (~10^{-10} cm^2/s) after a 3-day incubation in differentiation medium. The authors hypothesize that the altered integrin dynamics results from restriction by direct links to microfilaments.

Herein, SPT and FRAP were used to measure the changes in integrins' lateral diffusion upon altered ligand affinity using a well-studied protein mutant. The wild-type (αPS2CβPS) and high ligand affinity mutant (αPS2CβPS-V409D) integrins were expressed in S2 cells. The αPS2CβPS-V409D integrin contains a single-point mutation in the extracellular ligand binding domain of the β subunit, and has an ~4-fold higher ligand binding affinity compared to αPS2CβPS (Bunch et al. 2006; Smith et al. 2007). Using a well-characterized integrin mutant with a high ligand affinity overcomes issues associated with altering the composition of the extracellular medium (e.g. reducing the Ca^{2+} composition or increasing the Mn^{2+} composition) to alter ligand affinity, which may cause numerous changes to the composition or structure of the cell membrane, and indirect changes in the lateral mobility of the integrins. 16-nm QDs containing physisorbed RBB-Tiggrin, the recombinant version of the αPS2CβPS-ligand Tiggrin (Bunch et al. 2004; Fogerty et al. 1994;

Graner et al. 1998; Jannuzi et al. 2004), were used for SPT measurements to track the movement of individual integrins. QDs were chosen as the probe due to their small size, broad absorption and narrow emission bands, brightness, and resistance against photobleaching (Gao et al. 2005). The SPT data are compared to ensemble FRAP measurements using integrins tagged with Venus yellow fluorescent protein. The results show that different populations of receptors are studied with the two techniques, and that the lateral mobility of a subset of integrins depends on their ligand affinity.

Materials and Methods

Cell culture and preparation

All experiments were performed using *Drosophila* S2 cells transformed to express αPS2CβPS or αPS2CβPS-V409D integrins under the regulation of the heat shock protein 70 promoter. Transfection methods and culture techniques have been previously described (Bunch and Brower 1992; Bunch et al. 1988; Zavortink et al. 1993). Briefly, cells were cultured in Shields and Sang M3 insect medium (Sigma-Aldrich, St. Louis, MO) with heat-inactivated 10% fetal bovine serum (Irvine Scientific, Santa Ana, CA), 12.5 mM streptomycin, 36.5 mM penicillin, and 0.2 µM methotrexate (Fisher Scientific, Pittsburgh, PA) in a 22^{o}C incubator. Integrin expression was induced with a 36^{o}C heat shock followed by 3 h incubation at 22^{o}C. Cells were then centrifuged at 600 × *g* for 3 min and resuspended in serum-free medium to a final concentration of 5×10^{5} cells/mL. Preparation of RBB-Tiggrin-coated glass microscope slides have been previously described (Smith et al. 2007). Cells were allowed to spread on the ligand-coated glass slides for half an hour at room temperature in serum-free medium prior to incubation with ligand-coated QDs.

Preparation of ligand-coated QDs and incubation with cells

16-nm QDs functionalized with amine-derivatized polyethylene glycol (PEG), and with emission maxima at 605 nm were obtained from Life Technologies (Carlsbad, CA). Since the diameter of the QDs is similar to the integrins' cross section (Takagi et al. 2002; Xiong et al. 2001), it is unlikely that more than one integrin is bound to a single QD (i.e., we are testing the role of affinity in altering integrin diffusion, and not avidity). The QDs were coated with a physisorbed layer of RBB-Tiggrin. The conjugation of positively charged amine-derivatized PEG QDs with net-negatively charged RBB-Tiggrin was performed by mixing a ratio of 1 QD to 20 RBB-Tiggrin in 10 mM phosphate buffer, pH 8.5 for 2 h (Medintz et al. 2003; Delehanty et al. 2006; Xiao et al. 2010; Mattoussi et al. 2000). The ligand-coated QDs (QD-RBB-Tiggrin) were stored in aliquots at 4^{o}C prior to use, sonicated for 2 h before diluting to the required concentration, and were then used within half an hour to limit the aggregation of QDs. After cells were spread on the ligand-coated surface, they were rinsed and incubated with QD-RBB-Tiggrin diluted in BES Tyrodes buffer (200 mM BES, 10 mg/mL BSA, 1 mM $CaCl_2$, 0.1 M $MgCl_2$) at the concentration specified in the text for 30 min. Cells were rinsed and imaged with 20 mM BES Tyrodes buffer.

Instrumentation

A Nikon Eclipse TE2000U microscope (Melville, NY) operating in wide-field, epi-fluorescence mode with a 100× Plan Apo, 1.49 numerical aperture oil-immersion objective was used for all experiments. Fluorescence images were collected every 40 ms for a total of 30 s using a PhotonMAX 512 EMCCD camera (Princeton Instrument, Trenton, NJ) and mercury lamp illumination. A filter set from Omega Optical (XF304-1, Brattleboro, VT) was

used for excitation (425/45 nm) and to collect the QD emission (605/20 nm). FRAP experiments were performed and the data analyzed as previously described (Sander et al. 2012). A constrained diffusion with an immobile fraction model was found to best-fit all data. All imaging measurements were carried out at room temperature.

QD binding specificity

To quantify the specificity of QD-RBB-Tiggrin binding, four S2 cell lines were used: one expressing αPS2CβPS integrins, a second expressing αPS2CβPS-V409D, a third that did not express αPS2CβPS integrins and a fourth that expressed an αPS2CβPS-Venus fusion protein. The number of QDs in the images collected using different QD-RBB-Tiggrin concentrations was quantified with the Image J version 1.45s Particle Tracker plugin developed by I.F. Sbalzarini and P. Koumoutsakos (2005). To verify the results, QDs were manually counted in some images.

Localization and tracking of QDs

The Image J Particle Tracker plugin was used for the localization and tracking of single QD-RBB-Tiggrin complexes (Sbalzarini and Koumoutsakos 2005). A particle radius of 3 and cutoff value of zero were used. A displacement of 4-5 pixel was chosen based on the maximum step (Qian et al. 1991; Kevin et al. 2010). The intensity percentile ranged from 0.1-1.7 depending on the image. A link range parameter of 4-5 was chosen to account for short quantum dot blinking events, which were used to confirm a single QD generated the track (Nirmal et al. 1996; Dahan et al. 2003). Each trajectory was visually inspected to identify trajectories that likely resulted from more than one QD, which was rare. The

positional uncertainty of the localization was 14 nm as measured by imaging and analyzing stationary QDs.

Data analysis

The mean-square displacement (MSD) for different time lags (τ) was calculated for each trajectory using the formula:

$$\mathrm{MSD}(n\tau) = \frac{1}{N-n}\sum_{i=1}^{N-n}[(x((i+n)\tau) - x(i\tau))^2 + (y((i+n)\tau) - y(i\tau))^2] \ , \quad (1)$$

where τ is the acquisition time between two successive frames, N is the total number of frames in the sequence, x and y are coordinates of the particle at a specific time lag, $0 < n < N/4$ and $1 < i < (N-n)$ are positive integers. The SPT trajectories were analyzed with a time-dependent diffusion coefficient as described by Feder et al. (1996). The diffusion coefficient (D) is given by:

$$D = \frac{1}{4}(\Gamma \tau^{\alpha-1}) \ , \quad (2)$$

where Γ is the transport coefficient, τ is the time lag, and α is the time exponent. The value of Γ (intercept) and α (slope) for each trajectory was obtained by fitting the log MSD vs. log τ curve by linear regression with weighting to the standard deviation (Feder et al. 1996; Saxton and Jacobson 1997; Slattery 1995). The trajectories were classified into different modes of motion according to the α value: directed motion ($\alpha > 1.1$), Brownian diffusion ($0.9 \leq \alpha \leq 1.1$), anomalous/constrained diffusion ($0.1 \leq \alpha < 0.9$), and immobile ($\alpha < 0.1$) (Feder et al. 1996; Ghosh and Webb 1994). The time-dependent diffusion coefficient at 1 s was calculated as Γ/4 for all trajectories with $\alpha > 0.1$.

Results and Discussion

Specific binding of QD-RBB-Tiggrin to integrin-expressing cells

The primary purpose of this study was to elucidate how the ligand binding affinity affected the lateral dynamics of integrins using single particle tracking, and to compare the results to those obtained by fluorescence recovery after photobleaching. The first step was to find conditions where the ligand-coated QDs specifically bound to integrin-expressing cells. Non-specific binding would influence the measurement of lateral diffusion, and could increase the fraction of immobile integrins. Specific binding was tested using transformed S2 cells expressing αPS2CβPS or high ligand affinity αPS2CβPS-V409D integrins and non-transformed S2 cells, which do not express detectable levels of αPS2CβPS integrins. A number of peptide or protein ligands containing the RGD-tripeptide αPS2CβPS binding domain were sequentially tested. Only the QDs containing a physisorbed layer of the 53-amino acid RBB-Tiggrin (QD-RBB-Tiggrin) exhibited binding to the integrin-expressing cells (Fig. 1a, b) but no binding to the non-transformed S2 cells (Fig. 1c). Similar fluorescence patterns were observed for the QD-RBB-Tiggrin bound to integrin-expressing cells as observed for cells expressing an integrin-Venus fusion protein (Fig. 1d). Specifically, integrins are often concentrated at the periphery of the cell as demonstrated by the white arrows in Fig. 1d and a high concentration of QDs exhibit a circular pattern in Fig. 1a and to a minor extent in Fig. 1b. The bright region at the center of the cells in Fig. 1d was from intracellular integrins (Sander et al. 2012; Dibya et al. 2009). The lack of a high concentration of QDs in the center compared to other parts of the cell in Fig. 1a, b suggests that the QDs did not bind to intracellular integrins. Using 1 nM QD-RBB-Tiggrin an average of 11 QDs per cell was measured for the cells expressing αPS2CβPS integrins and the

average number decreased to 0.1 for non-transformed S2 cells at 1 nM QD-RBB-Tiggrin (Table 1). Thus, there is 1% non-specific binding at this concentration.

As expected, the high ligand affinity αPS2CβPS-V409D integrins bound more QD-RBB-Tiggrin (Fig. 1b) compared to the αPS2CβPS integrins (Fig. 1a) when measured at the same QD concentration. Comparing different QD-RBB-Tiggrin concentrations, a statistically similar number of QDs was counted using 1 nM QD-RBB-Tiggrin for αPS2CβPS integrin-expressing cells and 0.5 nM QD-RBB-Tiggrin for αPS2CβPS-V409D integrin-expressing cells (Table 1).

SPT classification of αPS2CβPS integrin motion

One hundred QD-RBB-Tiggrin trajectories, representing the motion of 100 αPS2CβPS receptors, were recorded from a total of 25 cells. Three types of integrin-motion were distinguishable based on the shape of the MSD versus time plots (Fig. 2). Brownian diffusion results in a best-fit straight line with a positive slope (Fig. 2a), anomalous/constrained diffusion results in a curve that plateaus to a value representative of the diffusion constraints imparted on the receptor (Fig. 2b), and immobile integrin shows a constant MSD vs. time lag plot (Fig. 2c). A more accurate method to classify the mode of motion is based on the time exponent value, α, calculated from log MSD versus log time lag plots. From the total 100 αPS2CβPS trajectories, 40% were mobile and 60% were immobile (Table 2). Further classifying the mobile trajectories, 8% showed Brownian motion, and 31% showed anomalous/constrained motion with a time dependent diffusion coefficient. Only one trajectory with directed motion was measured. The average time-exponent for all mobile particles ($\alpha > 0.1$) was 0.6 ± 0.3. The diffusion coefficient at 1 s was calculated for all mobile particles and ranged from nearly immobile to the theoretical value for two-dimensional

diffusion in a bilayer (0.004 to 21 $\times 10^{-9}$ cm^2/s). The average diffusion coefficient at 1 s for all mobile particles was $2 \pm 5 \times 10^{-9}$ cm^2/s (Table 2).

All 40 mobile αPS2CβPS trajectories are shown in Fig. 3a. Since the trajectories were measured from 25 different cells, the position of the trajectory on the graph depends on the location of the cell within the region of interest, the size of the cell, and the location of the QD in the cell. The position of the trajectory on the cell was found by overlapping the white light image of the cell with the fluorescence image of the trajectory. All the trajectories exhibiting Brownian diffusion (i.e., with $0.9 \leq \alpha \leq 1.1$) were located at the periphery of the cells. In these cases, the tracks partially outline the edge of the cell. The trajectories exhibiting constrained diffusion were located throughout the center portion of the membrane, but not at the edge of the cell. Constraints to integrin diffusion measured by SPT are the result of either heterogeneous membrane regions (e.g., lipid nanodomains/rafts or clustering) or interactions between integrin cytoplasmic domains and cytoplasmic proteins. Brownian diffusion measured at the edge of the cell may be the result of decreased membrane heterogeneity in this region or altered binding to cytoplasmic proteins at the edge of the cell.

SPT classification of αPS2CβPS-V409D integrin motion

To determine if the integrins' ligand affinity affects the diffusion coefficient and mobile fraction, trajectories were collected from 16 cells expressing high ligand affinity αPS2CβPS-V409D integrins. Out of 100 trajectories, 2% showed Brownian diffusion, 16% showed anomalous/constrained diffusion, and 82% were immobile (Table 2). The average diffusion coefficient at 1 s decreased 4-fold for the high ligand affinity integrins (0.5 ± 0.8 $\times 10^{-9}$ cm^2/s) compared to the wild-type integrins. In addition, the mobile fraction reduced from 40% for αPS2CβPS to 18% for αPS2CβPS-V409D.

The eighteen mobile trajectories observed from 16 different cells expressing αPS2CβPS-V409D integrins are shown in Fig. 3b. A qualitative comparison to the wild-type trajectories shown in Fig. 3a indicates that the αPS2CβPS trajectories that exhibited Brownian diffusion and traced a portion of the periphery of the cell were not measured for the αPS2CβPS-V409D integrin. Also based on the data graphed in Fig. 3, while the number of trajectories with anomalous/constrained diffusion decreased for the αPS2CβPS-V409D integrins, qualitatively there was no significant difference in the shape or position of these trajectories compared to the αPS2CβPS integrins.

One plausible explanation for the decreased diffusion coefficient for αPS2CβPS-V409D versus αPS2CβPS integrins is more clustering of the high ligand affinity integrins. Mutations that increase the integrins' ligand affinity also result in more integrin clustering, as previously reported (Smith et al. 2007; Bunch et al. 2006). There is ~3-fold more energy transfer measured in a clustering assay for αPS2CβPS-V409D compared to αPS2CβPS integrins. The measurement did not enable the mechanism for the increased clustering to be determined. For example, it is possible that the integrin clusters remained the same size, but more αPS2CβPS-V409D clusters formed. Alternatively, the number of clusters could stay the same, while their size increased. Finally for the sake of completeness, some combination of both may have occurred. The Saffman-Delbrück equation can be used to estimate the change in the diffusion coefficient for the extreme case of a single, unclustered integrin with a 5 nm radius added to a cluster containing 20 integrins (1975). Clusters larger than this could be observed in the optical image, but were not. In this case, the diffusion coefficient is estimated to decrease by 75% for the clustered integrin. The measured diffusion coefficient decreased by 75% for the αPS2CβPS-V409D integrin compared to the αPS2CβPS integrin. Given the

extreme case considered for the calculation, it is likely that integrin clustering was one reason for the decrease in the diffusion coefficient of the high ligand affinity integrin, but it may not be the only one.

Other possible reasons for the decrease in the diffusion coefficient and mobile fraction observed for the high ligand affinity αPS2CβPS-V409D integrins are altered interactions with other membrane proteins or cytoskeletal proteins. If these interactions are with mobile species or are transient on the SPT time scale, the diffusion constraints would increase. On the other hand if the interactions are with immobile membrane or cytoplasmic proteins and are of a long duration on the SPT time scale, the integrin mobile fraction would decrease. Leitinger and Hogg found that a mutant LFA-1 missing the I domain, with characteristics that mimic high affinity integrins, preferentially localizes into lipid nanodomains in T lymphocytes (2002). The wild-type LFA-1 with a low ligand affinity does not preferentially localize into lipid rafts until after it was exposed to Mn^{2+} or phorbal esters, which have been shown to increase ligand affinity for a number of integrins. A differential role of cholesterol in the clustering of αPS2CβPS-V409D and αPS2CβPS integrins has been previously reported, and this suggests that cholesterol-enriched nanodomains are functionally important to these integrins (Dibya et al. 2010). If αPS2CβPS-V409D integrins with higher ligand binding affinity than αPS2CβPS exhibit altered partitioning into lipid nanodomains, this could have a role in altering the integrins' diffusion coefficient or mobile fraction depending on the size of the domains and the temporal characteristics of the partitioning.

Comparison of average SPT and FRAP diffusion parameters

FRAP measurements were collected using fluorescent-protein tagged integrins to compare the ensemble diffusion parameters to those obtained by SPT (Table 2 and 3). For

αPS2CβPS integrins, both the diffusion coefficient and the time exponent, α, for the mobile fraction were the same within the statistical uncertainty of the SPT and FRAP measurements. The αPS2CβPS mobile fraction and the αPS2CβPS-V409D diffusion coefficient, mobile fraction, and α are larger when measured by FRAP compared to SPT. The differences between the FRAP and SPT measurements can be interpreted based on the population of integrins being measured and the nature of the fluorescent probe as schematically shown in Fig. 4. The FRAP experiment measures all integrin, whether they interact with ligand or not. The SPT measurement necessitates that the integrin under study be bound to ligand immobilized on the QD. Additionally, the population of integrins with Brownian diffusion at the periphery of the cell cannot be measured by FRAP, and the integrins measured by FRAP are in closer contact to the glass substrate than those measured by SPT (Fig 4). To these latter two points, more constrained diffusion may be expected for the FRAP measurement, but this would cause a decrease in α or the diffusion coefficient as measured by FRAP and this is not consistent with the experimental values (Table 2 and 3). Considering only the FRAP data (Table 3), there is no difference in the ensemble diffusion coefficient for αPS2CβPS and αPS2CβPS-V409D integrins. On the other hand, SPT reveals that a subset of ligand-bound, high ligand affinity integrins have a 75% slower diffusion coefficient than the subset of ligand-bound wild-type integrins.

Numerous studies report a slower diffusion coefficient measured by SPT than FRAP (Georgiou et al. 2002; Lee et al. 1991; Saxton and Jacobson 1997). This variability between FRAP and SPT has been attributed to the nature of the fluorescent probe: the mass and size of the QD (~2 MDa) is larger than the fluorescent protein (~27 kDa), while the fluorescent protein is covalently attached to the integrin—this modification has no affect on the

integrins' ligand affinity (data not shown). However, the differences in the diffusion coefficient measured by FRAP and SPT for the αPS2CβPS-V409D integrin is not likely from the probe since the same probe was used to study both αPS2CβPS and αPS2CβPS-V409D integrins, but no difference was measured for the αPS2CβPS integrins' diffusion coefficient. Other factors such as cross-linking of receptors by QDs must also be considered as a possible source for the differences in the diffusion parameters measured by the two techniques. However, the similar diameter of the QD (16 nm) and integrin (~10 nm) as well as steric constraints limit the possibility of receptor cross-linking.

For both αPS2CβPS and αPS2CβPS-V409D integrins there are smaller mobile fractions measured by SPT than measured by FRAP (Table 2 and 3). This may represent a decrease in the mobile fraction for the subset of ligand-bound integrins compared to the average of all integrins in the membrane. An alternative explanation is that these changes are the result of the probes used in these experiments since a decrease was measured for both integrins. Previous comparisons of SPT and FRAP measured smaller mobile fractions by SPT (Saxton and Jacobson 1997; Slattery 1995). For example, Kusumi et al. reports a 30% E-cadherin mobile fraction by SPT and 64% by FRAP (1993). This is similar to the difference reported herein. Non-specific binding of QD-RBB-Tiggrin to the cell could in theory artificially increase the immobile fraction measured by SPT. As discussed above, non-specific binding was limited to 1% and this is significantly lower than the difference in the mobile fraction measured by the two techniques.

In summary, the differences reported in the diffusion coefficient for the ligand-bound fraction of αPS2CβPS and αPS2CβPS-V409D integrins is the results of differences in the diffusion characteristics of these integrins, and not the result of experimental artifacts.

Whereas the origin for the 31 to 51% decrease in the mobile fraction of the ligand-bound fraction measured by SPT compared to the FRAP remains uncertain; comparing only the SPT values by themselves shows that the ligand-bound fraction of αPS2CβPS-V409D integrins is less mobile than the wild-type integrins.

Conclusions

Two primary conclusions have been presented: One the 'bulk' integrins, representing the majority, measured by FRAP do not have altered diffusion properties when the high ligand affinity receptor is compared to the wild-type receptor. Second as measured by SPT, a subset of ligand-bound, high ligand affinity integrins exhibits slower diffusion than the ligand-bound, wild-type integrins. Information about this population of integrins is lost in the ensemble FRAP measurement. Additionally, SPT reveals αPS2CβPS and αPS2CβPS-V409D integrins exhibit both Brownian and anomalous/constrained motion, but the fraction of trajectories exhibiting these motions is smaller for the high ligand affinity integrins. αPS2CβPS integrins also have a small population with directed motion that is absent for the higher ligand affinity integrins. The αPS2CβPS-V409D integrins are said to exhibit properties that mimic signaling from outside of the cell. Integrins with other functionally distinct mutations may behave uniquely and represent the lateral motion for other signaling states. This study is the first step to addressing how ligand affinity affects the lateral dynamics of these receptors.

Acknowledgements

This work is supported by the National Science Foundation under Grant CHE-0845236. The authors thank Dr. Javier Vela and Ms. Yijun Guo for providing QDs for initial experiments and Mr. Aleem Syed for helpful discussions.

References

Anderson CM, Georgiou GN, Morrison IE, Stevenson GV, Cherry RJ (1992) Tracking of cell surface receptors by fluorescence digital imaging microscopy using a charge-coupled device camera. Low-density lipoprotein and influenza virus receptor mobility at 4 degrees C. J Cell Sci 101 (Pt 2):415-425

Bakker GJ, Eich C, Torreno-Pina JA, Diez-Ahedo R, Perez-Samper G, van Zanten TS, Figdor CG, Cambi A, Garcia-Parajo MF (2012) Lateral mobility of individual integrin nanoclusters orchestrates the onset for leukocyte adhesion. Proc Natl Acad Sci U S A 109 (13):4869-4874

Bunch TA, Brower DL (1992) Drosophila PS2 integrin mediates RGD-dependent cell-matrix interactions. Development 116 (1):239-247

Bunch TA, Grinblat Y, Goldstein LS (1988) Characterization and use of the Drosophila metallothionein promoter in cultured Drosophila melanogaster cells. Nucleic Acids Res 16 (3):1043-1061

Bunch TA, Helsten TL, Kendall TL, Shirahatti N, Mahadevan D, Shattil SJ, Brower DL (2006) Amino acid changes in Drosophila alphaPS2betaPS integrins that affect ligand affinity. J Biol Chem 281 (8):5050-5057

Bunch TA, Miller SW, Brower DL (2004) Analysis of the Drosophila betaPS subunit indicates that regulation of integrin activity is a primal function of the C8-C9 loop. Exp Cell Res 294 (1):118-129

Chen H, Titushkin I, Stroscio M, Cho M (2007) Altered membrane dynamics of quantum dot-conjugated integrins during osteogenic differentiation of human bone marrow derived progenitor cells. Biophys J 92 (4):1399-1408

Chen Y, Lagerholm BC, Yang B, Jacobson K (2006) Methods to measure the lateral diffusion of membrane lipids and proteins. Methods 39 (2):147-153

Dahan M, Levi S, Luccardini C, Rostaing P, Riveau B, Triller A (2003) Diffusion dynamics of glycine receptors revealed by single-quantum dot tracking. Science 302 (5644):442-445

Delehanty JB, Medintz IL, Pons T, Brunel FM, Dawson PE, Mattoussi H (2006) Self-assembled quantum dot-peptide bioconjugates for selective intracellular delivery. Bioconjug Chem 17 (4):920-927

Dibya D, Arora N, Smith EA (2010) Noninvasive measurements of integrin microclustering under altered membrane cholesterol levels. Biophys J 99 (3):853-861

Dibya D, Sander S, Smith EA (2009) Identifying cytoplasmic proteins that affect receptor clustering using fluorescence resonance energy transfer and RNA interference. Anal Bioanal Chem 395 (7):2303-2311

Feder TJ, Brust-Mascher I, Slattery JP, Baird B, Webb WW (1996) Constrained diffusion or immobile fraction on cell surfaces: a new interpretation. Biophys J 70 (6):2767-2773

Fogerty FJ, Fessler LI, Bunch TA, Yaron Y, Parker CG, Nelson RE, Brower DL, Gullberg D, Fessler JH (1994) Tiggrin, a novel Drosophila extracellular matrix protein that functions as a ligand for Drosophila alpha PS2 beta PS integrins. Development 120 (7):1747-1758

Gao X, Yang L, Petros JA, Marshall FF, Simons JW, Nie S (2005) In vivo molecular and cellular imaging with quantum dots. Curr Opin Biotechnol 16 (1):63-72

Georgiou G, Bahra SS, Mackie AR, Wolfe CA, O'Shea P, Ladha S, Fernandez N, Cherry RJ (2002) Measurement of the lateral diffusion of human MHC class I molecules on HeLa cells by fluorescence recovery after photobleaching using a phycoerythrin probe. Biophys J 82 (4):1828-1834

Ghosh RN, Webb WW (1994) Automated detection and tracking of individual and clustered cell surface low density lipoprotein receptor molecules. Biophys J 66 (5):1301-1318.

Giancotti FG, Ruoslahti E (1999) Integrin signaling. Science 285 (5430):1028-1032

Graner MW, Bunch TA, Baumgartner S, Kerschen A, Brower DL (1998) Splice variants of the Drosophila PS2 integrins differentially interact with RGD-containing fragments of the extracellular proteins tiggrin, ten-m, and D-laminin 2. J Biol Chem 273 (29):18235-18241

Hillis GS, MacLeod AM (1996) Integrins and disease. Clin Sci (Lond) 91 (6):639-650

Huveneers S, Truong H, Danen HJ (2007) Integrins: signaling, disease, and therapy. Int J Radiat Biol 83 (11-12):743-751

Hynes RO (2002) Integrins: bidirectional, allosteric signaling machines. Cell 110 (6):673-687

Jacobson K, Ishihara A, Inman R (1987) Lateral diffusion of proteins in membranes. Annu Rev Physiol 49:163-175

Jacobson K, O'Dell D, August JT (1984) Lateral diffusion of an 80,000-dalton glycoprotein in the plasma membrane of murine fibroblasts: relationships to cell structure and function. J Cell Biol 99 (5):1624-1633

Jannuzi AL, Bunch TA, West RF, Brower DL (2004) Identification of integrin beta subunit mutations that alter heterodimer function in situ. Mol Biol Cell 15 (8):3829-3840

Kevin B, Dries V, Jo D, Stefaan De S (2010) Single Particle Tracking. In: Nanoscopy and Multidimensional Optical Fluorescence Microscopy. Chapman and Hall/CRC, pp 5-1-5-17

Kovaleski JM, Wirth MJ (1997) Peer Reviewed: Applications of Fluorescence Recovery after Photobleaching. Analytical Chemistry 69 (19):600A-605A

Kucik DF, O'Toole TE, Zheleznyak A, Busettini DK, Brown EJ (2001) Activation-enhanced alpha(IIb)beta(3)-integrin-cytoskeleton interactions outside of focal contacts require the alpha-subunit. Mol Biol Cell 12 (5):1509-1518

Kusumi A, Sako Y, Yamamoto M (1993) Confined lateral diffusion of membrane receptors as studied by single particle tracking (nanovid microscopy). Effects of calcium-induced differentiation in cultured epithelial cells. Biophys J 65 (5):2021-2040

Lee GM, Ishihara A, Jacobson KA (1991) Direct observation of brownian motion of lipids in a membrane. Proc Natl Acad Sci U S A 88 (14):6274-6278

Leitinger B, Hogg N (2002) The involvement of lipid rafts in the regulation of integrin function. J Cell Sci 115 (Pt 5):963-972

Luo BH, Carman CV, Springer TA (2007) Structural basis of integrin regulation and signaling. Annu Rev Immunol 25:619-647

Mattoussi H, Mauro JM, Goldman ER, Anderson GP, Sundar VC, Mikulec FV, Bawendi MG (2000) Self-Assembly of CdSe−ZnS Quantum Dot Bioconjugates Using an Engineered Recombinant Protein. Journal of the American Chemical Society 122 (49):12142-12150

Medintz IL, Clapp AR, Mattoussi H, Goldman ER, Fisher B, Mauro JM (2003) Self-assembled nanoscale biosensors based on quantum dot FRET donors. Nat Mater 2 (9):630-638

Mirchev R, Golan DE (2001) Single-particle tracking and laser optical tweezers studies of the dynamics of individual protein molecules in membranes of intact human and mouse red cells. Blood Cells Mol Dis 27 (1):143-147

Nirmal M, Dabbousi BO, Bawendi MG, Macklin JJ, Trautman JK, Harris TD, Brus LE (1996) Fluorescence intermittency in single cadmium selenide nanocrystals. Nature (London) 383 (Copyright (C) 2012 American Chemical Society (ACS). All Rights Reserved.):802-804

Qian H, Sheetz MP, Elson EL (1991) Single particle tracking. Analysis of diffusion and flow in two-dimensional systems. Biophys J 60 (4):910-921

Reddy KV, Mangale SS (2003) Integrin receptors: the dynamic modulators of endometrial function. Tissue Cell 35 (4):260-273

Saffman PG, Delbruck M (1975) Brownian motion in biological membranes. Proc Natl Acad Sci U S A 72 (8):3111-3113

Sander S, Arora N, Smith EA (2012) Elucidating the role of select cytoplasmic proteins in altering diffusion of integrin receptors. Anal Bioanal Chem 403 (8):2327-2337

Saxton MJ, Jacobson K (1997) Single-particle tracking: applications to membrane dynamics. Annu Rev Biophys Biomol Struct 26:373-399

Sbalzarini IF, Koumoutsakos P (2005) Feature point tracking and trajectory analysis for video imaging in cell biology. J Struct Biol 151 (2):182-195

Slattery JP (1995) Lateral Mobility of Fc[epsilon]RI on Rat Basophilic Leukemia Cells as Measured by Single Particle Tracking Using a Novel Bright Fluorescent Probe. Cornell University, May

Smith EA, Bunch TA, Brower DL (2007) General in vivo assay for the study of integrin cell membrane receptor microclustering. Anal Chem 79 (8):3142-3147

Stewart M, Hogg N (1996) Regulation of leukocyte integrin function: affinity vs. avidity. J Cell Biochem 61 (4):554-561

Takada Y, Ye X, Simon S (2007) The integrins. Genome Biol 8 (5):215

Takagi J, Petre BM, Walz T, Springer TA (2002) Global conformational rearrangements in integrin extracellular domains in outside-in and inside-out signaling. Cell 110 (5):599-511

van Kooyk Y, Figdor CG (2000) Avidity regulation of integrins: the driving force in leukocyte adhesion. Curr Opin Cell Biol 12 (5):542-547

Xiao Y, Forry SP, Gao X, Holbrook RD, Telford WG, Tona A (2010) Dynamics and mechanisms of quantum dot nanoparticle cellular uptake. J Nanobiotechnology 8:13

Xiong JP, Stehle T, Diefenbach B, Zhang R, Dunker R, Scott DL, Joachimiak A, Goodman SL, Arnaout MA (2001) Crystal structure of the extracellular segment of integrin alpha Vbeta3. Science 294 (5541):339-345

Zavortink M, Bunch TA, Brower DL (1993) Functional properties of alternatively spliced forms of the Drosophila PS2 integrin alpha subunit. Cell Adhes Commun 1 (3):251-264

Table 1 Average number ± standard deviation of QD-RBB-Tiggrin per cell analyzed from the indicated number of cells across three replicate experiments

S2 cells expressing:	**Average number QD per cell (QD-RBB-Tiggrin)**	**Concentration of QD-RBB-Tiggrin (nM)**	**Number of cells analyzed**
αPS2CβPS integrins	11 ± 6	1	20
αPS2CβPS-V409D integrins	15 ± 10	0.5	16
no αPS2CβPS integrins	0.1 ± 0.3	1	37

Table 2 Integrin diffusion parameters obtained from SPT experiments for wild-type integrins (αPS2CβPS) or high ligand affinity integrins (αPS2CβPS-V409D)

	αPS2CβPS			**αPS2CβPS-V409D**		
	Diffusion Coefficient at 1 second $\times 10^{-9}$ cm^2/s	α value	Fraction	Diffusion Coefficient at 1 second $\times 10^{-9}$ cm^2/s	α value	Fraction
Immobile	n/a	n/a	0.60	n/a	n/a	0.82
Directed	20	1.2	0.01	n/a	n/a	n/a
Brownian	6 ± 5	1.00 ± 0.03	0.08	1.3 ± 0.7	0.925 ± 0.007	0.02
Constrained /Anomalous	1 ± 1	0.5 ± 0.2	0.31	0.4 ± 0.8	0.4 ± 0.3	0.16
All Mobile	2 ± 5 (*25 cells*)	0.6 ± 0.3	0.40	0.5 ± 0.8 (*16 cells*)	0.5 ± 0.3	0.18

Table 3 Integrin diffusion parameters obtained from FRAP experiments for wild-type integrins tagged with Venus fluorescent protein (αPS2CβPS-Venus) or high ligand affinity integrins tagged with Venus (αPS2CβPS-V409D-Venus)

αPS2CβPS-Venus			**αPS2CβPS-V409D-Venus**		
Diffusion Coefficient at 1 second $\times 10^{-9}$ cm^2/s	α value	Mobile Fraction	Diffusion Coefficient at 1 second $\times 10^{-9}$ cm^2/s	α value	Mobile Fraction
3.4 ± 0.2 (*15 cells*)	0.56 ± 0.03	0.71 ± 0.02	3.3 ± 0.1 (*16 cells*)	0.69 ± 0.02	0.67 ± 0.01

Fig. 1 Fluorescence images of 5 nM QD-RBB-Tiggrin binding to S2 cells (a) expressing αPS2CβPS integrins, (b) expressing αPS2CβPS-V409D integrins, (c) that do not express αPS2CβPS integrins, and (d) expressing αPS2CβPS tagged with Venus yellow fluorescent protein. In (c) the white regions of interest highlight the location of cells. In (d) the *white arrows* highlight a high concentration of integrin at the periphery of the cell. Images (a), (b) and (c) were adjusted to same intensity range. The ten micron scale bar is the same for all images.

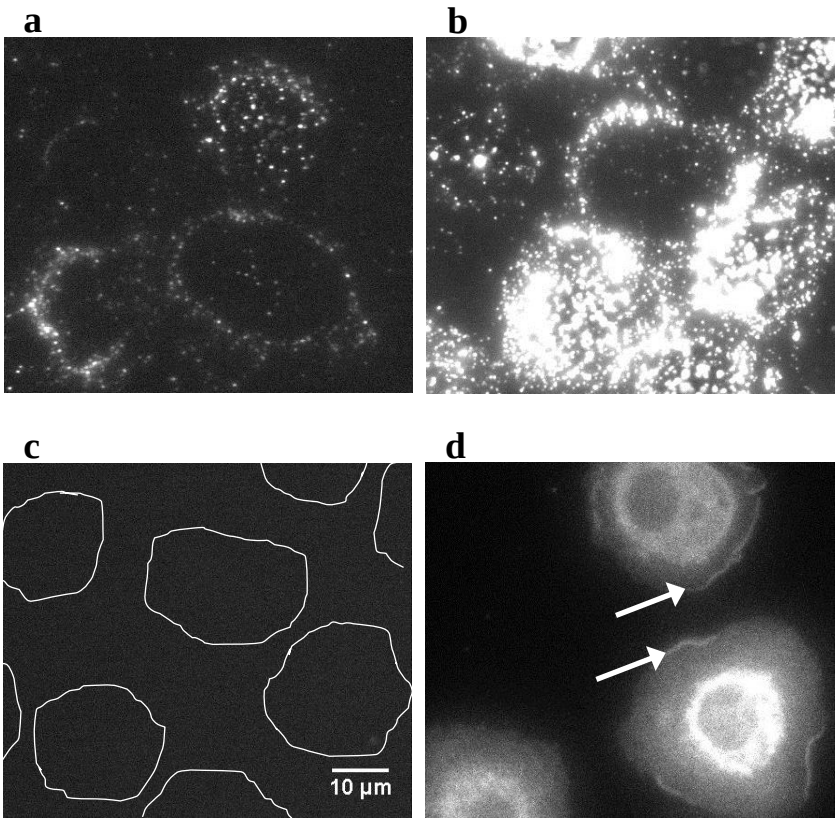

Fig. 2 Representative mean square displacement (MSD) versus time plots for QD-RBB-Tiggrin bound to S2 cells expressing αPS2CβPS integrins: (a) Brownian trajectory; (b) anomalous/constrained trajectory; (c) immobile trajectory. The inset graphs show the trajectory for each type of motion with X- and Y-coordinates plotted in microns.

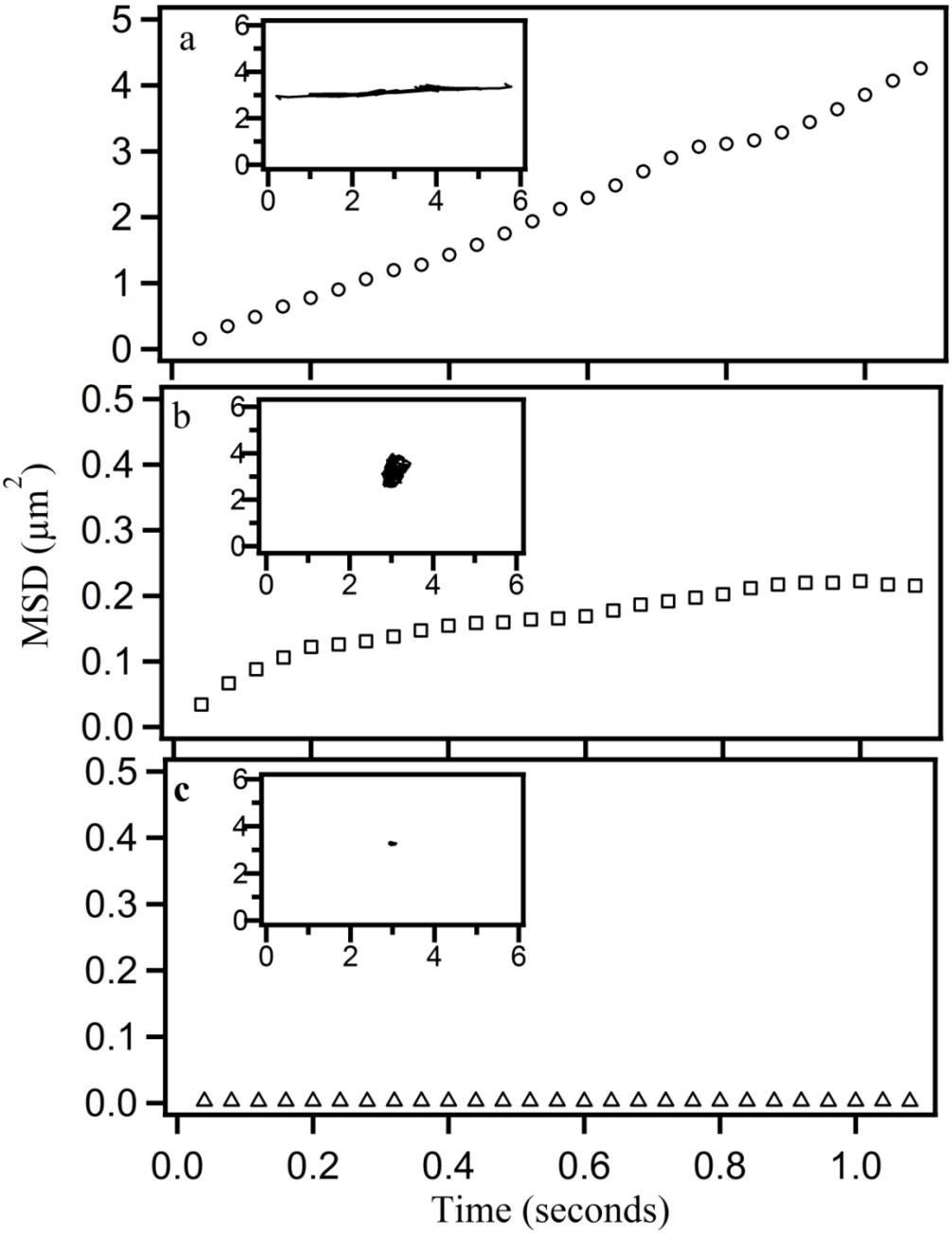

Fig. 3 All mobile trajectories (Brownian and anomalous/constrained) for: (a) αPS2CβPS or (b) αPS2CβPS-V409D integrins. The first number listed for each trajectory is the diffusion coefficient ($\times 10^{-9}$cm^2/s) and the second number is the time exponent, α, obtained by fitting the log MSD vs. log τ curve for each trajectory. Some of the trajectories are overlapped, in most cases the overlapped trajectories were obtained from the same cell, and it is possible they represent the same integrin at different time point. The inset shows a histogram of all diffusion coefficients for each cell line.

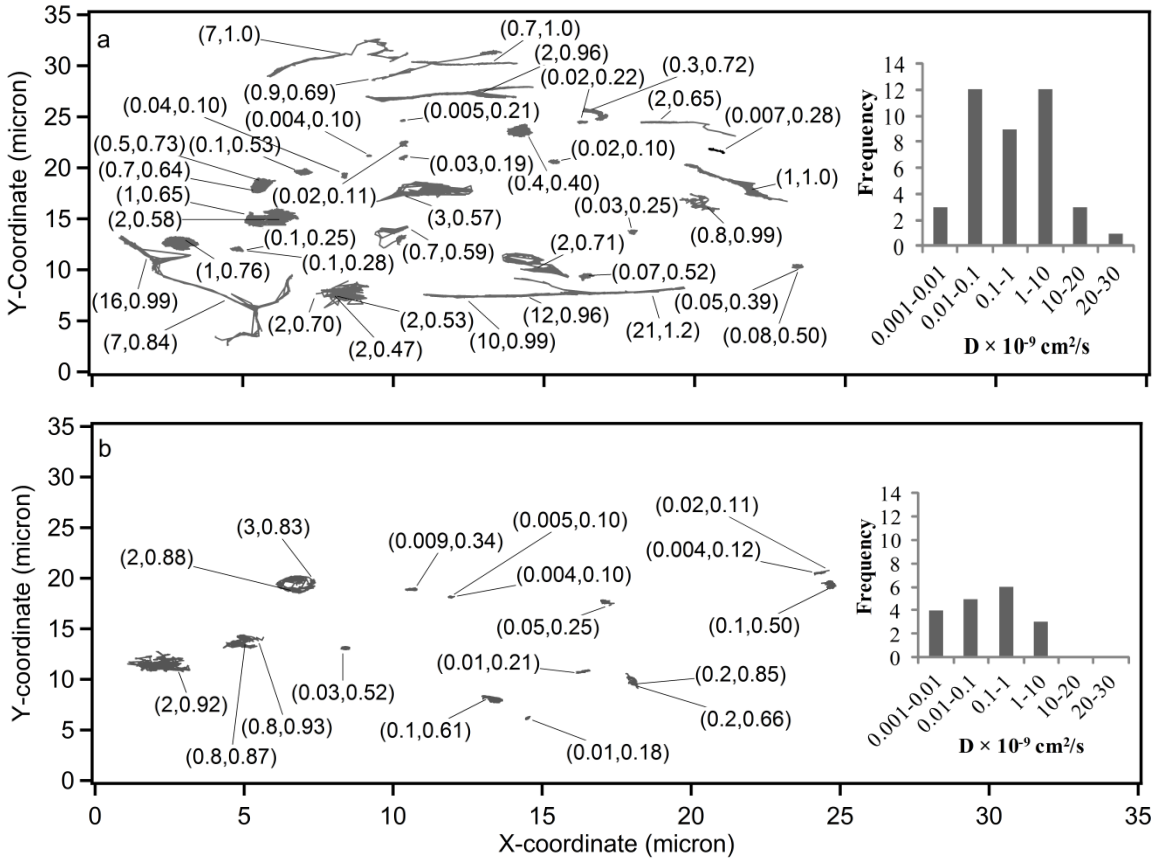

Fig. 4 Schematic of the FRAP and SPT measurements. Cells are spread on a ligand/BSA coated glass slide for both experiments. (a) FRAP measures the ensemble diffusion of all ligand bound and unbound integrins as shown by the *rectangular region*. (b) SPT measures the diffusion of only integrin that is bound to ligand-coated quantum dots as shown by the *rectangular region*. The figure is not drawn to scale.

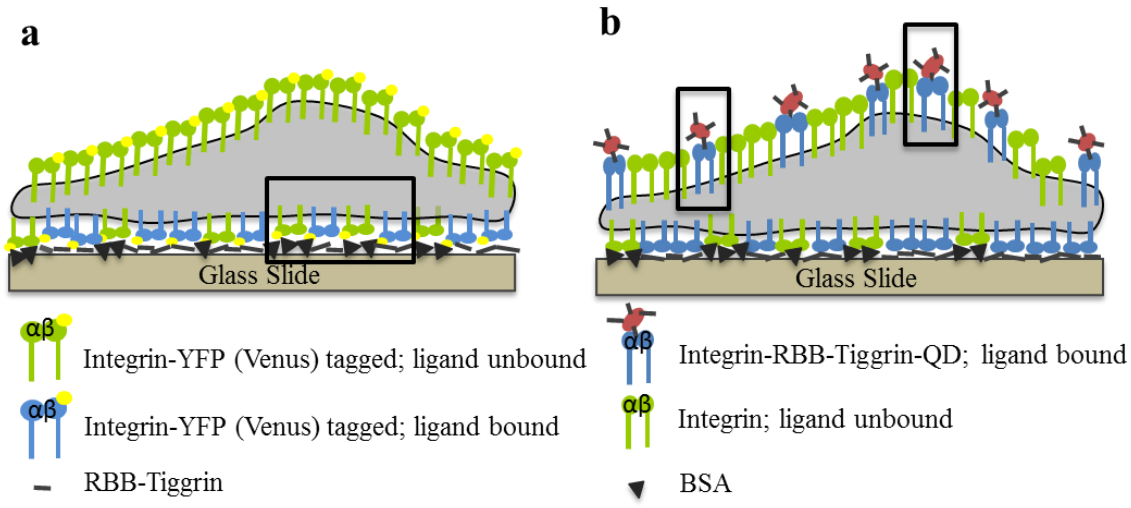

CHAPTER 3: SELECT CYTOPLASMIC AND MEMBRANE PROTEINS INCREASE THE PERCENTAGE OF IMMOBILE INTEGRINS BUT DO NOT AFFECT THE AVERAGE DIFFUSION COEFFICIENT OF MOBILE INTEGRINS

A paper published in *Analytical and Bioanalytical Chemistry*, 2013. 405, (26), 8561-8568

Dipak Mainali and Emily A. Smith

Department of Chemistry, Iowa State University, 1605 Gilman Hall, Ames, Iowa 50011

Keywords Single particle tracking, RNAi, αPS2CβPS integrins, S2 cells, Tiggrin-functionalized quantum dot

Abstract

Integrins are ubiquitous adhesion receptors that are important for signaling and integrating the extracellular matrix and cytoskeleton. The role of cytoplasmic proteins vinculin, focal adhesion kinase (FAK), integrin linked kinase (ILK), and membrane proteins epidermal growth factor receptor (EGFR) and Notch in altering αPS2CβPS integrin lateral diffusion was measured using single particle tracking (SPT) and RNA interference (RNAi). SPT measures heterogeneous diffusion properties and RNAi selectively reduces the concentration of a target protein. After systematically reducing the concentration of vinculin, FAK, ILK, EGFR, or Notch there was a 31 to 80% increase in the mobile integrin fraction, indicating that these five targeted proteins (or assemblies that contain these proteins) are

responsible for immobilizing a fraction of the integrins when all proteins are present at native concentrations. The average diffusion coefficient of all mobile integrins did not change after any of the RNAi treatments, and the percentage of Brownian, directed or anomalous/constrained trajectories relative to total mobile trajectories did not change after vinculin or EGFR RNAi. However, the fraction of anomalous/constrained trajectories relative to the total mobile trajectories increased 9 to 19% after FAK, ILK and Notch RNAi, when the concentration of these proteins was reduced. In the case of FAK, ILK and Notch, native concentrations of these proteins simultaneously increase the immobile fraction of integrins but decrease the diffusion constraints to those integrins that remain mobile. Comparisons of single receptor and ensemble measurements of diffusion, and what is known about the affect of these proteins in altering integrin clustering are discussed.

Introduction

Integrins comprise a family of type 1, transmembrane receptors that integrate the extracellular matrix with the intracellular cytoskeleton. This family of receptors is composed of non-homologous, non-covalently associated α- and β- subunits, with overall highly conserved heterodimer structure throughout the animal kingdom [1,2]. Primary integrin functions include cell- extracellular matrix adhesion, cell-cell adhesion, cell migration, growth, signaling, differentiation, and regulation of gene expression [3-5]. Integrins are important pharmacological targets because diverse human pathologies including cancer, inflammation, fibrosis, and thrombotic diseases are associated with integrin adhesion [6,7]. A significant body of research focuses on the structural, biochemical, and biophysical aspects of integrin function [8,9]. However, little is known about the role of specific cytoplasmic and

membrane proteins in altering integrins' lateral diffusion, which is a highly heterogeneous property.

The cytoplasmic domain of both α- and β-integrin subunits directly or indirectly associate with many cytoplasmic proteins. Integrins are a component of focal adhesions, which are signaling and adhesion platforms that incorporate numerous cytoplasmic proteins [10]. Vinculin and focal adhesion kinase (FAK) are required for focal adhesion formation and turnover [10]. Vinculin interacts with integrins via contacts with other cytoplasmic proteins and has a role in regulating integrins' residency time in focal adhesions and clustering [11-14]. FAK and integrin linked kinase (ILK) directly interact with integrins' β cytoplasmic tail [15,16]. Due to the complexity of the cytoskeleton, and in particular the proteins that interact with integrins, it is desirable to unravel specific effects of each protein in altering integrin lateral diffusion.

Similarly, a diverse group of membrane proteins form supramolecular complexes that contain integrins [17]. Co-immunoprecipitation assays have provided direct evidence of integrins' physical association with receptor tyrosine kinases [18-20]. For example, α5β1, α2β1, α6β1, and α6β4 integrins are known to associate with EGFR [21-25]. β1 integrins also interact with another cell surface receptor termed Notch [26]. The coupling and signaling pathways between β1 integrins, Notch, and EGFR are coordinated by lipid nanodomains termed caveolae [26]. Since integrins are known to associate and cooperate with EGFR and Notch in regulating cellular functions, it is necessary to address how these membrane receptors play a role in altering integrins' lateral diffusion.

Fluorescence recovery after photobleaching (FRAP), fluorescence correlation spectroscopy (FCS), and single particle tracking (SPT) are the main microscopy techniques

utilized to measure the lateral diffusion of membrane components [27,28]. We have used FRAP to elucidate the role of select cytoplasmic and membrane proteins in altering the ensemble diffusion properties of integrins [29,30]. Since FRAP is an ensemble technique that provides an average response from numerous receptors, the heterogeneity in integrin diffusion is not quantified. In contrast, SPT measures the mobility of an individual receptor, and enables the classification of each mobile receptor as exhibiting directed, Brownian, or anomalous/constrained motion. In addition, the dilute nature of the particles used in SPT provides an approximately two orders of magnitude better spatial resolution than that of FRAP, which enables the quantification of lateral mobility within domains smaller than the diffraction limit of light [31]. Several studies propose the existence of lipid nanodomains (e.g., caveolae, clathrin-coated pits) and cytoskeletal corrals that constrain receptor diffusion in the membrane [32-35]. SPT's superior spatial resolution can detect changes in integrins' mobility within these nanodomains.

Herein, the changes in integrins' lateral diffusion after systematically reducing the expression of the cytoplasmic proteins (vinculin, FAK, or ILK) and the membrane proteins (EGFR or Notch) are reported. The targeted proteins in this study were chosen based on their known interaction with integrins, their effect on integrins' lateral diffusion as measured with FRAP or due to a known effect on integrin clustering [30,29,36]. RNA interference (RNAi) was used to decrease the expression of the targeted cytoplasmic or membrane protein followed by characterization of integrin diffusion using SPT. Real-time polymerase chain reaction (RT-PCR) was used to quantify reductions in the target protein's mRNA concentration after RNAi treatment. The results help to unravel the role of other cellular components in altering heterogeneous populations of laterally diffusing integrins.

Materials and Methods

Cell culture and preparation. *Drosophila* S2 cells transformed to express αPS2CβPS integrins under the regulation of the heat shock protein 70 promoter were used to perform all experiments unless otherwise noted. The details of transfection methods and culture techniques have been previously described [37-39]. Untransformed S2 cells were maintained as previously described [40,30,29].

dsRNA synthesis and RNA interference. Double stranded RNA (dsRNA) synthesis and RNAi treatments have been previously described [41,36,30,29]. Cells were incubated with 10 µg dsRNA for 4 days at 22 ^{o}C to reduce the expression of targeted proteins before performing RT-PCR or SPT experiments. For SPT experiments, αPS2CβPS integrin expression in cells were induced on the fourth day of dsRNA incubation with a 36 ^{o}C heat shock followed by a 3 h incubation at 22 ^{o}C. Cells were then centrifuged at 600×g for 3 min and the cell pellet was resuspended to a final concentration of 4×10^{5} cells/mL in serum free medium. Cells were placed on RBB-Tiggrin-coated microscope slides and allowed to spread for 45 min before starting SPT experiments [42]. RBB-Tiggrin is a fragment of the protein Tiggrin, which is the natural ligand to αPS2CβPS integrins.

Real-Time Polymerase Chain Reaction (RT-PCR). Extraction of mRNA from the RNAi treated and no RNAi treated cell lysates was performed using the Dynabeads mRNA Direct kit (Invitrogen 610.12). After the quantification of mRNA using the absorbance value at 260 nm, a High Capacity RNA-to-cDNA kit (Applied Biosystems # 4387406) was used for the reverse transcription of mRNA to cDNA. Applied Biosystems TaqMan Gene Expression Assays and master mix were combined with 50 ng of cDNA and the RT-PCR

experiment was performed on a Roche LightCycler 480 (Roche Applied Science). The gene expression assays were EGFR: Dm01841622_g1; Notch: Dm01841974_g1; Vinculin: Dm01841855_g1; FAK: Dm01816810_m1; ILK: Dm01843539_g1; Myospheroid: Dm01843062_g1; PMCA: Dm01820605_g1; and gamma tubulin Dm01841764. Genomic S2 DNA isolated with Qiagen Kit # 69504 was used to construct the calibration curve and to calculate the reaction efficiency. The statistical significance and the relative expression level were quantified using the software REST 2009 (Qiagen, Hilden, Germany).

Quantum Dot (QD) preparation and incubation with cells. The preparation of RBB-Tiggrin-coated, 16-nm, amine-derivatized polyethylene glycol QDs (QD-RBB-Tiggrin) with emission maxima at 605 nm was performed as previously described [40]. Just prior to use, the QD-RBB-Tiggrin solution was sonicated for 2 h before diluting with a 1 % bovine serum albumin (BSA) solution to the required 0.1 nM concentration. Then the diluted QD-RBB-Tiggrin solution was gently shaken for half an hour followed by a 5 min sonication prior to incubation with 50 µL of cells for 5 min. The cells were then washed three times and imaged with BES Tyrodes buffer (20 mM BES, 0.14 M NaCl, 2.9 mM KCl, 0.1 % w/v glucose, 0.1 % w/v BSA).

QD tracking Instrumentation. The QDs were imaged using a Nikon Eclipse TE2000U microscope (Melville, NY, USA) operating in wide-field, epi-fluorescence mode with 100× Plan Apo, 1.49 numerical aperture oil-immersion objective. Fluorescence images for each SPT experiment were recorded for 30 s with continuous 40 ms acquisition using a 16-bit PhotonMax 512 EMCCD camera (Princeton Instrument, Trenton, NJ, USA) and mercury lamp illumination. Excitation of (425/45 nm) and emission from (605/20 nm) the QDs were

obtained through a filter set from Omega Optical (XF304-1, Brattleboro, VT, USA). All tracking experiments were performed at room temperature.

QD localization, tracking, and binding specificity. The Image J particle tracker 2D/3D plug-in implementing the algorithm developed by Sbalzarini and Koumoutsakos was used for QD localization, tracking, and to check binding specificity [43]. The particle radius was three, the cutoff value was zero, and the intensity percentile range was 0.1-1.5. A displacement value of four pixels was chosen based on the maximum step calculation for the fastest diffusion that can be theoretically attained on the membrane at the time resolution of single frame used in this experiment [44-46]. A single QD track was visually identified by using its blinking property and the short blinking events were accounted for in the trajectory by choosing the link range parameter of four [47,48]. The extracted trajectories were at least 4 s in duration. The positional accuracy was estimated to be ca.17 nm in a 2D plane as measured by imaging and analyzing stationary QDs. To verify the specific binding of 0.1 nM QD-RBB-Tiggrin with αPS2CβPS integrins, the number of bound QDs was quantified using a cell line expressing αPS2CβPS integrins or a second cell line that did not express integrins as discussed previously [40].

Data analysis. The mean square displacement (MSD) for each trajectory at different time lags was calculated using the formula:

$$\mathrm{MSD}(n\tau) = \frac{1}{N-n}\sum_{i=1}^{N-n}[(x((i+n)\tau) - x(i\tau))^2 + (y((i+n)\tau) - y(i\tau))^2], \qquad (1)$$

where τ is the acquisition time between two successive frames, N is the total number of frames in the sequence, x and y are coordinates of the particle at a specific time lag, $0 < n < N/4$ and $1 < i < (N-n)$ [49,28]. The diffusion coefficient for each trajectory was analyzed with

a time-dependent diffusion coefficient (D) as described by Feder et al. [50], which is given by:

$$D = \frac{1}{4}(\Gamma \tau^{\alpha-1}), \qquad (2)$$

where Γ is the transport coefficient, τ is the time lag, and α is the time exponent. The logarithmic plot of MSD versus the time lag was fitted by linear regression with weighting to the standard deviation to calculate Γ (intercept) and α (slope) [50,51,28]. The mode of diffusion/motion was assigned to each trajectory based on the α value: directed ($\alpha > 1.1$), Brownian ($0.9 \leq \alpha \leq 1.1$), anomalous/constrained ($0.1 \leq \alpha < 0.9$), and immobile ($\alpha < 0.1$) [52,50]. The time-dependent diffusion coefficient was calculated at 1 s using equation 2 for all trajectories with $\alpha > 0.1$.

Results and Discussion

Reduction in mRNA concentration for RNAi targeted proteins. The main goal of this study was to understand the influence of cytoplasmic (vinculin, FAK, or ILK) and membrane (EGFR or Notch) proteins on αPS2CβPS integrins' lateral diffusion using SPT to reveal heterogeneous populations (**Fig. 1**). The proteins selected for this study were chosen because they are known to affect the ensemble diffusion properties or clustering of integrins, but RNAi treatments for these proteins do not affect cell growth, viability or cell cycle regulation [53-55,36,30,29]. Details of how these proteins affect integrin diffusion still remain, and many of these details can be elucidated by studying individual populations of integrins, rather than an ensembled response. In this study, αPS2CβPS integrins' lateral diffusion was characterized into different modes of motion at native cytoplasmic and membrane protein

concentrations. Then, integrin diffusion was measured in a cell population with a reduced concentration of one target protein. To minimize the non-specific reduction of proteins other than the target, RNAi probes were chosen to have no calculated nonspecific targets [56,36].

The reduced mRNA expression for the RNAi targeted protein was confirmed by RT-PCR (**Table 1**). There was an 18 to 92% statistically significant reduction in mRNA concentration, with the targeted cytoplasmic proteins' mRNA reduced to a greater extent than the membrane proteins. This may be due to the differences in how mRNA is synthesized and processed for cytoplasmic versus membrane proteins [57,58]. Immunocytochemistry showed that a 62% or 78% decrease in mRNA concentration correlated to a corresponding 35% or 21% decrease in membrane protein expression for EGFR or Notch, respectively [29]. Similarly, for the cytoplasmic protein vinculin, an 84% decrease in mRNA concentration corresponded to a 36% decrease in protein expression [30,59]. Antibodies do not exist for the other targeted proteins and the S2 cell line.

Table 1: RT-PCR results of the relative expression of mRNA in RNAi treated cells compared to untreated cells.

	Treatment	**$\frac{\text{mRNA RNAi}}{\text{mRNA no RNAi}}$**
Cytoplasmic Proteins	Vinculin	0.08 ($p < 0.01$)*
	FAK	0.1 ($p < 0.01$)*
	ILK	0.08 ($p < 0.01$)*
Membrane Proteins	EGFR	0.6 ($p < 0.01$)*
	Notch	0.8 ($p < 0.01$)*

* A p value below 0.05 indicates a statistically significant difference in the mRNA expression when compared to the value before RNAi treatment at the 95% confidence level.

αPS2CβPS integrin diffusion at native protein concentrations. A total of 100 αPS2CβPS integrin trajectories were analyzed from 13 different cells at native membrane and cytoplasmic protein concentrations. Trajectories were classified as exhibiting directed, Brownian, anomalous/constrained, or immobile properties (**Fig. 2**). As expected, the directed and Brownian trajectories generally covered a larger area of the cell membrane than the anomalous/constrained integrins, and any "movement" observed in the immobile trajectories was within the positional uncertainty for these experiments. At native cytoplasmic and membrane protein concentrations there are 58% immobile and 42% mobile ligand-bound integrin (**Fig. 3a**). As a percentage of mobile integrins, there are 7%, 17%, and 76% directed, Brownian, and anomalous/constrained ligand-bound integrin, respectively. A majority of constrained/anomalously diffusing integrins measured by SPT is consistent with published ensemble FRAP measurements; the directed and Brownian diffusing populations are not measured by FRAP [30,29].

In SPT measurements, the specific binding of QDs to integrin is essential for the accuracy of the measurement. Therefore, the binding specificity of QD-RBB-Tiggrin to integrin at the concentration used for the SPT experiments was tested using 2 cell populations that: (i) expressed αPS2CβPS integrins or (ii) did not express integrins. An average of 10 and 0.1 QDs per cell was measured for the cells expressing integrins or not expressing integrins, respectively (**Table 2**). Nonspecific binding is 1%, suggesting minimal impact of this small fraction on the SPT results. In general, the nonspecific binding resulted in immobile trajectories; therefore nonspecific binding is expected to increase the immobile fraction by 1% at most.

Table 2: Average number of QDs bound per cell using 0.1 nM QD-RBB-Tiggrin.

S2 cells expressing	Average number of QD-RBB-Tiggrin per cell	No. Of cells analyzed
αPS2CβPS integrins	10	12
No integrins	0.1	36

The range of diffusion coefficients for mobile, ligand-bound integrins spans three orders of magnitude (0.002 to 5×10^{-9} cm^2/s) at native protein concentrations, indicating a high level of heterogeneity in integrin diffusion within the mobile population (**Fig. 3b**). The large heterogeneity in integrins' lateral diffusion is postulated to be the result of varying interactions with other membrane and cytoplasmic components. The average diffusion coefficient from all mobile SPT tracks was $0.7 \pm 1 \times 10^{-9}$ cm^2/s.

Reduced expression of cytoplasmic proteins vinculin, FAK, or ILK increases the ligand-bound integrin mobile population. A total of one-hundred αPS2CβPS integrin trajectories were collected and analyzed for each RNAi targeted cytoplasmic protein, and the results were compared to values obtained at native protein concentrations (i.e., prior to RNAi). After vinculin, FAK, or ILK RNAi, the mobile population increased by 50%, 80%, and 31%, respectively (Fig. 3a). The mobile fraction is larger after these RNAi treatments as measured by SPT compared to previously reported values measured by FRAP [30]. The previous FRAP experiments used integrin that was covalently attached to a fluorescent protein. In the FRAP experiments, the integrin did not need to be bound to ligand to

contribute to the signal. On the other hand, the SPT experiment only measures the trajectory of integrin that is bound to ligand (i.e., QD-RBB-Tiggrin). The difference in the mobile fraction measure by SPT and FRAP after these RNAi treatments suggests that vinculin, FAK and ILK have a greater impact on immobilizing ligand-bound integrin, which is the population measured by SPT, compared to integrin that is not ligand-bound, which will also contribute to the FRAP signal.

For vinculin RNAi treated cells there is an increase in the number of integrins exhibiting all modes of motion (directed, Brownian, and anomalous), but the fraction of each population relative to the total number of mobile trajectories is approximately the same as measured for the no RNAi cell population (Fig. 3a). This indicates vinculin does affect the number of integrins that are mobile, but it does not affect the mode of integrin diffusion. In contrast, FAK and ILK do affect the mode of integrin diffusion. There is a 19% (FAK RNAi) or 13% (ILK RNAi) increase in the anomalous/constrained population and a concurrent decrease in directed and Brownian populations. This indicates FAK and ILK expressed at native concentrations have a role in decreasing mobile integrins' diffusion constraints.

There is no statistically significant change in the average integrin diffusion coefficient after the RNAi treatment for vinculin ($1 \pm 3 \times 10^{-9}$ cm^2/s), FAK ($0.3 \pm 0.7 \times 10^{-9}$ cm^2/s), or ILK ($0.5 \pm 1 \times 10^{-9}$ cm^2/s) measured by SPT (this work) or as previously reported using FRAP [30]. However, histograms of diffusion coefficients provide additional information that the average values do not provide (Fig. 3b). Considering frequency changes of greater than 0.05, there are several significant changes. In the case of reduced FAK and ILK concentrations, the histograms show an increased frequency of integrins within the range 0.001 to 0.1×10^{-9} cm^2/s (FAK) or 0.001 to 0.01×10^{-9} cm^2/s (ILK, Fig. 3b). The increased

frequency of mobile integrins with slow diffusion coefficients is not evident in the average and ensemble diffusion coefficients due to the large standard deviation and heterogeneity, revealing the importance of single receptor measurements to reveal changes to individual populations. In the case of vinculin RNAi, there is a significant increase in the frequency of two populations, one diffusing faster than the average and the other diffusing slower than the average (Fig. 3b), essentially canceling each other out in the average.

It is well established that integrins provide a physical link between the extracellular matrix, actin cytoskeleton, and intracellular adaptor molecules at adhesion sites. The increase in integrins' mobile population after reducing vinculin, ILK or FAK concentrations is expected to be the result of alteration in extracellular matrix-integrin-cytoskeleton connections. Using the wealth of information known about vinculin as an example, it has been observed that focal adhesions are smaller and fewer in mouse embryo fibroblast cells devoid of vinculin, and the cells have reduced adhesion to a variety of extracellular matrix proteins [60,61]. Also, more dynamic focal adhesions in mouse embryo fibroblasts have been observed when the vinculin concentration was reduced [60,61]. Hence, because of these changes to focal adhesions, the decrease in vinculin concentration might favor an increase in the mobile integrin population by releasing binding constraints to immobile cytoplasmic assemblies.

The ligand-bound mobile population of integrins increases with reduced expression of membrane proteins EGFR or Notch. SPT results showed a 76% and 62% increase in the mobile population of integrins after EGFR or Notch protein reduction, respectively (**Fig. 4a**). Within reasonable experimental uncertainty, these are the same mobile fractions measured by FRAP after the reduction of these proteins [29]. In the case of EGFR RNAi, the fraction of

integrins exhibiting each mode of motion relative to the total number of mobile integrins was the same as measured before RNAi treatment; whereas anomalous/constrained integrin trajectories are the only mode of motion exhibiting an increased number of trajectories after Notch RNAi. In this regard, native concentrations of Notch, FAK and ILK generate a similar effect on integrin diffusion, which is less mobile integrins and decreased constrained diffusion on the remaining mobile population.

Statistically similar average integrin diffusion coefficients were measured after the RNAi treatment of EGFR ($0.5 \pm 1 \times 10^{-9}$ cm^2/s) or Notch ($0.6 \pm 1 \times 10^{-9}$ cm^2/s) compared to the average value before RNAi treatment ($0.7 \pm 1 \times 10^{-9}$ cm^2/s). After RNAi treatment there is an increase in the mobile integrin fraction with diffusion coefficients that spanned 0.001 to 1×10^{-9} cm^2/s; only the fastest diffusion coefficients exhibit no change (**Fig. 4b**).

Some plausible reasons for the increase in the mobile population of integrins after EGFR or Notch RNAi are decreases in integrin clustering, altered integrin organization within nanodomains or altered interactions with cytoplasmic proteins driven by the altered membrane composition, reduced membrane crowding or changes in ligand binding affinity. Using fluorescence resonance energy transfer less integrin clustering was measured at a reduced concentration of EGFR or Notch [29]. Reduced clustering as a result of the EGFR or Notch RNAi treatment is not the best explanation for the increase in the mobile fraction of integrins since *more* integrin clustering was measured after vinculin and FAK RNAi [36], and as reported above there was also an increase in the integrin mobile fraction after these treatments. Integrins are known to partition between lipid nanodomains and the bulk membrane in response to a variety of stimuli such as ligand binding [62,63]. Similarly, it has been reported that the lipid nanodomains can change their size and composition either by

including or by excluding proteins selectively in response to intra- or extracellular stimuli [64]. Another recent study described how adaptor proteins such as vinculin and FAK are enriched in certain lipid raft fractions [65]. Therefore, the reduced concentration of adapter proteins, EGFR or Notch could disrupt the composition or organization of lipid nanodomains or perturb the partitioning of integrins between nanodomains and the bulk membrane in a way that favors integrin mobility. This would explain the consistent increase in the integrin mobile fraction after all five RNAi treatments. The increase in the number of integrins with constrained diffusion after Notch, FAK and ILK RNAi treatments versus the consistent fraction of integrins with constrained diffusion before and after EGFR and vinculin RNAi treatment could suggest a different mechanism of disrupting the lipid nanodomain structure or composition.

Conclusions

A combination of SPT and RNAi was used to show that the reduction of select cytoplasmic (vinculin, FAK, or ILK) and membrane (EGFR or Notch) proteins play a role in affecting integrins' lateral mobility. Overall, after RNAi treatment, the fraction of ligand-bound integrins became more mobile and in some cases diffusion also became more constrained. The modification in extracellular matrix-integrin-cytoskeleton connections, and subsequent changes brought about as a consequence of this, are the hypothesized mechanism for the increase in integrin mobility after reduction of select cytoplasmic or membrane protein concentrations. The methodology reported here is suited to study the role of other cellular proteins in affecting the diffusion of numerous membrane proteins.

Acknowledgements

This work is supported by the National Science Foundation under Grant CHE-0845236.

References

1. Takada Y, Ye X, Simon S (2007) The integrins. Genome Biol 8 (5):215

2. Plow EF, Haas TA, Zhang L, Loftus J, Smith JW (2000) Ligand binding to integrins. J Biol Chem 275 (29):21785-21788

3. Hynes RO (2002) Integrins: bidirectional, allosteric signaling machines. Cell 110 (6):673-687

4. Giancotti FG, Ruoslahti E (1999) Integrin signaling. Science 285 (5430):1028-1032

5. Streuli CH, Akhtar N (2009) Signal co-operation between integrins and other receptor systems. Biochem J 418 (3):491-506

6. Millard M, Odde S, Neamati N (2011) Integrin targeted therapeutics. Theranostics 1:154-188

7. Goodman SL, Picard M (2012) Integrins as therapeutic targets. Trends in pharmacological sciences 33 (7):405-412

8. Luo BH, Carman CV, Springer TA (2007) Structural basis of integrin regulation and signaling. Annu Rev Immunol 25:619-647

9. Xiong JP, Stehle T, Zhang R, Joachimiak A, Frech M, Goodman SL, Arnaout MA (2002) Crystal structure of the extracellular segment of integrin alpha Vbeta3 in complex with an Arg-Gly-Asp ligand. Science 296 (5565):151-155

10. Petit V, Thiery JP (2000) Focal adhesions: structure and dynamics. Biol Cell 92 (7):477-494

11. Kroemker M, Rudiger AH, Jockusch BM, Rudiger M (1994) Intramolecular interactions in vinculin control alpha-actinin binding to the vinculin head. FEBS Lett 355 (3):259-262

12. Turner CE, Glenney JR, Jr., Burridge K (1990) Paxillin: a new vinculin-binding protein present in focal adhesions. J Cell Biol 111 (3):1059-1068

13. Menkel AR, Kroemker M, Bubeck P, Ronsiek M, Nikolai G, Jockusch BM (1994) Characterization of an F-actin-binding domain in the cytoskeletal protein vinculin. J Cell Biol 126 (5):1231-1240

14. Humphries JD, Wang P, Streuli C, Geiger B, Humphries MJ, Ballestrem C (2007) Vinculin controls focal adhesion formation by direct interactions with talin and actin. J Cell Biol 179 (5):1043-1057

15. Schaller MD, Otey CA, Hildebrand JD, Parsons JT (1995) Focal adhesion kinase and paxillin bind to peptides mimicking beta integrin cytoplasmic domains. J Cell Biol 130 (5):1181-1187

16. Hannigan GE, Leung-Hagesteijn C, Fitz-Gibbon L, Coppolino MG, Radeva G, Filmus J, Bell JC, Dedhar S (1996) Regulation of cell adhesion and anchorage-dependent growth by a new beta 1-integrin-linked protein kinase. Nature 379 (6560):91-96

17. Brown EJ (2002) Integrin-associated proteins. Curr Opin Cell Biol 14 (5):603-607

18. Schneller M, Vuori K, Ruoslahti E (1997) Alphavbeta3 integrin associates with activated insulin and PDGFbeta receptors and potentiates the biological activity of PDGF. EMBO J 16 (18):5600-5607

19. Woodard AS, Garcia-Cardena G, Leong M, Madri JA, Sessa WC, Languino LR (1998) The synergistic activity of alphavbeta3 integrin and PDGF receptor increases cell migration. J Cell Sci 111 (Pt 4):469-478

20. Soung YH, Clifford JL, Chung J (2010) Crosstalk between integrin and receptor tyrosine kinase signaling in breast carcinoma progression. BMB Rep 43 (5):311-318

21. Miyamoto S, Teramoto H, Gutkind JS, Yamada KM (1996) Integrins can collaborate with growth factors for phosphorylation of receptor tyrosine kinases and MAP kinase activation: roles of integrin aggregation and occupancy of receptors. J Cell Biol 135 (6 Pt 1):1633-1642

22. Moro L, Venturino M, Bozzo C, Silengo L, Altruda F, Beguinot L, Tarone G, Defilippi P (1998) Integrins induce activation of EGF receptor: role in MAP kinase induction and adhesion-dependent cell survival. EMBO J 17 (22):6622-6632

23. Yu X, Miyamoto S, Mekada E (2000) Integrin alpha 2 beta 1-dependent EGF receptor activation at cell-cell contact sites. J Cell Sci 113 (Pt 12):2139-2147

24. Falcioni R, Antonini A, Nistico P, Di Stefano S, Crescenzi M, Natali PG, Sacchi A (1997) Alpha 6 beta 4 and alpha 6 beta 1 integrins associate with ErbB-2 in human carcinoma cell lines. Exp Cell Res 236 (1):76-85

25. Mariotti A, Kedeshian PA, Dans M, Curatola AM, Gagnoux-Palacios L, Giancotti FG (2001) EGF-R signaling through Fyn kinase disrupts the function of integrin alpha6beta4 at hemidesmosomes: role in epithelial cell migration and carcinoma invasion. J Cell Biol 155 (3):447-458

26. Campos LS, Decker L, Taylor V, Skarnes W (2006) Notch, epidermal growth factor receptor, and beta1-integrin pathways are coordinated in neural stem cells. J Biol Chem 281 (8):5300-5309

27. Chen Y, Lagerholm BC, Yang B, Jacobson K (2006) Methods to measure the lateral diffusion of membrane lipids and proteins. Methods 39 (2):147-153

28. Saxton MJ, Jacobson K (1997) Single-particle tracking: applications to membrane dynamics. Annu Rev Biophys Biomol Struct 26:373-399

29. Arora N, Mainali D, Smith EA (2012) Unraveling the role of membrane proteins Notch, Pvr, and EGFR in altering integrin diffusion and clustering. Anal Bioanal Chem 404 (8):2339-2348

30. Sander S, Arora N, Smith EA (2012) Elucidating the role of select cytoplasmic proteins in altering diffusion of integrin receptors. Anal Bioanal Chem 403 (8):2327-2337

31. Mirchev R, Golan DE (2001) Single-particle tracking and laser optical tweezers studies of the dynamics of individual protein molecules in membranes of intact human and mouse red cells. Blood Cells Mol Dis 27 (1):143-147

32. Pralle A, Keller P, Florin EL, Simons K, Horber JK (2000) Sphingolipid-cholesterol rafts diffuse as small entities in the plasma membrane of mammalian cells. J Cell Biol 148 (5):997-1008

33. Leitner DM, Brown FL, Wilson KR (2000) Regulation of protein mobility in cell membranes: a dynamic corral model. Biophys J 78 (1):125-135

34. Sako Y, Kusumi A (1994) Compartmentalized structure of the plasma membrane for receptor movements as revealed by a nanometer-level motion analysis. J Cell Biol 125 (6):1251-1264

35. Edidin M, Zuniga MC, Sheetz MP (1994) Truncation mutants define and locate cytoplasmic barriers to lateral mobility of membrane glycoproteins. Proc Natl Acad Sci U S A 91 (8):3378-3382

36. Dibya D, Sander S, Smith EA (2009) Identifying cytoplasmic proteins that affect receptor clustering using fluorescence resonance energy transfer and RNA interference. Anal Bioanal Chem 395 (7):2303-2311

37. Bunch TA, Grinblat Y, Goldstein LS (1988) Characterization and use of the Drosophila metallothionein promoter in cultured Drosophila melanogaster cells. Nucleic Acids Res 16 (3):1043-1061

38. Bunch TA, Brower DL (1992) Drosophila PS2 integrin mediates RGD-dependent cell-matrix interactions. Development 116 (1):239-247

39. Zavortink M, Bunch TA, Brower DL (1993) Functional properties of alternatively spliced forms of the Drosophila PS2 integrin alpha subunit. Cell Adhes Commun 1 (3):251-264

40. Mainali D, Smith EA (2013) The effect of ligand affinity on integrins' lateral diffusion in cultured cells. Eur Biophys J 42 (4):281-290

41. Clemens JC, Worby CA, Simonson-Leff N, Muda M, Maehama T, Hemmings BA, Dixon JE (2000) Use of double-stranded RNA interference in Drosophila cell lines to dissect signal transduction pathways. Proceedings of the National Academy of Sciences 97 (12):6499-6503

42. Smith EA, Bunch TA, Brower DL (2007) General in vivo assay for the study of integrin cell membrane receptor microclustering. Anal Chem 79 (8):3142-3147

43. Sbalzarini IF, Koumoutsakos P (2005) Feature point tracking and trajectory analysis for video imaging in cell biology. J Struct Biol 151 (2):182-195

44. Saffman PG, Delbruck M (1975) Brownian motion in biological membranes. Proc Natl Acad Sci U S A 72 (8):3111-3113

45. Qian H, Sheetz MP, Elson EL (1991) Single particle tracking. Analysis of diffusion and flow in two-dimensional systems. Biophys J 60 (4):910-921

46. Kevin B, Dries V, Jo D, Stefaan De S (2010) Single Particle Tracking. In: Nanoscopy and Multidimensional Optical Fluorescence Microscopy. Chapman and Hall/CRC, pp 5-1 to 5-17

47. Nirmal M, Dabbousi BO, Bawendi MG, Macklin JJ, Trautman JK, Harris TD, Brus LE (1996) Fluorescence intermittency in single cadmium selenide nanocrystals. Nature (London) 383:802-804

48. Dahan M, Levi S, Luccardini C, Rostaing P, Riveau B, Triller A (2003) Diffusion dynamics of glycine receptors revealed by single-quantum dot tracking. Science 302 (5644):442-445

49. Saxton MJ (1997) Single-particle tracking: the distribution of diffusion coefficients. Biophys J 72 (4):1744-1753

50. Feder TJ, Brust-Mascher I, Slattery JP, Baird B, Webb WW (1996) Constrained diffusion or immobile fraction on cell surfaces: a new interpretation. Biophys J 70 (6):2767-2773

51. Slattery JP (1995) Lateral Mobility of Fc[epsilon]RI on Rat Basophilic Leukemia Cells as Measured by Single Particle Tracking Using a Novel Bright Fluorescent Probe. Cornell University, May

52. Ghosh RN, Webb WW (1994) Automated detection and tracking of individual and clustered cell surface low density lipoprotein receptor molecules. Biophys J 66 (5):1301-1318

53. Boutros M, Kiger AA, Armknecht S, Kerr K, Hild M, Koch B, Haas SA, Paro R, Perrimon N (2004) Genome-wide RNAi analysis of growth and viability in Drosophila cells. Science 303 (5659):832-835

54. Bjorklund M, Taipale M, Varjosalo M, Saharinen J, Lahdenpera J, Taipale J (2006) Identification of pathways regulating cell size and cell-cycle progression by RNAi. Nature 439 (7079):1009-1013

55. Bettencourt-Dias M, Giet R, Sinka R, Mazumdar A, Lock WG, Balloux F, Zafiropoulos PJ, Yamaguchi S, Winter S, Carthew RW, Cooper M, Jones D, Frenz L, Glover DM (2004) Genome-wide survey of protein kinases required for cell cycle progression. Nature 432 (7020):980-987

56. Schmidt EE, Pelz O, Buhlmann S, Kerr G, Horn T, Boutros M (2013) GenomeRNAi: a database for cell-based and in vivo RNAi phenotypes, 2013 update. Nucleic Acids Res 41:D1021-1026

57. Chen Q, Jagannathan S, Reid DW, Zheng T, Nicchitta CV (2011) Hierarchical regulation of mRNA partitioning between the cytoplasm and the endoplasmic reticulum of mammalian cells. Mol Biol Cell 22 (14):2646-2658

58. Lerner RS, Seiser RM, Zheng T, Lager PJ, Reedy MC, Keene JD, Nicchitta CV (2003) Partitioning and translation of mRNAs encoding soluble proteins on membrane-bound ribosomes. RNA 9 (9):1123-1137

59. Sander S (2012) Development of fluorescence-based methods to study the effect of cytoplasmic proteins, cholesterol, and extracellular ligand on integrin diffusion and clustering in single cells. Iowa State University, Ames

60. Saunders RM, Holt MR, Jennings L, Sutton DH, Barsukov IL, Bobkov A, Liddington RC, Adamson EA, Dunn GA, Critchley DR (2006) Role of vinculin in regulating focal adhesion turnover. Eur J Cell Biol 85 (6):487-500

61. Coll JL, Ben-Ze'ev A, Ezzell RM, Rodriguez Fernandez JL, Baribault H, Oshima RG, Adamson ED (1995) Targeted disruption of vinculin genes in F9 and embryonic stem cells changes cell morphology, adhesion, and locomotion. Proc Natl Acad Sci U S A 92 (20):9161-9165

62. Decker L, Baron W, Ffrench-Constant C (2004) Lipid rafts: microenvironments for integrin-growth factor interactions in neural development. Biochem Soc Trans 32 (Pt3):426-430

63. Runz S, Mierke CT, Joumaa S, Behrens J, Fabry B, Altevogt P (2008) CD24 induces localization of beta1 integrin to lipid raft domains. Biochem Biophys Res Commun 365 (1):35-41

64. Simons K, Toomre D (2000) Lipid rafts and signal transduction. Nat Rev Mol Cell Biol 1 (1):31-39

65. Wang R, Bi J, Ampah KK, Zhang C, Li Z, Jiao Y, Wang X, Ba X, Zeng X (2013) Lipid raft regulates the initial spreading of melanoma A375 cells by modulating β1 integrin clustering. The International Journal of Biochemistry & Cell Biology *In Press*

Fig. 1 Schematic of the experimental approach. First, the integrins' lateral diffusion characteristics are measured at native cytoplasmic and membrane protein concentrations using SPT with ligand-labeled quantum dots. Second, the cells were RNAi treated to reduce the select cytoplasmic or membrane protein concentration. Third, the integrins' lateral diffusion characteristics at the reduced cytoplasmic or membrane protein concentration are measured. The figure is not drawn to scale.

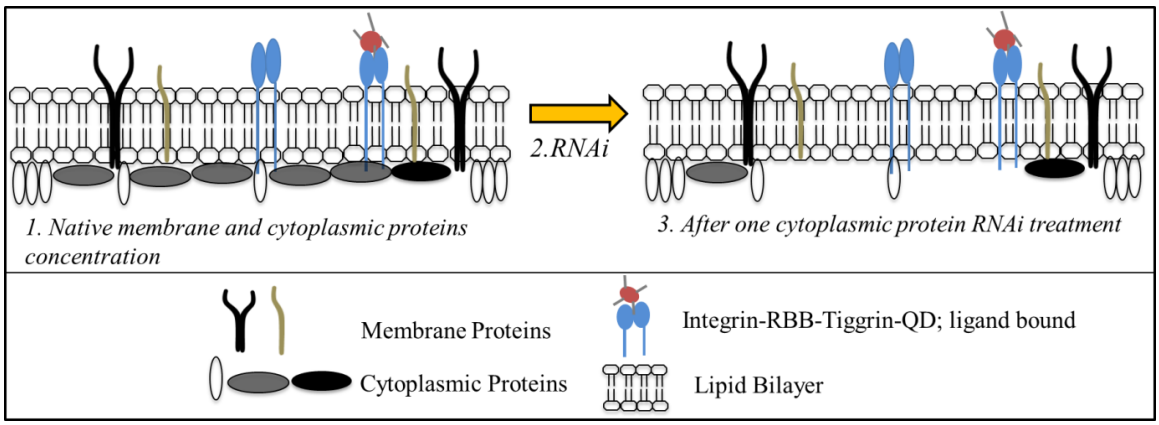

Fig. 2 Representative trajectories exhibited by αPS2CβPS integrins bound to QD-RBB-Tiggrin. (Left to right) Directed (α = 1.11), Brownian (α = 1.04), anomalous/constrained (α = 0.68), and immobile (α = 0.05) trajectory.

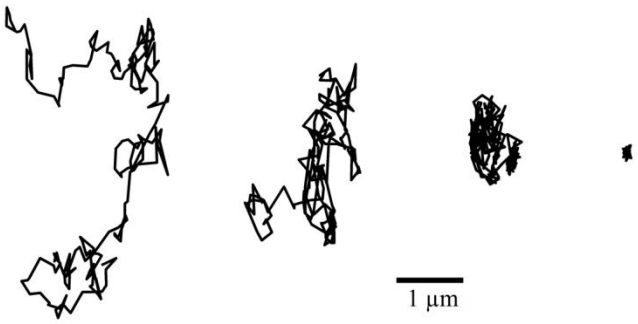

Fig. 3 Cytoplasmic Protein RNAi. **a** The total number of immobile and mobile trajectories exhibiting each mode of motion observed from 100 trajectories. For directed, Brownian and anomalous/constrained trajectories, the first number in the table is the percentage relative to all 100 trajectories and the second number is the percentage relative to only mobile trajectories. **b** histograms of diffusion coefficients for trajectories classified as mobile after vinculin, FAK, or ILK RNAi treatment.

a

	No RNAi		Vinculin		FAK		ILK	
	All	Mobile	All	Mobile	All	Mobile	All	Mobile
Immobile	58		37		24		45	
All Mobile	42		63		76		55	
Directed	3	7	4	6	1	1	1	2
Brownian	7	17	11	17	3	4	5	9
Anomalous	32	76	48	76	72	95	49	89

b

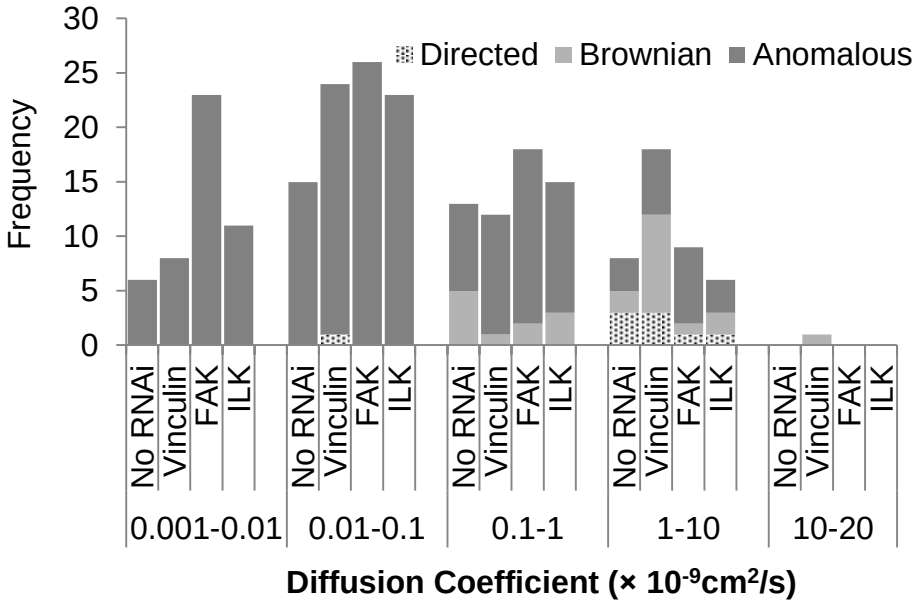

Fig. 4 Membrane Protein RNAi. **a** The total number of immobile and mobile trajectories exhibiting each mode of motion observed from 100 trajectories. For directed, Brownian and anomalous/constrained trajectories, the first number in the table is the percentage relative to all trajectories and the second number is the percentage relative to only mobile trajectories. **b** histograms of diffusion coefficients for trajectories classified as mobile after EGFR or Notch RNAi treatment.

a

	No RNAi		EGFR		Notch	
	All	Mobile	All	Mobile	All	Mobile
Immobile	58		26		32	
All Mobile	42		74		68	
Directed	3	7	4	5	3	4
Brownian	7	17	12	16	7	10
Anomalous	32	76	58	78	58	85

b

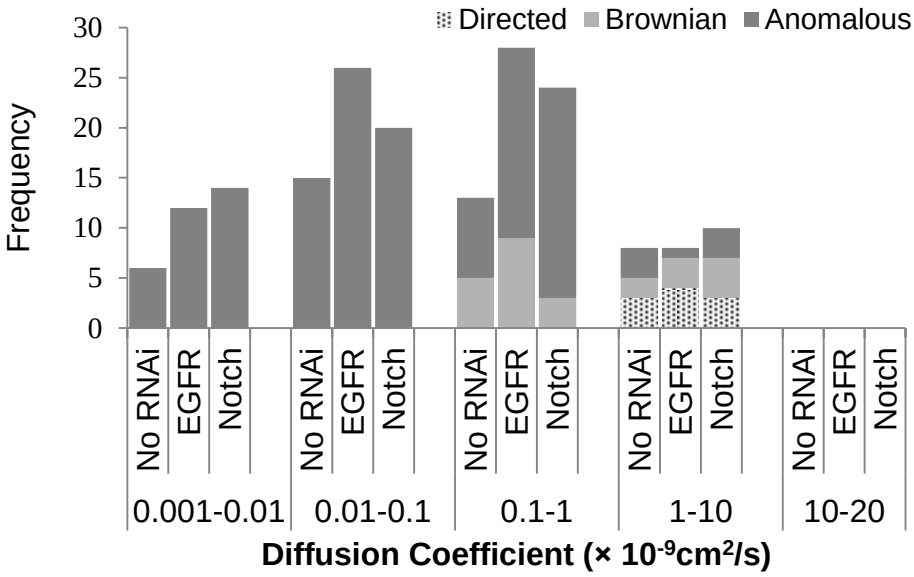

CHAPTER 4: ROLE OF INSULIN RECEPTOR AND INSULIN SIGNALING ON αPS2CβPS INTEGRINS' LATERAL DIFFUSION

Dipak Mainali, Aleem Syed, Neha Arora, Emily A. Smith

Abstract

Integrins are ubiquitous transmembrane receptors with adhesion and signaling properties. The influence of insulin receptor and insulin signaling on αPS2CβPS integrins' lateral diffusion was studied using single particle tracking (SPT) in S2 cells before and after reducing the insulin receptor expression or insulin stimulation. The expression of the insulin receptor was reduced using RNA interference. Insulin signaling was monitored by measuring the level of phospho-Akt by Western blotting. There was a 38% increase in the mobile population of integrins after reducing the concentration of the insulin receptor, and a 6% increase when the concentration of the insulin receptor was reduced in combination with insulin stimulation. After both treatments there was also a 6 to 13% increase in trajectories exhibiting Brownian diffusion relative to the total mobile population, indicating there were relatively fewer integrins in confined domains. For integrins that remained in confined domains after reducing the concentration of insulin receptor there was a 49% increase in the average diameter of confined domains and a 29% increase in the time integrins spend in confined domains. No change in integrins' diffusion coefficient was measured for any conditions included in this study. Insulin stimulation alone has no measured effect on altering integrin diffusion, but reduced expression of the insulin receptor alters integrin diffusion properties. The addition of insulin stimulation under conditions of reduced insulin receptor

expression partially restores changes to integrin diffusion properties, possibly as a result of other insulin signaling pathways that are activated at reduced insulin receptor conditions.

Keywords cell membrane biophysics, single particle tracking, RNA interference (RNAi), S2 cells, quantum dots

Abbreviations

SPT	Single particle Tracking
QDs	Quantum dots
RT-PCR	Real-time polymerase chain reaction
RNAi	RNA interference
RTKs	Receptor Tyrosine Kinases

Introduction

Integrins are adhesion and bi-directional signaling receptors [1,2]. The association of extracellular ligands or cytoplasmic proteins with integrins initiate events such as cytoskeleton reorganization, regulation of gene expression, activation of mitogen-activated protein kinase, and phosphorylation of focal adhesion kinase and paxillin [3-9]. Binding to extracellular ligand or intracellular components is not the only mechanism to activate integrins' signaling pathways. Signaling is a complex phenomenon and cross-talk can exist between different receptors' signaling processes [10].

Integrins and receptor tyrosine kinases (RTKs) are two families of cell surface receptors whose signaling processes are known to cooperate for an integrated control of cellular function. Cross-talk between integrins and RTKs can be through signaling pathways without direct interaction or through direct physical association [5,11-13]. For example, certain growth factors modulate integrin-mediated cell adhesion to the extracellular matrix, and adhesion to extracellular matrix is one of the prerequisites for cells to respond to growth factors [14-18]. Similarly, integrin-dependent cell migration is induced by growth factors [19].

A member of the RTK family that exhibits cross-talk with integrins is insulin receptors. Both insulin-triggered signaling and direct physical association modulate this cross-talk [4,13,20,21]. For example, insulin treatment on CHO-T cells has increased the adhesion of cells to a fibronectin matrix mediated by $\alpha_5\beta_1$ integrins [20]. Similarly, $\alpha_5\beta_1$ signaling enhances insulin receptor kinase activity and formation of complexes containing insulin receptor substrate-1(IRS-1) and PI-3 kinase [20]. $\alpha_v\beta_3$ integrins co-immunoprecipitate with activated insulin receptor indicating a direct association [13]. Also, $\alpha_v\beta_3$ association with IRS-1 and insulin receptor was enhanced in response to insulin stimulation [21,13]. During insulin mediated signaling, insulin receptor and downstream targets interact with cholesterol containing domains [22-24]. Upon insulin stimulation, single particle tracking experiments on insulin receptor showed reduced lateral diffusion and increased confinement within 100-nm scale membrane domains [25].

Integrins' lateral mobility and rearrangement in the cell membrane are essential to initiate many cellular functions. Integrin clustering can lead to increased adhesion and signal activation while diffusion affects the rate at which integrins interact with other cellular

components [26,27]. Integrin-mediated adhesion, migration, and association with other membrane receptors depend on its lateral diffusion. Monitoring the lateral mobility of integrins in the cell membrane in response to insulin receptor signal stimulation or insulin receptor depletion can provide valuable insight into the mechanism of cross-talk between these receptors.

Herein, the role of insulin signaling and the insulin receptor on integrins' lateral dynamics as measured by SPT is reported. SPT is a method for measuring heterogeneous properties of receptor diffusion with high spatial resolution [28]. *Drosophila* S2 cells expressing αPS2CβPS integrins are stimulated with insulin or the insulin receptors are targeted by RNA interference. The basic mechanisms of insulin signaling are conserved in *Drosophila* and mammalian systems [29,30]. Western blot analysis to measure phospho-Akt expression can verify successful insulin stimulation. Akt, also called protein kinase B (PKB), is activated by insulin in a signaling pathway involving PI3 kinase [31,32]. Real-time polymerase chain reaction (RT-PCR) quantifies insulin receptor's mRNA concentration. This research provides new insight on how insulin signaling and the insulin receptor affect integrins' lateral dynamics and adds new evidence to the mechanism of cross-talk between these receptors.

Materials and Methods

Cell culture

Drosophila S2 cells were used to perform all experiments. Cells were transformed to express αPS2CβPS integrins under the regulation of the heat shock promoter, unless otherwise noted. Transfection methods and culture techniques have been previously described [33-36].

RNA interference and RT-PCR

For RNA interference, cells were incubated with 10 µg of double-stranded RNA (dsRNA) specific to the insulin receptor (RNAi reagent identifier: HFA16717, http://www.genomernai.org/) for 4 days at 22 ^{o}C before performing RT-PCR or SPT experiments. dsRNA synthesis and RT-PCR experiments were performed as described previously [37-41]. Applied Biosystems TaqMan Gene Expression Assay (Dm02136224_g1) for insulin receptor (INR) was obtained from Life Technologies (Carlsbad, CA, USA).

Insulin stimulation and Western Blot analysis

Insulin stimulation was achieved with the treatment of 10 µg/mL human insulin (Sigma Aldrich, Saint Louis, MO) for 5 minute [30]. To measure phospho-Akt levels by Western blot analysis, cells were lysed using SDS sample buffer (62.5 mM Tris-HCl pH 6.5 at RT, 2 % (w/v) SDS, 10 % glycerol, 41.6 mM DTT), followed by sonication for 2 min to complete lysis. The lysed samples were then heated for 5 min at 95 ^{o}C and cooled on ice before loading to 4-12 % gradient SDS-PAGE gel. The separated proteins from SDS-PAGE were transferred to polyvinylidene fluoride (PVDF) membrane. The membrane blots were washed for 5 min with TBS (20 mM Tris-HCl, 500 mM NaCl, pH 7.5) and blocked in TBST (TBS, 0.1 % Tween 20) with 5 % w/v nonfat dry milk for 1 h. The blots were then washed with TBST three times at 5 min intervals and incubated overnight at 4 ^{o}C with phospho-Akt (Ser473) Rabbit mAb (Cell Signaling Technology # 4060, Beverly, MA, USA) at a dilution of 1:2000. After washing three times with TBST, the blots were then incubated with Anti-Rabbit IgG, HRP-linked antibody (Cell Signaling Technology # 7074, Beverly, MA, USA) at a dilution of 1:1000 for 1 h at room temperature. Finally, after washing the membrane three

times for 5 min each with TBST, the blots were developed using Clarity Western ECL Substrate (Bio-Rad, # 170-5060, Hercules, CA, USA).

Quantum dot preparation and imaging

The 16-nm amine-derivatized polyethylene glycol quantum dots (Life Technologies, Carlsbad, CA) were conjugated with a recombinant version of the αPS2CβPS integrins' ligand RBB-Tiggrin [33,37]. The conjugated product (here after QD-RBB-Tiggrin) was sonicated for 2 h and diluted to 1 nM before incubating for 5 min with cells to bind with integrins [37]. The QD imaging experiments were performed at room temperature using a Nikon Eclipse TE2000U microscope (Melville, NY, USA) operating in wide-field, epi-fluorescence mode with a 100× objective and mercury lamp illumination [33,37]. Fluorescence images were collected every 40 ms for a total of 30 s using a PhotonMAX 512 EMCCD camera (Princeton Instrument, Trenton, NJ, USA). Filter sets for excitation (425/45 nm) and emission (605/20 nm) were obtained from Omega Optical (XF304-1, Brattleboro, VT, USA).

QD-RBB-Tiggrin binding specificity, localization, and tracking

The ImageJ particle tracker 2D/3D plug-in implementing the algorithm developed by Sbalzarini and Koumoutsakos was used for quantifying QD-RBB-Tiggrin binding specificity, localization, and tracking [42,37]. A single QD-RBB-Tiggrin was visually identified by its blinking property and the extracted trajectories were at least 4 s in duration. S2 cells expressing αPS2CβPS integrins or not expressing αPS2CβPS integrins were used to verify the specific binding of 1 nM QD-RBB-Tiggrin. Specific binding was ~99 %.

SPT data analysis

SPT trajectories were analyzed using APM_GUI (Analyzing Particle Movement with Graphical User Interface), which is a MatLab-implemented application based on an algorithm reported by Simpson and co-workers [43-45]. Trajectories were classified as exhibiting either confined or non-confined (Brownian) motion based on how long the particle stays in a given region. The confinement index (L) was calculated for each trajectory to highlight regions of confined behavior as described previously [44]. The larger the value of L, the greater the probability a trajectory is in a confined domain. The confinement index (L) and critical time t_c were the two parameters used to classify modes of motion. For a given trajectory, a confined domain is defined by the regions where L increases above a critical threshold L_c for a duration of time longer than a critical time t_c. Based on the simulation of Brownian trajectories, those with $L > 3.16$ for a duration $t_c > 1.1$ s have a 99.93% likelihood to be in a confined domain. The size of the confined region, the duration of the confinement, and the diffusion coefficients inside the confined zones and outside the confined regions were further analyzed for each trajectory classified as confined. The characteristic diffusion coefficient of a given region and the instantaneous diffusion coefficient for each segment of a trajectory were calculated by analyzing the plot of mean square displacement (MSD) vs. time [43].

Results and Discussions

Insulin treatment has no significant effect on integrins' lateral dynamics

The goal of this study was to understand how insulin-mediated signaling and more generally the insulin receptor affect integrins' lateral dynamics. The first step is to measure

integrins' diffusion properties at native cellular conditions. SPT was used to measure a total of 100 trajectories, which were classified as exhibiting non-confined/Brownian diffusion, confined diffusion, or immobility. Integrins were considered to be immobile if the diffusion coefficient was below 0.001 μm^2/sec. At native cellular conditions, there were 62% ligand-bound mobile trajectories; 39 trajectories showed confined diffusion and 23 trajectories displayed Brownian diffusion (Fig.1). Confined trajectories consisted of at least one or up to six confined regions whereas Brownian trajectories have no confined regions (Fig.2). As one may expect, the average diffusion coefficient inside the confined region (0.01 μm^2/sec) was an order of magnitude slower compared to the average diffusion coefficient outside the confined regions (0.1 μm^2/sec). The average diameter and the duration within the confined region were 110 nm and 2.1 s, respectively. The presence of confined and immobile integrins is assumed to be the result of interactions with other biomolecules and possibly with large biocomplexes.

Insulin-mediated signaling was activated by treating cells with 10 µg/mL insulin, and verified by measuring phospho-Akt levels. Cells treated with insulin showed a non-integrin dependent 40% increase in phospho-Akt (Fig. 3). Based on the analysis of 100 trajectories after insulin stimulation, 65% of integrins were mobile and 35% were immobile. The integrin mobility before and after insulin stimulation was similar (Fig. 1). Additionally, there is no statistically significant difference in the integrin diffusion coefficient, confinement domain size, or the duration in confined domains when compared to cells that are not stimulated with insulin (Table 1, Fig. 4). These results indicate that a downstream activation of insulin-signaling, as measured by phospho-Akt level, doesn't have a measurable impact on integrins' lateral diffusion.

Insulin receptors constrain integrin diffusion in a native cellular environment

Insulin receptor expression was reduced by performing RNA interference. The decreased expression of insulin receptor mRNA was confirmed by RT-PCR, which revealed a 72% statistically significant reduction after RNAi treatment. Compared to cells with a native expression of insulin receptor, cells that were RNAi treated for insulin receptor showed an elevated phospho-Akt activity in the absence of insulin stimulation (Fig. 3). A similar observation has been made when insulin receptor expression was depleted in renal mesangial cells [46]. In insulin receptor RNAi treated cells, the intensity of the phospho-Akt band after insulin stimulation was 20% higher when compared to the phospho-Akt band observed without insulin stimulation. This may be the result of less than 100% reduction in the insulin receptor expression after RNAi, or the result of signaling pathways that don't involve the insulin receptor. Actin, which was detected as a loading control, had similar intensity in cells with and without insulin simulation (Fig. 3).

After reducing the expression of insulin receptors, a total of 100 ligand-bound integrin trajectories were collected and analyzed, and the results were compared to values obtained at a native cellular environment. The ligand-bound integrin mobile population increased to 86%; and there was an increase in the number of both Brownian and confined populations of integrins (Fig. 1). Relative to the total number of mobile integrin trajectories, there is a larger increase in trajectories exhibiting Brownian diffusion relative to those with confined domains. Based on the Welch's t-test, there is a statistically significant increase in the average diameter of confinement domains and the average duration that mobile integrins reside inside confined domains when values after insulin receptor RNAi are compared to a native cellular environment (Table 1 and Fig. 4). The average diameter of the confinement

domain increases to 160 nm from 110 nm and the average duration of time inside the confined domains increases to 2.7 s from 2.1 s. There is no statistically significant difference in the integrin diffusion coefficients inside or outside the confined regions (Table 1). The increase in the amount of time integrins spend in confined domains may be correlated with the increase in the diameter of the confined domains; however, based only on considerations of area one would expect the duration in confined domains to quadruple. As this does not happen, other factors must be controlling the amount of time integrins reside in confined domains.

The increase in integrins' mobile population and the relative (based on only the mobile trajectories) decrease in the percentage of integrins with confined motion with reduced insulin receptor expression may be due to the release of physical interactions between these two receptors. The physical association of integrins with insulin receptor has been reported [13,21]. Reduced membrane crowding may also play a role, although this is unlikely to be the sole explanation for the changes in integrin diffusion given the diversity of proteins and protein density in the cell membrane. Integrins and insulin receptor localize in lipid nanodomains that have been considered important sites for signal transduction and receptor interaction [47-49]. When insulin receptor expression is reduced, changes in the composition of lipid nanodomains or partitioning of integrins into lipid nanodomains may favor integrin mobility. Similarly, insulin receptor also localizes with other RTKs, such as EGFR or platelet derived growth factor (PDGF) receptor, at lipid nanodomains. These receptors have known interactions with integrins. Insulin receptor RNAi may alter the organization of other RTKs, which in turn may increase integrin mobility. There is an increased concentration and enhanced activity of insulin-like growth factor 1 receptor in

insulin receptor depleted cells [46]; increased integrin mobility after insulin receptor RNAi may be indirectly the result of this type of cellular alteration, which is consistent with increased phospho-Akt levels after insulin receptor RNAi.

After insulin receptor RNAi or insulin stimulation, elevated phosho-Akt levels were measured compared to native cellular conditions (Fig. 3). In order to unravel why different integrin diffusion properties were measured after these treatments, and to test if the absence of the insulin receptor alone is responsible for the changes in integrin diffusion after insulin receptor RNAi, a combination of insulin receptor RNAi and insulin treatment was performed. As measured by SPT, there is a 66% mobile integrin fraction and a 34% immobile fraction (Fig. 1). Out of 66 mobile integrin trajectories, 33 exhibited Brownian diffusion and 33 exhibited confined diffusion (Fig. 1). There is small increase in the total mobile fraction compared to the fraction measured at a native cellular environment and 43% more integrins exhibiting Brownian trajectories. There is no statistically significant difference in integrin diffusion coefficient inside confined regions, in the confined domain size, and the duration in confined domains when compared to cells at native cellular environment (Table 1, Fig. 4). The combined effect of insulin receptor RNAi and insulin stimulation is a 23% smaller mobile fraction compared to when only insulin receptor RNAi was performed. While the reduced expression of the insulin receptor alters integrin diffusion properties, they are nearly (but not entirely) restored by the combined effects of insulin receptor RNAi and insulin treatment. This is hypothesized to be the result of other insulin signaling pathways that are activated under conditions of reduced insulin receptor expression, as discussed above. One area to be explored is the nature of these signaling pathways and what other alterations they cause to cell membrane dynamics.

Conclusion

In summary, the cross-talk between αPS2CβPS integrins and insulin receptors affects integrin diffusion. The cellular changes that result when reducing the expression of the insulin receptor by RNAi have a more dominant effect on altering the lateral dynamics of integrins than insulin signaling in the presence or absence of the insulin receptor.

Acknowledgements

This work was supported by the National Science Foundation (CHE-0845236).

References:

1. Hynes RO (1999) Cell adhesion: old and new questions. Trends Cell Biol 9 (12):M33-37

2. Giancotti FG, Ruoslahti E (1999) Integrin signaling. Science 285 (5430):1028-1032

3. Dedhar S, Hannigan GE (1996) Integrin cytoplasmic interactions and bidirectional transmembrane signalling. Curr Opin Cell Biol 8 (5):657-669

4. Clark EA, Brugge JS (1995) Integrins and signal transduction pathways: the road taken. Science 268 (5208):233-239

5. Schwartz MA, Schaller MD, Ginsberg MH (1995) Integrins: emerging paradigms of signal transduction. Annu Rev Cell Dev Biol 11:549-599

6. Burridge K, Turner CE, Romer LH (1992) Tyrosine phosphorylation of paxillin and pp125FAK accompanies cell adhesion to extracellular matrix: a role in cytoskeletal assembly. J Cell Biol 119 (4):893-903

7. Yurochko AD, Liu DY, Eierman D, Haskill S (1992) Integrins as a primary signal transduction molecule regulating monocyte immediate-early gene induction. Proc Natl Acad Sci U S A 89 (19):9034-9038

8. Chen Q, Kinch MS, Lin TH, Burridge K, Juliano RL (1994) Integrin-mediated cell adhesion activates mitogen-activated protein kinases. J Biol Chem 269 (43):26602-26605

9. Guan JL (1997) Role of focal adhesion kinase in integrin signaling. Int J Biochem Cell Biol 29 (8-9):1085-1096

10. Taniguchi CM, Emanuelli B, Kahn CR (2006) Critical nodes in signalling pathways: insights into insulin action. Nat Rev Mol Cell Biol 7 (2):85-96

11. Ross RS (2004) Molecular and mechanical synergy: cross-talk between integrins and growth factor receptors. Cardiovasc Res 63 (3):381-390

12. Miyamoto S, Teramoto H, Gutkind JS, Yamada KM (1996) Integrins can collaborate with growth factors for phosphorylation of receptor tyrosine kinases and MAP kinase activation: roles of integrin aggregation and occupancy of receptors. J Cell Biol 135 (6 Pt 1):1633-1642

13. Schneller M, Vuori K, Ruoslahti E (1997) Alphavbeta3 integrin associates with activated insulin and PDGFbeta receptors and potentiates the biological activity of PDGF. EMBO J 16 (18):5600-5607

14. Schlessinger J, Geiger B (1981) Epidermal growth factor induces redistribution of actin and alpha-actinin in human epidermal carcinoma cells. Exp Cell Res 134 (2):273-279

15. Bockus BJ, Stiles CD (1984) Regulation of cytoskeletal architecture by platelet-derived growth factor, insulin and epidermal growth factor. Exp Cell Res 153 (1):186-197

16. Kadowaki T, Koyasu S, Nishida E, Sakai H, Takaku F, Yahara I, Kasuga M (1986) Insulin-like growth factors, insulin, and epidermal growth factor cause rapid cytoskeletal reorganization in KB cells. Clarification of the roles of type I insulin-like growth factor receptors and insulin receptors. J Biol Chem 261 (34):16141-16147

17. Lillien LE, Sendtner M, Raff MC (1990) Extracellular matrix-associated molecules collaborate with ciliary neurotrophic factor to induce type-2 astrocyte development. J Cell Biol 111 (2):635-644

18. Schubert D, Kimura H (1991) Substratum-growth factor collaborations are required for the mitogenic activities of activin and FGF on embryonal carcinoma cells. J Cell Biol 114 (4):841-846

19. Klemke RL, Yebra M, Bayna EM, Cheresh DA (1994) Receptor tyrosine kinase signaling required for integrin alpha v beta 5-directed cell motility but not adhesion on vitronectin. J Cell Biol 127 (3):859-866

20. Guilherme A, Torres K, Czech MP (1998) Cross-talk between insulin receptor and integrin alpha5 beta1 signaling pathways. J Biol Chem 273 (36):22899-22903

21. Vuori K, Ruoslahti E (1994) Association of insulin receptor substrate-1 with integrins. Science 266 (5190):1576-1578

22. Kim K-B, Kim B-W, Choo H-J, Kwon Y-C, Ahn B-Y, Choi J-S, Lee J-S, Ko Y-G (2009) Proteome analysis of adipocyte lipid rafts reveals that gC1qR plays essential roles in adipogenesis and insulin signal transduction. PROTEOMICS 9 (9):2373-2382

23. Maffucci T, Brancaccio A, Piccolo E, Stein RC, Falasca M (2003) Insulin induces phosphatidylinositol-3-phosphate formation through TC10 activation. EMBO J 22 (16):4178-4189

24. Muller G, Jung C, Wied S, Welte S, Frick W (2001) Insulin-mimetic signaling by the sulfonylurea glimepiride and phosphoinositolglycans involves distinct mechanisms for redistribution of lipid raft components. Biochemistry 40 (48):14603-14620

25. Al-Qatati A, Winter PW, Wolf-Ringwall AL, Chatterjee PB, Van Orden AK, Crans DC, Roess DA, Barisas BG (2012) Insulin receptors and downstream substrates associate with membrane microdomains after treatment with insulin or chromium(III) picolinate. Cell Biochem Biophys 62 (3):441-450

26. Stewart M, Hogg N (1996) Regulation of leukocyte integrin function: affinity vs. avidity. J Cell Biochem 61 (4):554-561

27. van Kooyk Y, Figdor CG (2000) Avidity regulation of integrins: the driving force in leukocyte adhesion. Curr Opin Cell Biol 12 (5):542-547

28. Saxton MJ, Jacobson K (1997) Single-particle tracking: applications to membrane dynamics. Annu Rev Biophys Biomol Struct 26:373-399

29. Fernandez R, Tabarini D, Azpiazu N, Frasch M, Schlessinger J (1995) The Drosophila insulin receptor homolog: a gene essential for embryonic development encodes two receptor isoforms with different signaling potential. EMBO J 14 (14):3373-3384

30. Kim SE, Cho JY, Kim KS, Lee SJ, Lee KH, Choi KY (2004) Drosophila PI3 kinase and Akt involved in insulin-stimulated proliferation and ERK pathway activation in Schneider cells. Cell Signal 16 (11):1309-1317

31. Burgering BM, Coffer PJ (1995) Protein kinase B (c-Akt) in phosphatidylinositol-3-OH kinase signal transduction. Nature 376 (6541):599-602

32. Franke TF, Yang SI, Chan TO, Datta K, Kazlauskas A, Morrison DK, Kaplan DR, Tsichlis PN (1995) The protein kinase encoded by the Akt proto-oncogene is a target of the PDGF-activated phosphatidylinositol 3-kinase. Cell 81 (5):727-736

33. Mainali D, Smith EA (2013) The effect of ligand affinity on integrins' lateral diffusion in cultured cells. Eur Biophys J 42 (4):281-290

34. Bunch TA, Grinblat Y, Goldstein LS (1988) Characterization and use of the Drosophila metallothionein promoter in cultured Drosophila melanogaster cells. Nucleic Acids Res 16 (3):1043-1061

35. Bunch TA, Brower DL (1992) Drosophila PS2 integrin mediates RGD-dependent cell-matrix interactions. Development 116 (1):239-247

36. Zavortink M, Bunch TA, Brower DL (1993) Functional properties of alternatively spliced forms of the Drosophila PS2 integrin alpha subunit. Cell Adhes Commun 1 (3):251-264

37. Mainali D, Smith EA (2013) Select cytoplasmic and membrane proteins increase the percentage of immobile integrins but do not affect the average diffusion coefficient of mobile integrins. Anal Bioanal Chem 405 (26):8561-8568

38. Arora N, Mainali D, Smith EA (2012) Unraveling the role of membrane proteins Notch, Pvr, and EGFR in altering integrin diffusion and clustering. Anal Bioanal Chem 404 (8):2339-2348

39. Sander S, Arora N, Smith EA (2012) Elucidating the role of select cytoplasmic proteins in altering diffusion of integrin receptors. Anal Bioanal Chem 403 (8):2327-2337

40. Dibya D, Sander S, Smith EA (2009) Identifying cytoplasmic proteins that affect receptor clustering using fluorescence resonance energy transfer and RNA interference. Anal Bioanal Chem 395 (7):2303-2311

41. Clemens JC, Worby CA, Simonson-Leff N, Muda M, Maehama T, Hemmings BA, Dixon JE (2000) Use of double-stranded RNA interference in Drosophila cell lines to dissect signal transduction pathways. Proceedings of the National Academy of Sciences 97 (12):6499-6503

42. Sbalzarini IF, Koumoutsakos P (2005) Feature point tracking and trajectory analysis for video imaging in cell biology. J Struct Biol 151 (2):182-195

43. Menchon SA, Martin MG, Dotti CG (2012) APM_GUI: analyzing particle movement on the cell membrane and determining confinement. BMC Biophys 5:4

44. Simson R, Sheets ED, Jacobson K (1995) Detection of temporary lateral confinement of membrane proteins using single-particle tracking analysis. Biophys J 69 (3):989-993

45. Meilhac N, Le Guyader L, Salome L, Destainville N (2006) Detection of confinement and jumps in single-molecule membrane trajectories. Phys Rev E Stat Nonlin Soft Matter Phys 73 (1 Pt 1):011915

46. Yano N, Suzuki D, Endoh M, Zhang W, Xu YC, Padbury JF, Tseng YT (2012) In vitro silencing of the insulin receptor attenuates cellular accumulation of fibronectin in renal mesangial cells. Cell Commun Signal 10 (1):29

47. Decker L, Baron W, Ffrench-Constant C (2004) Lipid rafts: microenvironments for integrin-growth factor interactions in neural development. Biochem Soc Trans 32 (Pt3):426-430

48. Couet J, Li S, Okamoto T, Ikezu T, Lisanti MP (1997) Identification of peptide and protein ligands for the caveolin-scaffolding domain. Implications for the interaction of caveolin with caveolae-associated proteins. J Biol Chem 272 (10):6525-6533

49. Runz S, Mierke CT, Joumaa S, Behrens J, Fabry B, Altevogt P (2008) CD24 induces localization of beta1 integrin to lipid raft domains. Biochem Biophys Res Commun 365 (1):35-41

Table 1. Average integrin diffusion coefficients, diameter of confined domains of diffusion, and duration in confined domains of diffusion as measured for 100 trajectories.

	No Treatment	Insulin Receptor RNAi	Insulin Stimulated	Insulin Stimulated and Insulin Receptor RNAi
Non-confined/Brownian motion				
Diffusion coefficient (μm^2/sec)	0.1	0.1 (p=0.5)	0.1 (p=0.6)	0.1 (p=0.4)
Confined motion				
Diffusion coefficient inside confined zones (μm^2/sec)	0.01	0.02 (p=0.05)	0.01 (p=0.6)	0.01 (p=0.7)
Diffusion coefficient outside confined zones (μm^2/sec)	0.1	0.05 (p=0.8)	0.1 (p=0.7)	0.04 (p=0.4)
Diameter of confined zones (μm)	0.110	0.160 (p=0.001)	0.120 (p=0.4)	0.120 (p=0.3)
Duration in confined zones (s)	2.1	2.7 (p=0.005)	2.1 (p=0.7)	2.3 (p=0.3)

[a] p-values in parenthesis were obtained from a Welch's t-test comparison to No Treatment values

Fig. 1 Percentage of trajectories exhibiting confined diffusion, Brownian diffusion or immobility at native cellular conditions or after the indicated treatment.

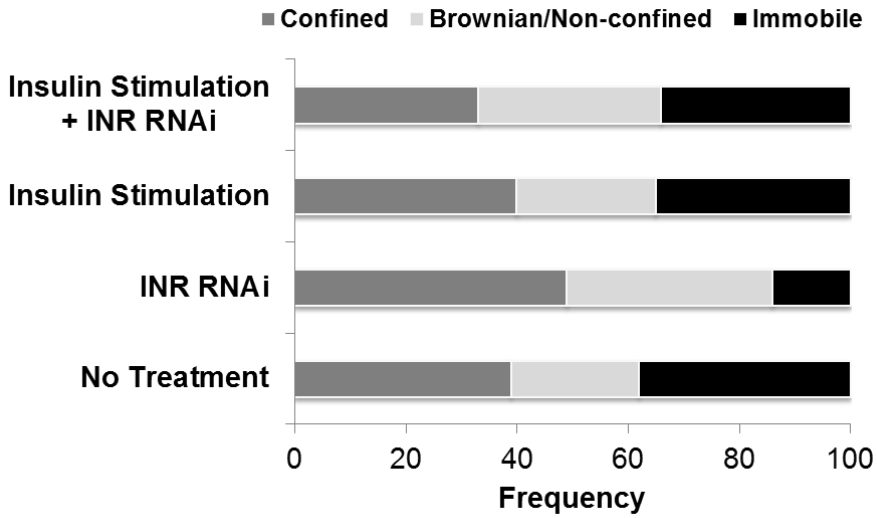

Fig. 2 Trajectory exhibiting: a) confined diffusion with three confined domains as depicted by the dark circles; b) non-confined/Brownian diffusion with no confined zones. (c, d) Plots showing instantaneous diffusion coefficient (grey curve) and confinement index (black curve) for the trajectory on the left. Dashed lines in c and d indicate the critical threshold value of the confinement index (L=3.16). The duration of the trajectory depends on the time between quantum dot blinking events, which is statistically random. For all data sets in this study, the average duration and standard deviation of all trajectories was 14 ± 8 s.

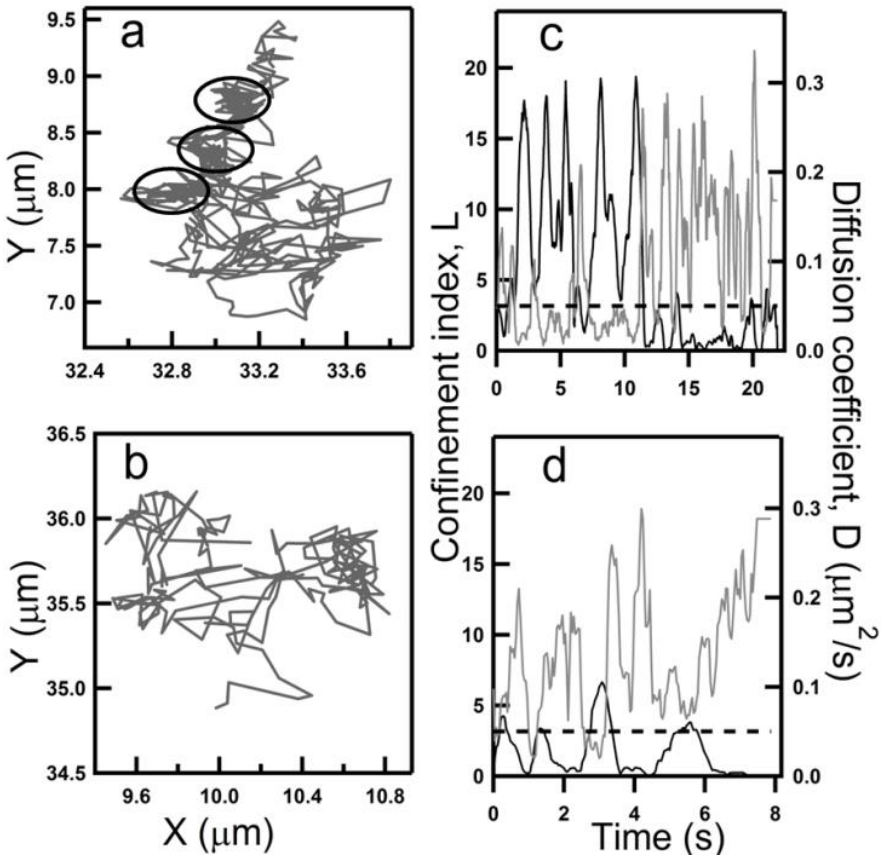

Fig. 3 Western blot image of phospho-Akt and actin level in S2 cells. A plus indicates αPS2CβPS expression (1, 2, 5, 6), insulin receptor RNAi treatment (5, 6), or insulin stimulation (1, 3, and 5)

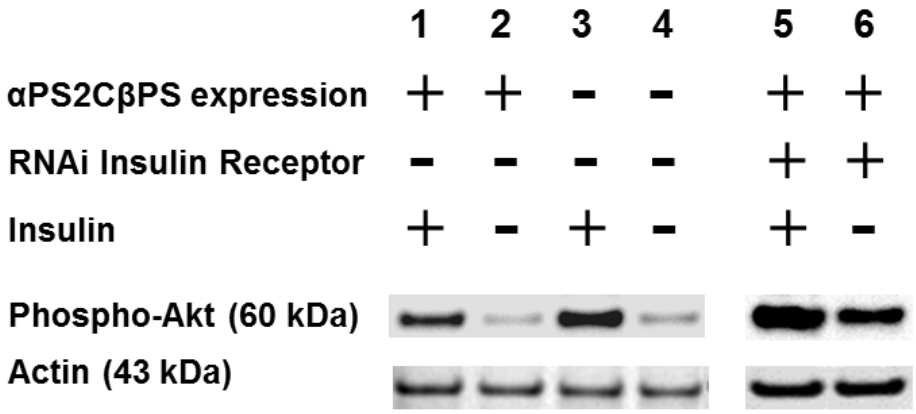

Fig. 4 Histograms of the size of confined domains (a-d) and the duration in confined domains (e-h). (a ,e) no treatment; (b, f) insulin receptor RNAi; (c, g) insulin stimulation; (d, h) insulin receptor RNAi and insulin stimulation. The frequency was normalized to the total number of confined mobile trajectories.

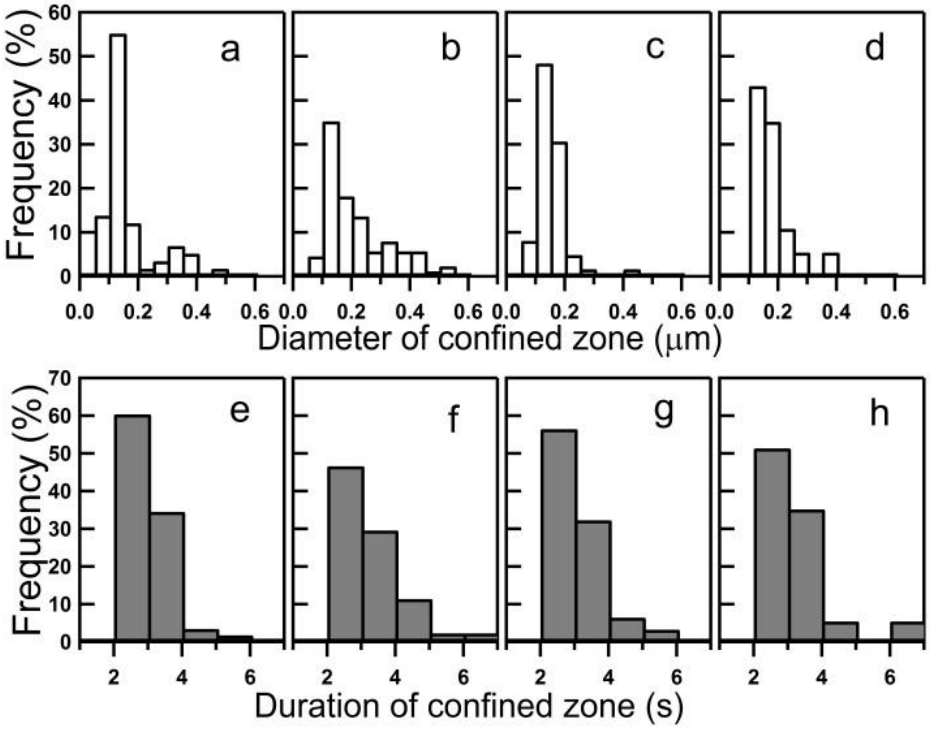

CHAPTER 5: GENERAL CONCLUSIONS

Single particle tracking is an important tool to measure the lateral mobility of cell membrane receptors. Because of SPT technique's high spatial resolution and the ability to measure individual receptor diffusion property, the information obtained from SPT can provide information that is often obscured by ensemble technique FRAP. In addition to revealing more detailed information, SPT data will help to better understand the results obtained by FRAP. The information obtained from these two techniques, when taken together, provides valuable insights on the lateral mobility of receptors. The thesis work presented here utilizes SPT technique in combination with molecular biology technique RNA interference to measure the lateral mobility of integrins at different cellular conditions.

The second chapter underscores the role of ligand affinity on integrins' lateral diffusion by addressing the lateral mobility results of wild-type and high-ligand affinity integrins obtained from SPT and FRAP techniques. As measured by SPT, high-ligand affinity integrins exhibited 75 % slower diffusion coefficient and 22 % lower mobile population when compared to wild-type integrins. However, no statistical difference in diffusion coefficient and mobile fraction was measured by FRAP. The difference in results was explained by the different population of integrins that are measured by these two techniques. Only ligand-bound integrins are measured by SPT whereas both ligand-bound and unbound are measured by FRAP. Therefore, based on the data, subset of ligand-bound high-ligand affinity integrins exhibits slower diffusion and lower mobile fraction compare to the ligand-bound wild-type integrins.

Chapter 3 combines SPT with RNA interference to address the influence of three cytoplasmic (Vinculin, FAK, ILK) and two membrane proteins (EGFR, Notch) role in

integrins' lateral diffusion. This study reports the increase in the number of ligand-bound integrins' mobile population after systematically reducing the concentration of targeted proteins. The percentage of integrins' mode of motion relative to total mobile population didn't alter after vinculin and EGFR concentration reduction. There was an increase of 9 to19 % increase in constrained population after Notch, ILK, or FAK concentration reduction. The five targeted proteins in this study are responsible for altering integrins' lateral mobility when present at native concentration.

Continuing the use of SPT and RNA interference technique, chapter 4 highlights the affect of insulin receptor and insulin signaling on integrins' lateral dynamics. No profound effect in integrins' lateral mobility was observed after the activation of signaling cascades initiated by insulin stimulated cells. However, after reducing the concentration of insulin receptor, integrins' mobile population increased indicating that the insulin receptor is responsible for constraining integrins' lateral mobility through direct association/interaction.

The techniques and the approaches used in this thesis work can be easily extended to the study of other membrane receptors in the same system as in S2 cells or in different systems such as mammalian cells. Similarly, one aspect that can be explored further would be the area of signaling effects on integrins' lateral mobility. For example, the effect of other signaling cascades initiated by growth factors and their receptors such as epidermal growth factor receptor (EGFR) or platelet derived growth factor (PDGF) could be explored.

APPENDIX: DEVELOPMENT OF A COMPREHENSIVE NEAR INFRARED SPECTROSCOPY CALIBRATION MODEL FOR RAPID MEASUREMENTS OF MOISTURE CONTENT IN MULTIPLE PHARMACEUTICAL PRODUCTS

A paper published in *Journal of Pharmaceutical and Biomedical Analysis*, 2014. 95, 169-175

Dipak Mainali[a], *Jane Li*[b §], *Peter Yehl*[b] *and Nicholas Chetwyn*[b]

a. Department of Chemistry, Iowa State University, 1605 Gilman Hall, Ames, IA 50011

b. Small Molecules Analytical Chemistry and Quality Control, Genentech, 1 DNA Way, South San Francisco, CA 94080

§ Corresponding author. Email address: li.jane@gene.com; Tel +001-650-225-7466

Abstract

Near infrared (NIR) spectroscopy has been widely used for the determination of water content in a wide variety of samples. With few exceptions, all methods employ a calibration model developed and applicable for a single product. The current study describes a NIR method using a single, comprehensive calibration model to predict the water content in tablets containing different active pharmaceutical ingredients (API). The calibration model was developed for water content range of 2 - 13% w/w using tablets containing three different APIs and different formulation compositions. To develop a robust comprehensive model, individual calibration models were sequentially developed starting from a simple model for one product to including tablets from all three projects in the final model using

partial least square analysis method. Data pretreatments and spectral region selections were performed during the method development to optimize the number of factors and the correlation coefficients for cross-validation and prediction by the comprehensive model. The model reliably predicted the water content in tablet samples of these three products, and can be updated for water measurements of new drug products by adding to the model two samples of the new product for calibration purpose.

Keywords

Near infrared spectroscopy, comprehensive model, moisture content, water analysis, tablets, pharmaceutical products

1. Introduction

Near infrared spectroscopy as an analytical tool has been widely used in pharmaceutical analysis for many years [1-9]. Over the last decade or so, pharmaceutical companies have been progressively adopting the Quality-by-Design principles expected by regulatory agencies[10] and implementing Process Analytical Technologies (PAT) to achieve full understanding of manufacturing processes and quality attributes of products [11-13]. NIR spectroscopy, capable of holistic and non-destructive sample analysis, has proven to be an invaluable PAT tool with distinctive advantages of little sample preparation, fast data acquisition, and flexibility with probes for at-line, on-line or in-line applications [12, 14-16]. Typical applications include timely monitoring of critical quality attributes (CQA) of drug products such as moisture content, blend and content uniformity and coating thickness [7, 17-21].

Water can affect the shelf life, physical and chemical stability and overall quality of pharmaceutical products [22-24]. The traditional wet chemistry method such as Karl Fischer titration for water content measurement is time-consuming, laborious and sample destructive. KF titration can be costly due to the use of organic solvents and treatment of chemical waste generated from the solvents use and destroyed samples. NIR spectroscopy, with its intrinsic advantages, is well suited for water determination because water shows strong absorption bands in NIR region that can provide the sensitivity and reproducibility needed for accurate measurements. Depending on the chemical and physical environment of the water molecule, the two most prominent absorption bands for water are the first overtone band of OH stretching at around 6800-7100 cm^{-1} (1470-1408 nm) and the combination band of OH stretching and bending at around 5100-5300 cm^{-1} (1960- 1887 nm) [19, 22, 25]. Numerous reported NIR methods for water analysis clearly demonstrated the wide applicability of this technique to materials from small molecule APIs and drug products to biologics [9, 20, 22, 26-29].

Quantitative water analysis by NIR spectroscopy is achieved through multivariate calibration methods to extract relevant chemical information from complex spectroscopic data and build calibration models for quantitation. Because the validity of a calibration model could be jeopardized by changes in instruments or sample composition and matrix [30], most of NIR water methods employ one calibration model for each relatively well-defined type of product or process to ensure the method accuracy. A unique example of universal quantitative models for determination of moisture content in beta-lactam powder injections by NIR was reported for feasibility and limits of the models and model extensions when applied for samples of same INN (International Nonproprietary Name) from diverse

formulations and sources [31]. This demonstrated that universal models can be developed to accommodate physical and chemical variations of the products, however, they quickly became very complicated with the increase of multiplicity of spectral variations. In addition, this example only utilized samples containing the same active ingredient.

For the present study, a comprehensive model for water analysis in compressed tablets was built with a set of standards that encompass significant variations in compositions and can reliably predict the water content in tablets differing in shape, size and containing different excipients and APIs. Performance between the individual and the comprehensive models was compared based on root mean square error of calibration (RMSEC), root mean square error of cross-validation (RMSECV), root mean square error of predication (RMSEP) and relative square errors of calibration and predication (RSEC and RSEP). No significant deterioration in the performance of the model was observed even as more products were included, although the minimal number of factors did increase as expected due to the increased complexity of the models. This method can be expanded for new products by updating the model with only two samples of the new products, and offers a fast and effective way to determine the moisture content in tablets to support product development.

2. Materials and methods

2.1. *Materials*

Uncoated tablets produced in house at Genentech (South San Francisco, CA, USA) with three different proprietary Genentech APIs were used for the study. API I and API III are both highly hygroscopic. Tablets containing API I were exposed to different humidity levels at ambient temperature to generate the reference samples with moisture level between

2 and 13% w/w for building NIR calibration method. The main excipient in all the tablets is microcrystalline cellulose (Avicel PH101, 102 or 103) purchased from FMC Biopolymer (Philadelphia, PA, USA). Tablets of API II also contained lactose monohydrate (Foremost Farms USA, Baraboo, WI, USA) at the amount similar to MCC. All tablets were manufactured using roller compaction process under different process conditions that were optimized for each product through Design of Experiments (DOE).

2.2. *FT-NIR instrument and data acquisition*

NIR spectra of the tablets were acquired with an Antaris II Fourier-Transform Near Infrared (FT-NIR) analyzer from Thermo Scientific (Madison, WI) equipped with Integrating Sphere and an Indium Gallium Arsenide (InGaAs) detector in diffuse reflectance mode. Thermo Scientific OMNIC software version 8.3 accompanying the instrument was used for the collection of all spectra. One spectrum was collected for each face of the round, oval or oblong shaped tablet. Each spectrum was the average of 16 scans in the range of 10,000 cm^{-1} to 4000 cm^{-1} with 8 cm^{-1} resolution. For each tablet, spectra from the two faces were averaged as one for calibration or quantitation.

2.3. *Karl Fischer*

Coulometric Karl Fischer 851 Titrando (Metrohm, Switzerland) equipped with 774 oven sample processor and Tiamo 2.3 software was used as the reference method to measure water content in the tablet samples. Each tablet was weighed, ground into powder, transferred to titration vials and sealed for the KF measurements. Precaution was taken to complete the grinding, powder transfer and vial sealing within 5 minutes for each sample after NIR spectra collection. This was especially important for tablets of API I and III due to their high

hygroscopicity, so that potential changes in water content because of the sample exposure to ambient conditions can be minimized.

2.4. *NIR Calibration model*

In order to build the calibration models over an expanded range of moisture content, tablets containing the API I were exposed to different humidity levels at ambient temperature to generate the reference samples with moisture level between 2 and 13% w/w. Samples of the lowest moisture content were stored with desiccant, and samples stored under ambient conditions without desiccant had moisture level of ~5% w/w. Higher moisture levels (>5% w/w) were obtained by exposing the tablets overnight to various high humidity conditions created by saturated salt solutions. These reference samples were analyzed by NIR and KF for moisture content. Of the thirty tablets analyzed, twenty-five were used for building NIR calibration models and five were used for validation of the models to allow the calculation of RMSEP and performance index (PI) values of the models. Table 1 summarizes the reference samples and their moisture contents by KF.

Chemometric software package TQ Analyst version 8 by Thermo Scientific (Madison, WI) was used to build the NIR calibration models. The models were built with partial least square (PLS) method by assigning KF data to the corresponding NIR spectra. Spectral pretreatments that were performed to build each calibration model included Savitzky-Golay smoothing with no, first-degree or second-degree derivative. Seven data points and third order polynomial were used for Savitzky-Golay smoothing. The best model was chosen based on the resulting chemometric parameters.

3. Results and Discussions

3.1 *Development of the calibration models*

The main goal of the study is to develop a single calibration model that can predict the water content for drug product samples containing different API. Round and oblong shaped tablets of API I as presented in Table 1, representing different strengths, were used to develop the first calibration model. Fig. 1 is the overlaid NIR spectra for these calibration samples with and without the first derivative pretreatment with Savitzky-Golay smoothing. Two spectral regions related to water absorption (5015-5303 cm^{-1}, 6503-7008 cm^{-1}) were selected to build the calibration model I, and the strongest correlation in the moisture level and signal intensity was observed at 5000-5500 cm^{-1} region that is attributed to the combination band of OH stretching and bending.

The calibration model I shown in Figure 2 (a) used 4 PLS factors, and the root mean square error of calibration (RMSEC) was 0.177 with correlation coefficient of 0.998. Individual calibration models using the round or oblong tablets for API I only were compared with the model I to assess any potential effect of tablet shape on model performance. Table 2 summarized the parameters for the models with different spectral pre-treatment approaches and Savitzky-Golay smoothing.

For the model using round tablets only, pre-treating the spectra significantly reduced the RMSEC; however, the RMSEP was much higher than the RMSEC indicating that the model was likely over-fitted. For the oblong tablets, first derivative resulted in the best fitted model with RMSEC 0.137 and RMSEP 0.13. The combined model I had higher RMSEC (0.177) than both due to the increased complexity with all the samples. However, the RMSEP value was similar for all three models of API I tablets, suggesting that the tablet shape had limited impact on the NIR spectra and thus the validity of the calibration model I.

The calibration model I was used to predict the water content in tablets of API I, API II, and API III. As expected, the calibration model I was able to reliably predict the water content of API I tablets, however failed to predict the correct water contents for tablets of API II and API III. This is not surprising considering that the change in API probably caused significant changes in the NIR spectra and thus invalidated the calibration model built with API I samples alone.

To render the calibration model useful for more than one product, calibration model I was updated using the reference samples of API II and API III tablets. Model updating is a common approach in incorporating differences or changes in samples or NIR instruments and enhancing the applicability of a calibration model for samples of different matrix and instrument settings [30]. Similar to the tablets of API I, the main component in tablets of API II and API III is microcrystalline cellulose (MCC). Compared to the other two products, tablets of API II also contained significant amount of lactose monohydrate (~40% wt) and had much lower drug loading (10% wt). All tablets contain other minor ingredients needed for the performance of the tablets; however, the most significant difference is the active pharmaceutical ingredients, the contribution of which to the NIR spectra and thus the calibration model must be adjusted in order to maintain the validity of the models. The model updated using tablets of API II was referred to as calibration model II, and the model updated using tablets of both API II and API III was referred to as calibration model III. Fig. 3 (a) is the overlaid NIR spectra for tablets of all three APIs, and Fig. 3 (b) is the spectra with first derivative pre-treatment.

Calibration model II was built with tablets of both API I and API II, including tablets of different shapes that represent different strengths for each product. Fig. 3 is the overlaid

NIR spectra of all calibration samples, clearly showing the higher baseline and different spectral features for the spectra of API II samples. This may be due to the presence of lactose monohydrate in these samples but not those of the other two APIs. Because of these significantly different spectral features, one extra spectral region (5321-5601cm^{-1}) was used to build the calibration model II in addition to the two regions (5014-5303cm^{-1}, 6503-7008cm^{-1}) used for the calibration model I. This model used 6 PLS factors and showed good quality of calibration and predication (RMSEC = 0.123, RMSEP = 0.186). Without this third region (5321-5601cm^{-1}), a simpler model with only three PLS factors could be established; however, the quality of the model was much worse (RMSEC = 0.382, RMSEP = 0.387). API II is not hygroscopic, and its tablets equilibrated to about 5% w/w of water when stored under normal laboratory conditions. As shown in Table 1, three tablet samples of API II were added to the calibration model, resulting in total of 23 individual calibration standards and 5 validation standards (Fig. 2 (b)). Compared to the model I, the RMSEC of the updated model II actually slightly decreased to 0.123 from 0.177 for the model I, however the number of factors used for the model increased from 4 to 6.

To further expand the scope of the calibration model and applicability of the method, calibration model III was built with the addition of API III tablets to the calibration standard set used for calibration model II. API III is very hygroscopic, and moisture absorption can result in various polymorphs for the API. For this study, only tablets stored with desiccants were used, since these were the only tablets manufactured and available. Because of the complicated polymorph situation, no samples for this API were prepared by exposing to different humidity levels. The addition of two tablet samples for API III brought the total number of individual calibration standards to 25 (Table 1). The calibration model III was

shown in Fig. 2 (c). For this calibration model, only two main spectral regions related to water absorption (5014-5302 cm^{-1} and 6503-7008 cm^{-1}) were selected (Fig. 3). Even though one additional product was added to the calibration set, the model remained relatively simple with 6 factors and RMSEC and RMSEP being 0.193 and 0.233, respectively. Inclusion of the third region (5321 - 5601 cm^{-1}) that was used for model II resulted in a slightly more complicated (8 factors) and over-fitted calibration model (RMSEC = 0.083, RMSEP = 0.212), which would reduce the reliability of prediction when the unknown samples were analyzed.

The comprehensive calibration model III used 6 PLS factors, same as the model II. Its RMSEC was 0.193, slightly greater than that of the model I. Both parameters strongly suggested that the addition of another set of different samples did not significantly increase the complexity of the calibration method, and it is possible to continue expanding the scope of the method to samples of additional APIs.

3.2 Validation of the Calibration Models

All NIR calibration models need to be validated for accuracy of predication before being used for actual analysis. Independent validation samples are generally selected to verify and confirm the quality of the calibration model. For this study, four tablet samples of API I and one tablet sample of API II were analyzed along with the calibration samples but utilized as validation standards to obtain the root mean square error of prediction (RMSEP) and the performance index [25] values. The calibration models were also cross-validated using the leave-one-out cross-validation approach. Although not widely used, the performance index (PI) measures how accurately a calibrated method can quantify or classify the validation standards and complements RMSEP in evaluating the performance of a calibration method for unknown sample analysis. The PI was calculated based on the difference of the

calculated vs. the actual moisture content; a PI value near 100 indicates a good method. Table 3 summarized the validation standards used, the RMSEP and PI for each of the three calibration models.

The PI values slightly decreased from the Model I to III, however were all above 90. RMSEP showed a slight increase from Model I to III. For each model, the RMSEP value was comparable to the RMSEC value (Table 4), a good indicator on the effectiveness of the models for the analysis of the unknown samples. The quality of calibration and predication of these calibration models was also demonstrated by the low Relative Standard Errors (RSE) as shown in Table 4 (RSEC for calibration and RSEP for predication).

3.3 Comparison of the Calibration Models

The three calibration models were compared to see how the performance would have deteriorated as the sample variety increased. The three models primarily differ in the number of standard samples incorporated from different drug product tablets and the region selected for calibration. Table 4 shows the chemometric parameters obtained from three calibration models. The values of RMSEC/P and RSEC/P clearly showed that the quality of calibration and predication did not appear to significantly deteriorate as the models became increasingly complicated. On the other hand, RSMECV for all three models was higher than RSMEC. This is consistent with NIR methods reported in the literature [16, 22, 32]. The extent of the difference between RMSEC and RMSECV may be due to the limited number of validation standards employed, especially for the comprehensive model III.

While building the models, the spectra in the standard samples were subjected to different pretreatment and smoothing methods. The model with less number of factors and higher performance index value was selected as the final model for each calibration set. The

PRESS (predicted residual error sum of squares) diagnostic from the software was used to obtain the RMSECV value and to observe the number of factors used in each model (Fig. 4). The PRESS diagnostic used the cross validation technique to calculate a PRESS value for each factor that may be used to generate the calibration model in PLS method. And the PRESS value normally decreases each time a factor was added to the calibration model if the factor is providing useful information for the calibration. For each model, the number of factors as suggested by the software was used. The loading spectra were checked to make sure that the factors with significant noise were not used in the model.

The robustness of the calibration models, as the calibration standards expanded to include more samples of different API and compositions, was also demonstrated by the analysis of tablet samples of API I using the three models (Table 5).

The results using the three calibration models for the same batches of samples of API I tablets were in excellent agreement with each other, strongly suggesting that the increased complexity of the calibration sample set did not compromise the quality of the calibration model. Except one oblong tablet sample with high water content (#10), all results based on NIR analysis were within 0.5% absolute value of KF measurements. In addition, the precision in measurements for the three NIR models was very similar based on the standard deviations for replicate measurements of the API I samples. The measurement precision and accuracy using the comprehensive calibration model evidently demonstrated the applicability of this model for the moisture analysis of complicated samples with differences in compositions and manufacturing process.

3.4 Prediction of moisture level for unknown samples

As the main purpose of the study was to develop a model that can be used for water analysis for drug product samples of difference APIs, the model that serves the intended purpose was model III. Included in Table 6 are the results from NIR analysis using the model III for independent samples of API I, II and III. The standard deviation for all results was also included to show the degree of the variation in the water measurements by both NIR and KF. Except sample #10, all average predicted results using the calibration model III were with 0.5% (absolute difference) of the average results measured by KF. The absolute difference over 1% (or ~12% relative) for sample #10 may be attributed to the inherent difference in water content from tablet to tablet of this sample and the possible inaccuracy in the KF measurements for this particular sample because of the rapid loss of water during the sample preparation for KF measurement. However, the predicted results with the demonstrated degree of accuracy were still valuable in quickly assessing the overall quality of a drug product considering the ease and speed of NIR analysis of intact tablets. Good precision (RSD < 3%) was also achieved by NIR measurements for all samples except API I sample #10 and the API III sample. For the API I sample #10, both KF and NIR measurements had worse precision than other samples; therefore, the poor precision for the NIR method may be attributed to the samples and the KF measurements as discussed above. The precision of KF measurements for the API III sample was comparable to others (except API I sample #10), and the poor precision on the NIR measurements pointed to the challenges in moisture analysis for highly hygroscopic materials even for techniques such as NIR where sample exposure time to the environment could be minimized.

4. Conclusions

A comprehensive calibration model was built for the analysis of water content in tablets containing different active ingredients. The model was shown to be robust and accurate with good precision in moisture analysis for tablets over the range of 2-13% w/w, and can potentially be further expanded for other drug products. The key in expanding the method applicability is to continuously update the model with new samples or products to be analyzed. The current study showed that this can be accomplished by adding as few as two samples to the model for the new product. As more products are brought into the scope of the method, the calibration model becomes more complicated in terms of number of PLS factors to be used and the degree of decrease in the performance index and RMSEC/CV/P. It remains to be explored on the number of factors that can be used before a new model becomes a necessity.

This method could be applicable to samples or dosage forms other than tablets, and could provide a fast and reliable approach for moisture analysis where many samples need to be analyzed and compared quickly to support pharmaceutical development. The speed of analysis by NIR spectroscopy and the non-destructive nature of the technique make it especially attractive for water determination of hygroscopic samples.

Acknowledgements

The authors would like to acknowledge Mr. Hong Lin of Genentech for technical discussions.

References

[1] J.E. Sinsheimer, N.M. Poswalk, Pharmaceutical applications of the near infrared determination of water, J Pharm Sci, 57 (1968) 2007-2010.

[2] A. Peinado, J. Hammond, A. Scott, Development, validation and transfer of a near infrared method to determine in-line the end point of a fluidised drying process for commercial production batches of an approved oral solid dose pharmaceutical product, J Pharm Biomed Anal, 54 (2011) 13-20.

[3] M. Blanco, A. Peguero, Analysis of pharmaceutical by NIR spectroscopy without a reference method, TRAC-Trend Anal Chem., 29 (2010) 1127-1136.

[4] M. Blanco, R. Cueva-Mestanza, A. Peguero, NIR analysis of pharmaceutical samples without reference data: Improving the calibration, Talanta, 85 (2011) 2218-2225.

[5] C.M. McGoverin, L.C.H. Ho, J.A. Zeitler, C.J. Strachan, K.C. Gordon, T. Rades, Quantification of binary polymorphic mixtures of ranitidine hydrochloride using NIR spectroscopy, Vibrational Spectroscopy, 41 (2006) 225-231.

[6] T. Schonbrodt, S. Mohl, G. Winter, G. Reich, NIR spectroscopy-a non-destructive analytical tool for protein quantification within lipid implants, J Control Release, 114 (2006) 261-267.

[7] J.J. Moes, M.M. Ruijken, E. Gout, H.W. Frijlink, M.I. Ugwoke, Application of process analytical technology in tablet process development using NIR spectroscopy: blend uniformity, content uniformity and coating thickness measurements, Int J Pharm, 357 (2008) 108-118.

[8] I. Paris, A. Janoly-Dumenil, A. Paci, L. Mercier, P. Bourget, F. Brion, P. Chaminade, A. Rieutord, Near infrared spectroscopy and process analytical technology to master the process

of busulfan paediatric capsules in a university hospital, J Pharm Biomed Anal, 41 (2006) 1171-1178.

[9] X. Zhou, P. Hines, M.W. Borer, Moisture determination in hygroscopic drug substances by near infrared spectroscopy, J Pharm Biomed Anal, 17 (1998) 219-225.

[10] U.S.F.D.A. (FDA), Guidance for Industry Pharmaceutical Development, 2009. http://www.fda.gov/Drugs/GuidanceComplianceRegulatoryInformation/Guidances/default.htm

[11] J. Luypaert, S. Heuerding, D.L. Massart, Y.V. Heyden, Direct orthogonal signal correction as data pretreatment in the classification of clinical lots of creams from near infrared spectroscopy data, Anal Chim Acta, 582 (2007) 181-189.

[12] C. De Bleye, P.F. Chavez, J. Mantanus, R. Marini, P. Hubert, E. Rozet, E. Ziemons, Critical review of near-infrared spectroscopic methods validations in pharmaceutical applications, J Pharm Biomed Anal, 69 (2012) 125-132.

[13] J. Mantanus, E. Rozet, K. Van Butsele, C. De Bleye, A. Ceccato, B. Evrard, P. Hubert, E. Ziemons, Near infrared and Raman spectroscopy as Process Analytical Technology tools for the manufacturing of silicone-based drug reservoirs, Anal Chim Acta, 699 (2011) 96-106.

[14] E.M. Agency, Guideline on the use of Near Infrared Spectroscopy (NIRS) by the pharmaceutical industry and the data requirements for new submissions and variations (draft), http://www.ema.europa.eu/docs/en_GB/document_library/Scientific_guideline/2012/02/WC500122769.pdf

[15] D.A. Burns, E. W. Ciurczak, Handbook of Near-Infrared Analysis, 3rd ed., CRC Press, New York 2008.

[16] L. Martínez, A. Peinado, L. Liesum, In-line quantification of two active ingredients in a batch blending process by near-infrared spectroscopy: Influence of physical presentation of the sample, Int. J. Pharm. 451 (2013) 67-75.

[17] J. Luypaert, D.L. Massart, Y. Vander Heyden, Near-infrared spectroscopy applications in pharmaceutical analysis, Talanta, 72 (2007) 865-883.

[18] T.R.M. De Beer, P. Vercruysse, A. Burggraeve, T. Quinten, J. Ouyang, X. Zhang, C. Vervaet, J.P. Remon, W.R.G. Baeyens, In-line and real-time process monitoring of a freeze drying process using Raman and NIR spectroscopy as complementary process analytical technology (PAT) tools, J Pharm Sci, 98 (2009) 3430-3446.

[19] H. Grohganz, M. Fonteyne, E. Skibsted, T. Falck, B. Palmqvist, J. Rantanen, Role of excipients in the quantification of water in lyophilised mixtures using NIR spectroscopy, J Pharm Biomed Anal, 49 (2009) 901-907.

[20] H. Grohganz, D. Gildemyn, E. Skibsted, J.M. Flink, J. Rantanen, Towards a robust water content determination of freeze-dried samples by near-infrared spectroscopy, Anal Chim Acta, 676 (2010) 34-40.

[21] J. Mantanus, E. Ziemons, P. Lebrun, E. Rozet, R. Klinkenberg, B. Streel, B. Evrard, P. Hubert, Active content determination of non-coated pharmaceutical pellets by near infrared spectroscopy: method development, validation and reliability evaluation, Talanta, 80 (2010) 1750-1757.

[22] C.C. Corredor, D. Bu, D. Both, Comparison of near infrared and microwave resonance sensors for at-line moisture determination in powders and tablets, Anal Chim Acta, 696 (2011) 84-93.

[23] S. Airaksinen, M. Karjalainen, A. Shevchenko, S. Westermarck, E. Leppanen, J. Rantanen, J. Yliruusi, Role of water in the physical stability of solid dosage formulations, J Pharm Sci, 94 (2005) 2147-2165.

[24] Y. Matsunaga, R. Ohta, N. Bando, H. Yamada, H. Yuasa, Y. Kanaya, Effects of water content on physical and chemical stability of tablets containing an anticancer drug TAT-59, Chem Pharm Bull (Tokyo), 41 (1993) 720-724.

[25] B. Czarnik-Matusewicz, S. Pilorz, Study of the temperature-dependent near-infrared spectra of water by two-dimensional correlation spectroscopy and principal components analysis, Vibrational Spectroscopy, 40 (2006) 235-245.

[26] C. Hakemeyer, U. Strauss, S. Werz, G.E. Jose, F. Folque, J.C. Menezes, At-line NIR spectroscopy as effective PAT monitoring technique in Mab cultivations during process development and manufacturing, Talanta, 90 (2012) 12-21.

[27] J. Mantanus, E. Ziemons, P. Lebrun, E. Rozet, R. Klinkenberg, B. Streel, B. Evrard, P. Hubert, Moisture content determination of pharmaceutical pellets by near infrared spectroscopy: method development and validation, Anal Chim Acta, 642 (2009) 186-192.

[28] Y. Zheng, X. Lai, S.W. Bruun, H. Ipsen, J.N. Larsen, H. Lowenstein, I. Sondergaard, S. Jacobsen, Determination of moisture content of lyophilized allergen vaccines by NIR spectroscopy, J Pharm Biomed Anal, 46 (2008) 592-596.

[29] A. Dunko, A. Dovletoglou, Moisture assay of an antifungal by near-infrared diffuse reflectance spectroscopy, J Pharm Biomed Anal, 28 (2002) 145-154.

[30] R.N. Feudale, N.A. Woody, H. Tan, A.J. Myles, S.D. Brown, J. Ferré, Transfer of multivariate calibration models: a review, Chemometrics and Intelligent Laboratory Systems, 64 (2002) 181-192.

[31] X.B. Zhang, Y.C. Feng, C.Q. Hu, Feasibility and extension of universal quantitative models for moisture content determination in beta-lactam powder injections by near-infrared spectroscopy, Anal Chim Acta, 630 (2008) 131-140.

[32] M. Ito, T. Suzuki, S. Yada, A. Kusai, H. Nakagami, E. Yonemochi, K. Terada, Development of a method for the determination of caffeine anhydrate in various designed intact tablets [correction of tables] by near-infrared spectroscopy: a comparison between reflectance and transmittance technique, J Pharm Biomed Anal, 47 (2008) 819-827.

Table 1 Reference Samples with moisture content in the range of 2-13% (w/w).

API	Sample	Tablet	Water by KF (% w/w)
I	1	Round	2.77
	2	Round	3.13
	3	Round	4.41
	4	Round	5.52
	5	Round	5.60
	6	Round	6.33
	7	Round	12.37
	8	Round	12.80
	9	Oblong	3.59
	10	Oblong	3.62
	11	Oblong	5.21
	12	Oblong	5.31
	13	Oblong	5.30
	14	Oblong	6.12
	15	Oblong	6.20
	16	Oblong	6.17
	17	Oblong	7.08
	18	Oblong	6.95
	19	Oblong	10.41
	20	Oblong	8.93
II	21	Round	4.99
	22	Round	4.98
	23	Oval	5.28
III	24	Oblong	2.25
	25	Oblong	2.18

Table 2 Chemometrics results for models using round or oblong tablets of API I only.

Sample	Spectral Pre-treatment	RMSEC and coefficient	RMSEP and coefficient	Factors Used	Regions
Round Tablets	No	0.15; 0.999	0.151; 1	3	5014-5303, 5321-5601, 6503-7008
	First Derivative	0.0134; 1	0.205; 1	5	5014-5303, 6503-7008
Oblong Tablets	First Derivative	0.137; 0.998	0.13; 1	2	5014-5303, 6503-7008
	Second Derivative	0.119; 0.998	0.127; 1	2	5014-5303, 6503-7008

Table 3 Summary of RMSEP and PI for the calibration models I, II and III.

Calibration Model	Validation Standards	RMSEP	PI
I	4 (API I)	0.143	95.6
II	5 (API I and II)	0.186	94.3
III	5 (API I and II)	0.233	92.8

Table 4 Chemometric parameters obtained from three calibration models.

	Calibration I	**Calibration II**	**Calibration III**
Pretreatment	1st Derivative	1st Derivative	1st Derivative
Smoothing	Savitzky-Golay	Savitzky-Golay	Savitzky-Golay
Region (cm^{-1})	5014-5303, 6503-7008	5014-5303, 5321-5601, 6503-7008	5014-5302, 6503-7008
RMSEC	0.177	0.123	0.193
RMSEC Corr.	0.998	0.998	0.997
RMSEP	0.143	0.186	0.233
RMSEP Corr.	0.997	0.995	0.991
PLS Factors	4	6	6
RMSECV	0.331	0.371	0.413
RMSECV Corr.	0.993	0.989	0.988
RSEC	2.55 %	1.83 %	3.00 %
RSEP	2.03 %	2.77 %	3.50 %

Table 5 Comparison of actual % moisture (KF) and predicted % moisture (NIR) for API I tablets using three calibration models[a]

Sample Type	Sample #	% wt (KF)[b]	% wt (NIR)[c]		
			Model I	Model II	Model III
Round	1	2.95	2.97 ± 0.08	3.02 ± 0.06	2.84 ± 0.07
	2	4.41	4.16 ± 0.05	4.26[d] ± 0.06	4.20[d] ± 0.03
	3	5.56	5.44 ± 0.08	5.20 ± 0.10	5.47 ± 0.08
	4	6.35	6.21 ± 0.15	6.00 ± 0.13	6.26 ± 0.15
	5	12.59	12.18 ± 0.28	12.09 ± 0.26	12.18 ± 0.28
Oblong	6	3.66[e]	3.32 ± 0.17	3.27 ± 0.11	3.35 ± 0.04
	7	5.27	5.19 ± 0.11	5.18 ± 0.12	5.20 ± 0.13
	8	6.17	6.15 ± 0.14	6.23 ± 0.20	6.10 ± 0.12
	9	7.03	6.98 ± 0.06	6.99 ± 0.07	6.92 ± 0.06
	10	9.57	10.78 ± 1.14	10.80 ± 1.39	10.74 ± 1.15

[a] All values shown were average ± standard deviation based on replicate measurements for each sample
[b] Average of two independent measurements for round tablets, and average of three independent measurements for oblong tablets;
[c] Average of ten independent measurements for round tablets, and average of three independent measurements for oblong tablets;
[d] Average of eight independent measurements;
[e] Average of two independent measurements.

Table 6 Comparison of actual % moisture (KF) and predicted % moisture (NIR) for tablets of all three APIs using calibration model III

Sample Type	Sample #	% moisture (KF) [a]	% moisture (NIR) [b]	% RSD NIR measurement
API I Round	1	2.95 ± 0.25	2.84 ± 0.07	2.46
	2	4.41 ± 0.01	4.20 ± 0.03	0.71
	3	5.56 ± 0.06	5.47 ± 0.08	1.46
	4	6.35 ± 0.03	6.26 ± 0.15	2.40
	5	12.59 ± 0.32	12.18 ± 0.28	2.30
API I Oblong	6	3.66 ± 0.10	3.35 ± 0.04	1.19
	7	5.27 ± 0.06	5.20 ± 0.13	2.50
	8	6.17 ± 0.04	6.10 ± 0.12	1.97
	9	7.03 ± 0.07	6.92 ± 0.06	0.87
	10	9.57 ± 0.76	10.74 ± 1.15	10.71
API II, Round	11	5.07 ± 0.02	5.16 ± 0.13	2.52
API II, Oval	12	4.71 ± 0.02	4.61 ± 0.09	1.95
API III	13	2.22 ± 0.05	2.30 ± 0.24	10.43

[a] *Average ± standard deviation of two independent measurements for API I round and API III tablets, and of three independent measurements for others.*
[b] *Average ± standard deviation of ten independent measurements for API I round tablets, of four independent measurements for API III samples, and of three independent measurements for others.*

Fig. 1. (a) Overlaid NIR spectra of API I tablet samples used for calibration; (b) overlaid NIR spectra with first derivative pretreatment.

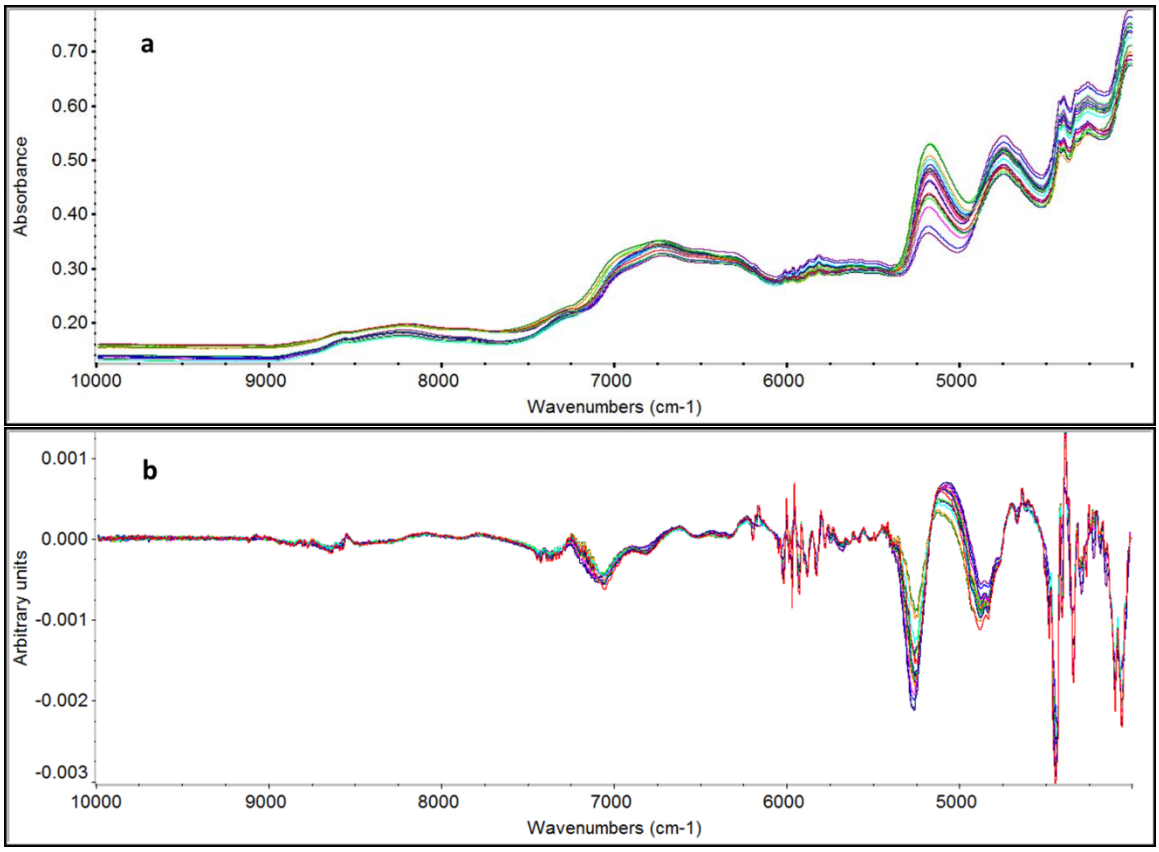

Fig. 2. Calibration plots for three models. (a) Model I. (b) Model II. (c) Model III. Actual = % (w/w) moisture by KF; calculated = % (w/w) moisture by NIR.

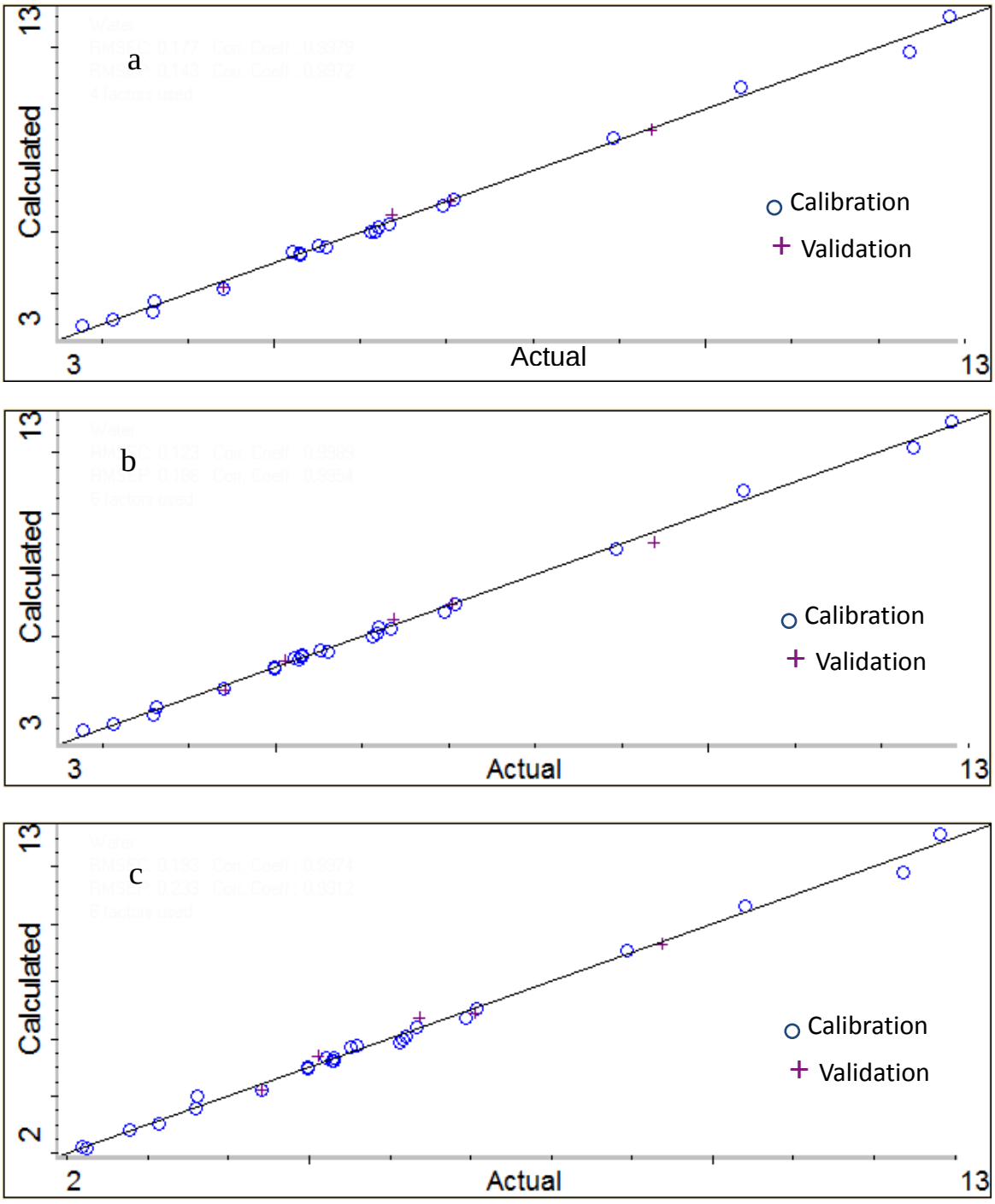

Fig. 3. (a) Overlaid spectra of all tablet samples used for calibration that includes API I, API II, API III; the spectra with higher baseline (the one on the top of all spectra) were those of API II tablets; (b) 1st derivative pretreatment overlaid spectra of all tablet samples used for calibration; the three spectra that were not totally overlapped (visible ~ 5100 cm^{-1} region) were those of API II tablets.

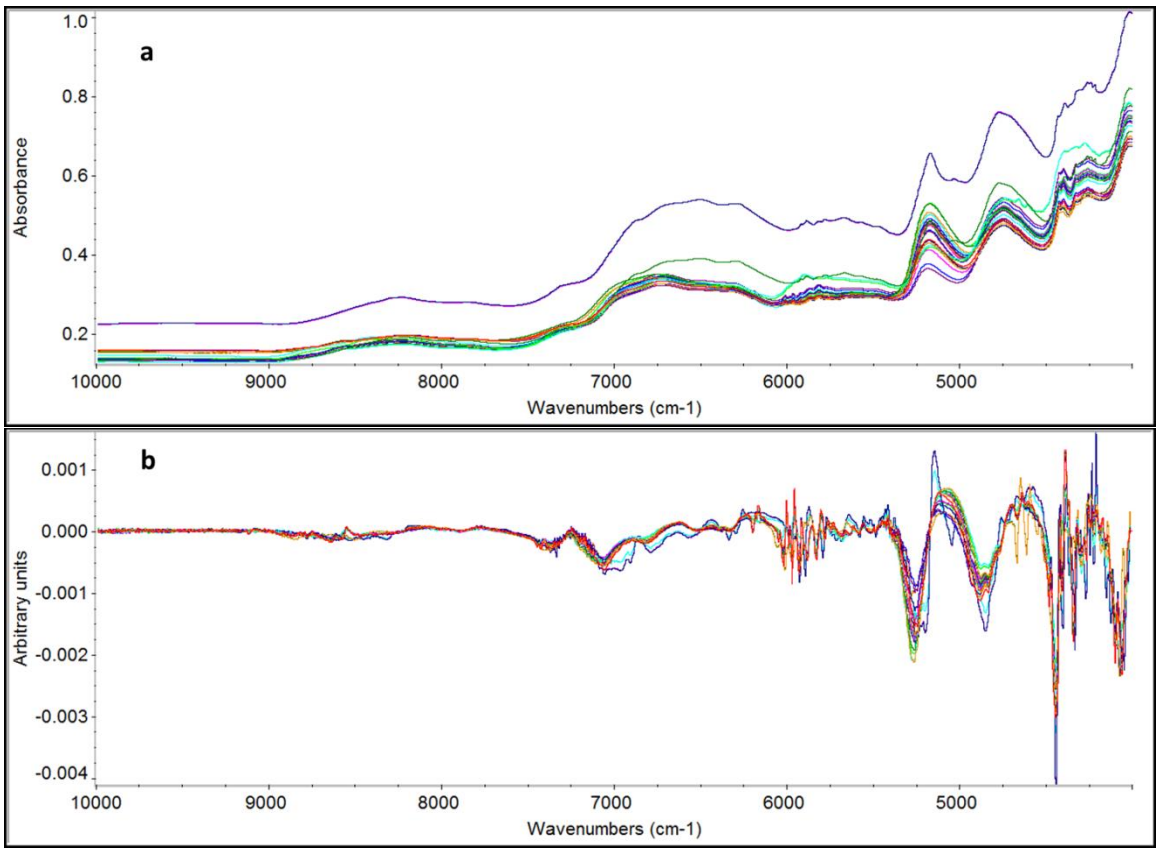

Fig. 4. PRESS plot for calibration model III.